

Collective light-matter interactions: From Purcell to Dicke.

Alexander N. Poddubny

Weizmann Institute of Science, Rehovot 7610001, Israel

`poddubny@weizmann.ac.il`

May 16, 2025

Contents

Preface	vii
1 Introduction	1
2 Overview of experimental systems	3
2.1 Practical implementations	4
2.2 Additional reading and references	8
3 Scattering on a single emitter	13
3.1 Brute-force approach	14
3.1.1 Wave equation	14
3.1.2 Emitter polarizability	15
3.2 Green function approach	19
3.3 Summary	21
3.4 Additional reading	22
4 Two-dimensional arrays	23
4.1 Reflection calculation	23
4.2 Additional reading	27
5 Scattering on two emitters	29
5.1 Multiple scattering approach	30
5.2 Non-Hermitian Hamiltonian method	32
5.3 Complex eigenmodes	33
5.4 Purcell enhancement	36
5.5 Super- and subradiant modes for $N = 2$	38

5.6	Non-Markovian effects	41
5.7	Summary	43
5.8	Additional reading	44
6	2×2 non-Hermitian Hamiltonian	47
6.1	Derivation of the Hamiltonian	47
6.2	Exceptional points. Strong and weak coupling	49
6.3	Friedrich-Wintgen condition	50
6.4	Summary	52
6.5	Additional reading	53
7	Light interaction with $N > 2$ periodically spaced emitters.	55
7.1	Collective super- and subradiant modes for N emitters	55
7.2	Transfer matrix method	59
7.2.1	General approach	59
7.3	Polariton dispersion	62
7.3.1	Reflection and transmission from a periodic structure	66
7.4	Bragg-spaced arrays	67
7.5	Borrmann effect	71
7.6	Summary	73
7.7	Additional reading	75
8	Chiral light-matter interaction	79
8.1	Spin-momentum locking: photonic bicycles	80
8.2	Chiral atom-light interaction	83
8.3	Summary	85
8.4	Additional reading	87
9	Arrays in a cavity	89
9.1	Empty cavity response	89
9.1.1	Reflection, transmission and Fabry-Pérot modes	89
9.1.2	Empty cavity Green function	91
9.1.3	Input-output theory for an empty cavity	93
9.2	Purcell factor in a cavity	97

9.3	Collective Rabi splitting	98
9.4	Additional reading	101
10	Array of quantum emitters	103
10.1	Jaynes–Cummings model	103
10.2	Collective Dicke states and Tavis-Cummings model	104
10.3	Weak coupling: collective spontaneous emission	107
10.4	Additional reading	110
11	Dicke superradiance	111
11.1	Superradiant burst	111
11.2	Dicke phase transition	113
11.3	Additional reading	117
12	Multiple-excited subradiant states	119
12.1	Subradiant states in the Dicke ladder	120
12.2	Subradiant states in waveguide QED	120
12.3	Additional reading	125
A	Resonant susceptibility	127
B	Green function for the Helmholtz equation	129
C	Electromagnetic Green function in free space	133
D	Emitter polarizability with radiative corrections	137
E	Lattice summation details	141
F	Lindblad master equation for an emitter array	145

Preface

We receive most of the information about the surrounding world via vision. As a result, optics has become the cornerstone of physics research at the same time that modern science was born, starting at least as early as Galileo's telescope and the experiments of Newton and Hooke. Electromagnetism became the first field theory and radio waves have connected the continents. The advent of quantum physics, in the beginning, was also paved with optics experiments, from the photoeffect to the spectra of stars. Later on, lasers became an indispensable tool and even an integral part of popular culture. Interaction of electromagnetic waves with matter is also an essential tool, from taking an X-ray image in a hospital to the characterization of materials in a lab. Very often, the setup involves several electromagnetic wave emitters, and it becomes an important question how these emitters will interact with electromagnetic waves: independently, or collectively. Collective light-matter interaction is the central subject of this book.

The incredible abundance of electromagnetic phenomena across different areas of science has led to the variety of terms, languages and traditions. Science has become scattered. I have had the luck to work closely with amazing colleagues from various communities studying very related phenomena, from radio physics to the physics of metamaterials, semiconductor physics, and atomic optics. I was really puzzled by how different the languages are and how little people from different communities interact with each other. It took quite an effort to bridge quantum and classical understandings of the Purcell effect (faster spontaneous emission in a cavity), although the results were already well-known in the literature. Quantum optics people would not read books or papers by radiophysics or x-ray people and vice versa. I am guilty of that as well. There are very basic collective interaction effects for X-ray diffraction theory, such as the Borrmann effect of suppression of absorption, that seem to be completely forgotten and have to be rediscovered each time when seen in experiments. The superradiance, collective

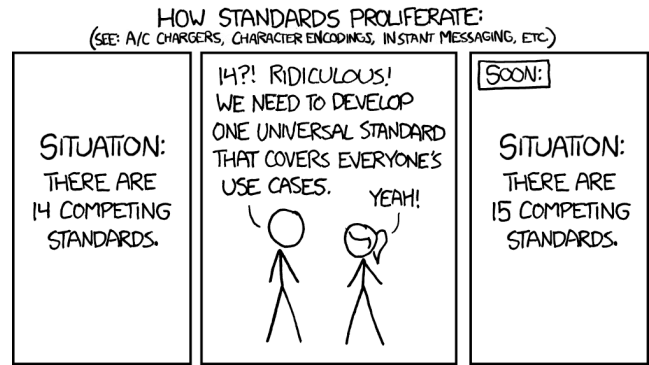


Figure 1: [xkcd comics #927](#) on competing standards. Maybe, [the same happens for textbooks](#)

enhancement of spontaneous emission in emitter arrays, is now seeing a renaissance of research. At the same time, there is not much collaboration between the specialists on various times of emitters, such as real atoms and artificial atoms (quantum dots).

The current book aims to bridge these communities at least partially by considering some basic effects of collective light-matter interactions occurring in various arrays of emitters from a hopefully universal viewpoint. In the first part, I will focus on the linear response regime, that is realized either for very low light intensity (below single photon) or for classical light in the linear optics regime. I will discuss collective enhancement and suppression of the light-matter interaction strength, the difference between strong and weak coupling regimes, Purcell effect, vacuum Rabi splitting. I know there is a little chance of success, as elucidated by the XKCD comic in Fig. 1. The whole concept of a textbook might vanish in the age of AI. But I still think it is worth a try. The book does not require knowledge of advanced quantum mechanics or quantum electrodynamics. It is mostly sufficient to know free-space electrodynamics at the undergraduate level.

Chapter 1

Introduction

This book deals with light interaction with arrays of emitters. The central idea is illustrated in Fig. 1.1. If the emitters are far from each other in space, or they are very different, they will interact with light independently. That is, each emitter will absorb and emit photons as if the others were not present, see Fig. 1.1(a). On the other hand, if emitters are similar to each other and interact with the same photonic modes, collective enhancement or suppression of emission becomes possible, as illustrated in Fig. 1.1(b,c) for two emitters. This happens because of either constructive or destructive interference of photons from different emitters.

Such an idea of collective emission is rather basic. It can be implemented in practice for very different systems of emitters, that we will discuss in the following Chapter 2. We also stress, that the picture in Fig. 1.1 is entirely classical. That is, it applies in the same way, for example, for classical antennas and for two-level atoms. There exist purely quantum effects, that can not be seen for antenna arrays, such as Dicke superradiance, that do not have a exact classical analogues. However, the understanding of the essential idea of constructive and destructive interference and even doing actual research on emission by emitter arrays does not require much knowledge of quantum mechanics or quantum electrodynamics. However, there is still a lot to study, even in the case of classical model.

It is instructive to compare the optical model of array of emitters coupled to propagating photons, or to photons trapped in a cavity, with, for example a condensed matter model of atoms bonded by chemical bonds in solids. First, the photon emitted by an emitter can propagate and be later reabsorbed by another emitter at a large distance. As such, the coupling of atoms via propagating photons can be long-ranged. The characteristic differences between

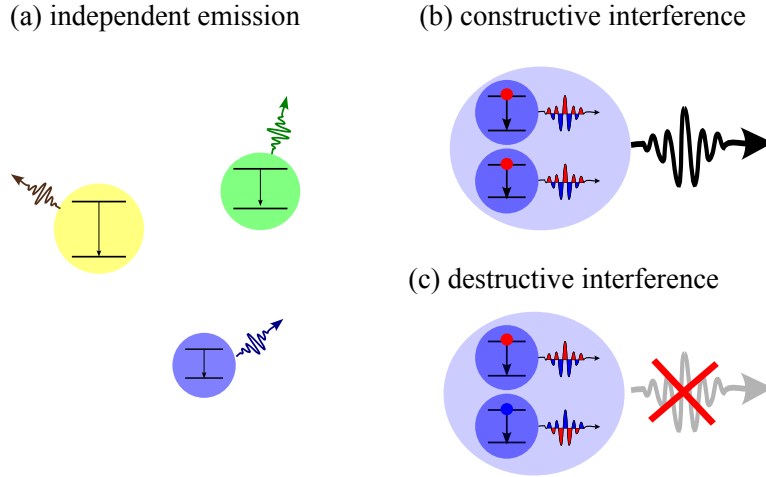


Figure 1.1: Schematics illustration of (a) independent emission of light from different emitters (b) constructive interference, enhancing rate and intensity of radiation from the two emitters, (c) destructive interference, suppressing rate and intensity of radiation.

coupled emitters can be easily on the order of microns, exceeding the length of chemical bonds by 5 orders of magnitude. Second, the emitted photon can just fly away without any reabsorption. As such, the photon-induced coupling in arrays of emitters is typically described by non-Hermitian coupling matrices, rather than usual Hermitian Hamiltonians in solids. Nowadays one often calls these matrices non-Hermitian Hamiltonians. They can be decomposed into two parts, the Hermitian one, responsive for the coupling between the emitters, and the anti-Hermitian one, responsible for the loss. The concept of non-Hermitian Hamiltonian is rather subtle and requires a lot of care, however, it is an important and useful idea that we will discuss in detail. Third, contrary to the most condensed matter setups, one usually studies not current response to the electric field, but optical response functions. For example, this can be the photon reflection spectrum, showing photon reflection probability depending on its frequency. The spectral positions of the resonances in the reflection spectra will provide energies of the excitations in the emitter array, and the linewidth of the resonances will provide their decay rate.

In this book, we will discuss all these features of collective light-matter interaction in detail. We will start by showing how the interaction depends on the spacing between the emitters, on the type of the photonic modes they interact with and on their number. The remaining chapters will be focused on the more quantum effects, such as Dicke phase transition and superradiant bursts.

Chapter 2

Overview of experimental systems

Let us now discuss several practical realizations of ordered arrays with multiple emitters that exhibit collective coupling to light. In order for collective coupling to be manifested, the emitters must share the same optical mode. Typically, in this book we will imply a waveguide quantum electrodynamics setup, where the photonic mode propagates in one spatial dimension along the waveguide and is trapped in the two remaining dimensions, perpendicular to the waveguide axis. Such an array is illustrated in Fig. 2.1. Later on, in Chapter 9, we will also consider emitters interacting with a photon mode that is trapped in a cavity in all three dimensions.

We start by defining the main parameters, characterizing the structure. The first important parameter is the characteristic emission frequency ω_0 is in resonance with photons. For an ideal two-level atom, this frequency is determined just by the difference between the energies of the ground and excited states. In practice, emitters can be far from the two-level atom approximation, but the characteristic resonance frequency can still be introduced. The second obvious parameter is the number of resonant emitters in the array N . Two more parameters are the photon emission rate and the emission directionality. In particular, it is important to distinguish between the coupling of the emitter to the resonant photonic mode and the coupling to all other modes. Suppose the emitter has been excited to a certain resonant level. After a certain time, the level will get de-excited, for example, by the spontaneous emission of a photon. However, the photon can be emitted both into the resonant waveguide mode (with the rate γ_{rm1D}) and into free space (with the rate γ). In the first case, the photon has a larger chance to propagate along the waveguide, and then to be reabsorbed by another emitter, and

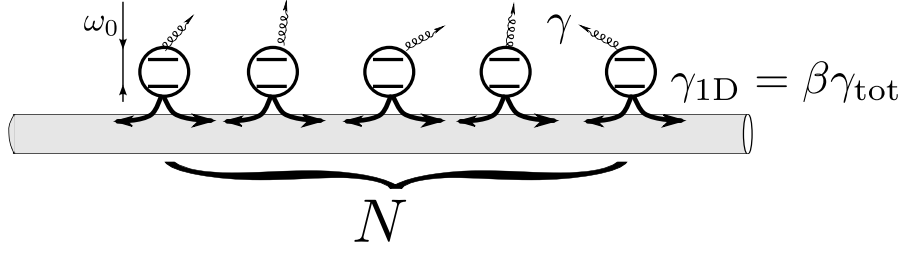


Figure 2.1: Schematics illustration of an array of N emitters, coupled to the waveguide photon mode

thus contribute to the collective coupling between the distant emitters. In the second case of free-space radiation, the chances that the photon will be reabsorbed by another emitter quickly decay with the distance between the emitters. From now on, we will make a strong simplifying assumption that the emission into the free-space mode with the rate γ does not contribute to the collective coupling: all emitted into free space photons are lost. This assumption will also allow us to incorporate all other decay and dephasing mechanisms of the emitter into the rate γ : since the free space photons are never reabsorbed, they can be just considered lost. This is a rather strong simplification. In realistic structures, the interaction via the free-space modes can also be important, and more details on that can be found in [1–3].

Under the stated assumptions, the main parameter, characterizing the efficiency of the emitter coupling to the waveguide photons, is the β -factor,

$$\beta = \frac{\gamma_{1D}}{\gamma_{1D} + \gamma} . \quad (2.1)$$

By definition, it is the fraction of the emission going into the waveguide mode and contributing to the collective coupling. The closer this factor is to unity, the stronger the interaction of the single emitter to the waveguide modes, and the stronger the collective coupling between the emitters will be manifested.

2.1 Practical implementations

Figure 2.2 compares resonant frequencies (a), coupling efficiencies β and typical numbers of emitters N (b). Table 2.1 presents the numerical values of these parameters for several representative systems. This compilation is not full and aims to demonstrate the variety of various structures rather than to list all possible systems. What is important, however, is that all the systems in Fig. 2.2 share a lot of basic physics that will be discussed later in the book.

In addition to giving the values of ω_0 , β , and N we also try to distinguish between the

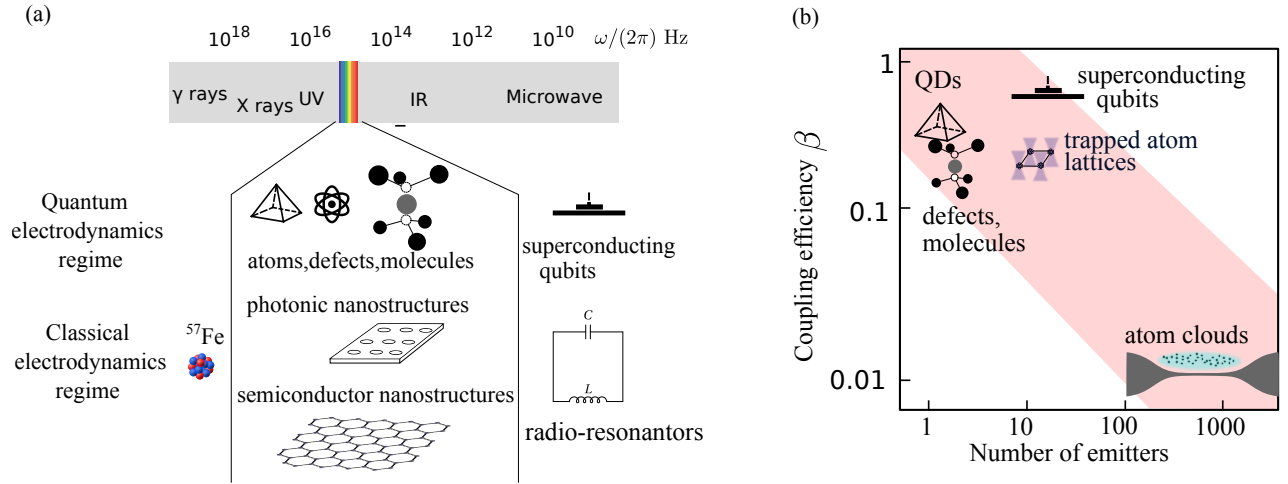


Figure 2.2: Comparison of various resonant structures with emitter arrays (a) spectral range and (b) coupling efficiency to the waveguide β vs number of emitters.

systems that are strongly sensitive to the quantum nature of light and the classical systems. The former, quantum ones, can be thought of as two-level atoms, that can host only one photon excitation. The latter, classical ones, can host many photon excitations at the same time. The quantum systems change their optical response after having absorbed a photon, since there is no room for a second one to be absorbed—which means that they exhibit strong optical nonlinearity at the level of an individual photon. In another words, they operate in the quantum nonlinear optics regime [4]. The latter, classical, structures have room for multiple photon excitations, and do not manifest such a strong optical nonlinearity. The two types of structures also call for different theoretical frameworks. The “quantum” structures in principle, require a quantum electrodynamical description when subjected to more than a single photon excitation. The classical structures can be, as expected, described by a usual classical electrodynamics, that is, Maxwell equations with resonant polarizabilities. It is important to note, that the word “quantum” is overloaded in physics literature and can imply different systems. Depending on the particular field of study, “quantum” can refer to the light and matter excitations, and it is usually not explicitly stated which ones are meant. For example, semiconductor quantum dots are true artificial atoms that can not host a lot of excitations at the same time and that operate in the quantum nonlinear optics regime. On the other hand, semiconductor quantum wells, where the electrons and holes are trapped only in one spatial dimension, are quantum in a sense of quantum confinement of electron and hole motion perpendicular to the well surface, but they do not exhibit a strong quantum nonlinear response. The reason is simple: electrons and holes can still freely propagate along the quantum well

2.1. PRACTICAL IMPLEMENTATIONS

Material system	Number of resonant emitters, N	Transition energy, $\hbar\omega_0$	radiative decay rate, $\gamma_{1D}/2\pi$	Coupling efficiency, β
quantum electrodynamics regime				
atom cloud + nanofiber	$1 \div 10^3$	1.5 eV	5.2 MHz	10^{-2}
Trapped atoms + waveguide	$1 \div 3$	1.4 eV	4.6 MHz	0.5
2D atomic array	$1 \div 2$	1.6 eV	~ 4 MHz	~ 0.5
Superconducting qubits	10	0.03 meV (7 GHz)	$10 \div 100$ MHz	0.999
Quantum dots	1	1.4 eV	0.2 GHz	0.99
Si vacancies in diamonds	2	1.7 eV	100 MHz	~ 0.5
Organic molecules	1	1.6 eV	30 MHz	0.2
classical electrodynamics regime				
Quantum well arrays	$1 \div 100$	1.5 eV	~ 25 MHz (0.1 meV)	$\sim 0.1 \div 0.5$
Plasmonic multilayers	$1 \div 10$	1.5 eV	0.2 eV	~ 0.5
Resonant dielectric metasurface	1	~ 2 eV	$10 \text{ neV} \div 0.2 \text{ eV}$	$\lesssim 1$
multilayered 2D materials	$1 \div 10$	1.6 eV	~ 0.25 THz (1 meV)	$\sim 0.1 \div 0.5$
Iron nuclei	$1 \div 100$	1.44×10^4 eV	0.1 MHz (1 neV)	~ 0.5

Table 2.1: Parameters of different state-of-the-art platforms waveguide quantum electrodynamics. The indicated numerical values are approximate and have been taken from Refs. [6], [7], [8], [9],[10], [11],[12],[13], [14],[15], [16],[17],[18] respectively. For iron nuclei the data scales as $\gamma_{1D} \sim 1/x^2$ where $x = \cos \theta$ is the incidence angle and is given for $x = 10^{-2}$.

surface, which means that there are a lot of degrees of freedom, so a lot of photons can be independently absorbed at the same time.

Importantly, when probed by a single photon, both quantum and classical structures share a lot of the same physics. Indeed, a single photon has no other photon to interact with, so the quantum nonlinearity, if any, is not manifested. In this regime, the quantum emitter arrays can even be described by the same Maxwell equations with resonant polarizabilities as the passive optical structures, for example, arrays of holes in dielectric slabs, or arrays of metallic nanoparticles, showing plasmonic resonances, or classical radiofrequency resonators.

There are also several other important distinctions between emitter platforms. First, the operating spectral range can be very different. The low-frequency side of the spectrum is occupied by the microwave structures, that is superconducting qubits and their classical counterparts, radio-frequency resonators. The type of superconducting qubits typically used in quantum optical setup are so-called transmon qubits [5]. In a nutshell, these can be thought of as electromagnetic resonant circuits with embedded Josephson junctions, that provide very strong anharmonicity of the energy spectrum. They can be made very coherent and are (almost) ideal two-level atoms, that operate in the microwave spectral range. The parameters of the qubits, such as resonant frequency, can be controlled externally. The disadvantage of the superconducting qubits is that they have to operate at very low temperatures, on the order of 10 mK. This is determined by the condition $k_B T \ll \hbar\omega_0$, the noise due to the background microwave radiation has to be freezed out.

The most high-frequency resonant emitters, where collective effects have been actively studied, that I am aware of, are arrays of nuclei, featuring γ -ray resonances with the photon energy in the order of 10 keV [19–21]. These are studied in crystals, where the nuclei are trapped in the lattice nodes, and do not move even when absorbing a highly energetic γ -quantum. As a result, the energy is not lost due to the recoil, as it would happen for an atom in free space. This is termed Mössbauer effect. As a result, the γ -rays exhibit sharp resonances. The system of resonant nuclei in crystals is probably the first one, where the resonant collective interaction of light with emitters has been studied experimentally. Naturally, most of the research has been focused on the optical frequency range, where one can study various natural and artificial atoms. The natural atoms are typically rubidium and cesium and the artificial atoms are semiconductor quantum dots. There also exist organic molecules as well as defects in crystals.

Figure 2.2(b) shows a tradeoff between the coupling efficiency and the number of emitters, see . Namely, one can either create arrays with just a few emitters, controllably strongly coupled to the waveguide mode, or one can compromise with the coupling efficiency per single emitter but increase the emitter number. For example, one can trap atoms in optical tweezers, and then move the trapped atoms close to the optical waveguide or organize them in a free-space lattice. At the moment, such studies are still limited to tens or hundreds of atoms. Another approach is to prepare a magneto-optical trap with a cloud of free atoms, where their positions are not fixed in space. The efficiency of coupling to the given photonic mode β will then be weaker. On the other hand, such cloud can include thousands and tens of thousands of atoms, so that the product βN will still be considerable.

We also note, that the setup of Fig. 2.1 does not necessarily require an optical waveguide. Its main property is that the emitters share a common propagating photonic mode. However, this can be realized in free space, provided that emitters do not scatter light to the side, see Fig. 2.3. How to realize such unidirectional scattering? One of the ways is to create an ordered two-dimensional periodic array of emitters, with the lattice spacing a smaller than the light wavelength λ , as shown in Fig. 2.3(b). In such case, the waves scattered sideways will interfere destructively and cancel each other. The array can scatter light only forward or backwards. The interaction of such an array with light is described by exactly the same equation as an interaction of individual emitter with the waveguide mode. We will consider such arrays in more detail in Sec. 4. They can be realized as lattices of trapped atoms [8] or arrays of plasmonic or dielectric nanoparticles. An ultimate case of such an atomic array is presented

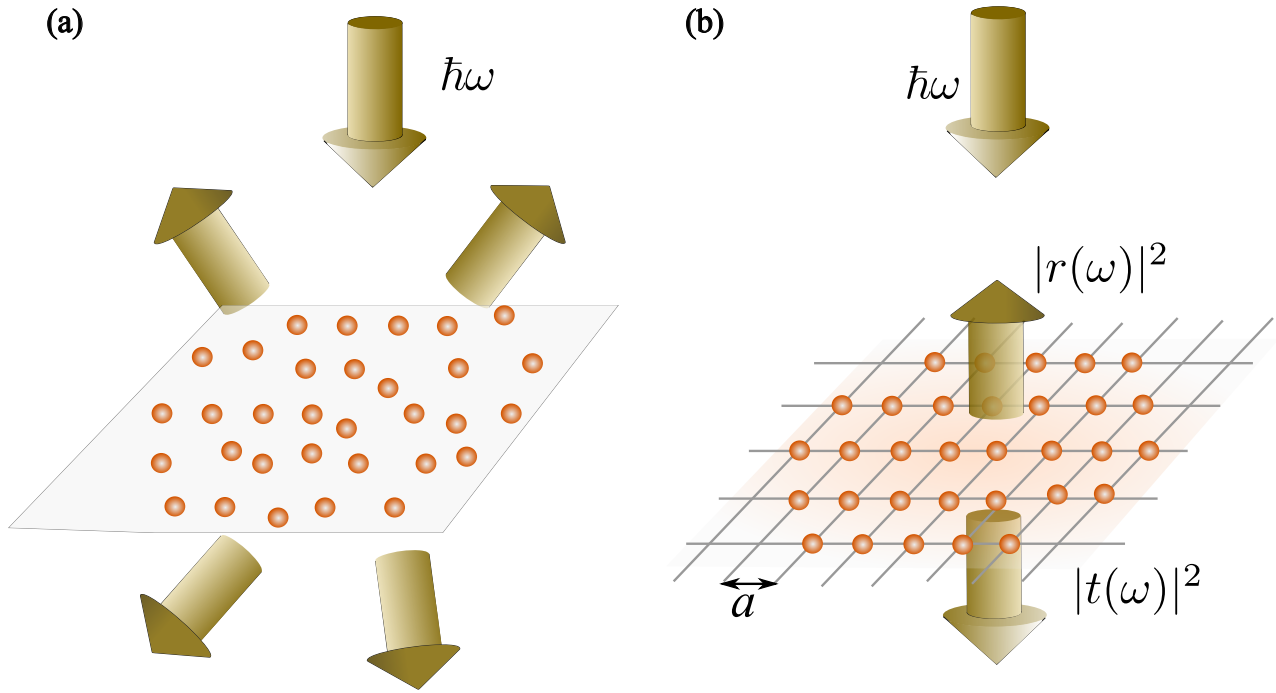


Figure 2.3: (a) nonperiodic array of atoms scatters light in all directions (b) periodic two-dimensional array scatters light only forward or backward

by a so-called two-dimensional quantum materials, such as MoS_2 . Those feature sharp optical resonances and can be stacked together [22]. One can also realize nuclei multilayers, resonantly scattering γ -rays [23].

2.2 Additional reading and references

Review on quantum well structures vs nuclei multilayers: A. Poddubny and E. Ivchenko, “Resonant diffraction of electromagnetic waves from solids (a review)”, [Phys. Solid State 55, 905–923 \(2013\)](#)

Review on waveguide QED: A. S. Sheremet et al., “Waveguide quantum electrodynamics: collective radiance and photon-photon correlations”, [Rev. Mod. Phys. 95, 015002 \(2023\)](#)

Introduction into superconducting qubits: P. Krantz et al., “A quantum engineer’s guide to superconducting qubits”, [Applied Physics Reviews 6, 021318 \(2019\)](#).

Bibliography

- ¹D. F. Kornovan, A. S. Sheremet, and M. I. Petrov, “Collective polaritonic modes in an array of two-level quantum emitters coupled to an optical nanofiber”, [Phys. Rev. B **94**, 245416 \(2016\)](#).
- ²A. Asenjo-Garcia, M. Moreno-Cardoner, A. Albrecht, H. J. Kimble, and D. E. Chang, “Exponential improvement in photon storage fidelities using subradiance and “selective radiance” in atomic arrays”, [Phys. Rev. X **7**, 031024 \(2017\)](#).
- ³M. B. M. Svendsen and B. Olmos, “Modified dipole-dipole interactions in the presence of a nanophotonic waveguide”, [Quantum **7**, 1091 \(2023\)](#).
- ⁴D. E. Chang, V. Vuletić, and M. D. Lukin, “Quantum nonlinear optics—photon by photon”, [Nature Photonics **8**, 685–694 \(2014\)](#).
- ⁵P. Krantz, M. Kjaergaard, F. Yan, T. P. Orlando, S. Gustavsson, and W. D. Oliver, “A quantum engineer’s guide to superconducting qubits”, [Applied Physics Reviews **6**, 021318 \(2019\)](#).
- ⁶N. V. Corzo, B. Gouraud, A. Chandra, A. Goban, A. S. Sheremet, D. V. Kupriyanov, and J. Laurat, “Large Bragg reflection from one-dimensional chains of trapped atoms near a nanoscale waveguide”, [Phys. Rev. Lett. **117**, 133603 \(2016\)](#).
- ⁷A. Goban, C.-L. Hung, J. Hood, S.-P. Yu, J. Muniz, O. Painter, and H. Kimble, “Superradiance for atoms trapped along a photonic crystal waveguide”, [Phys. Rev. Lett. **115**, 063601 \(2015\)](#).
- ⁸J. Rui, D. Wei, A. Rubio-Abadal, S. Hollerith, J. Zeiher, D. M. Stamper-Kurn, C. Gross, and I. Bloch, “A subradiant optical mirror formed by a single structured atomic layer”, [Nature **583**, 369–374 \(2020\)](#).
- ⁹M. Mirhosseini, E. Kim, X. Zhang, A. Sipahigil, P. B. Dieterle, A. J. Keller, A. Asenjo-Garcia, D. E. Chang, and O. Painter, “Cavity quantum electrodynamics with atom-like mirrors”, [Nature **569**, 692–697 \(2019\)](#).

- ¹⁰A. P. Foster, D. Hallett, I. V. Iorsh, S. J. Sheldon, M. R. Godsand, B. Royall, E. Clarke, I. A. Shelykh, A. M. Fox, M. S. Skolnick, I. E. Itskevich, and L. R. Wilson, “Tunable photon statistics exploiting the Fano effect in a waveguide”, [Phys. Rev. Lett. **122**, 173603 \(2019\)](#).
- ¹¹A. Sipahigil et al., “An integrated diamond nanophotonics platform for quantum-optical networks”, [Science **354**, 847–850 \(2016\)](#).
- ¹²S. Faez, P. Türschmann, H. R. Haakh, S. Göttinger, and V. Sandoghdar, “Coherent interaction of light and single molecules in a dielectric nanoguide”, [Phys. Rev. Lett. **113**, 213601 \(2014\)](#).
- ¹³B. Jusserand, A. N. Poddubny, A. V. Poshakinskiy, A. Fainstein, and A. Lemaitre, “Polariton resonances for ultrastrong coupling cavity optomechanics in GaAs/AlAs multiple quantum wells”, [Phys. Rev. Lett. **115**, 267402 \(2015\)](#).
- ¹⁴R. Taubert, D. Dregely, T. Stroucken, A. Christ, and H. Giessen, “Octave-wide photonic band gap in three-dimensional plasmonic Bragg structures and limitations of radiative coupling”, [Nat. Comm. **3**, 691 \(2012\)](#).
- ¹⁵C. W. Hsu, B. Zhen, J. Lee, S.-L. Chua, S. G. Johnson, J. D. Joannopoulos, and M. Soljačić, “Observation of trapped light within the radiation continuum”, [Nature **499**, 188–191 \(2013\)](#).
- ¹⁶H. H. Fang, B. Han, C. Robert, M. A. Semina, D. Lagarde, E. Courtade, T. Taniguchi, K. Watanabe, T. Amand, B. Urbaszek, M. M. Glazov, and X. Marie, “Control of the exciton radiative lifetime in van der Waals heterostructures”, [Phys. Rev. Lett. **123**, 067401 \(2019\)](#).
- ¹⁷A. K. Geim and I. V. Grigorieva, “Van der waals heterostructures”, [Nature **499**, 419–425 \(2013\)](#).
- ¹⁸A. I. Chumakov, G. V. Smirnov, A. Q. R. Baron, J. Arthur, D. E. Brown, S. L. Ruby, G. S. Brown, and N. N. Salashchenko, “Resonant diffraction of synchrotron radiation by a nuclear multilayer”, [Phys. Rev. Lett. **71**, 2489–2492 \(1993\)](#).
- ¹⁹J. Hannon and G. Trammell, “Coherent γ -ray optics”, [Hyperfine Interactions **123**, 127–274 \(1999\)](#).
- ²⁰Y. Kagan, “Theory of coherent phenomena and fundamentals in nuclear resonant scattering”, [Hyperfine Interactions **123**, 83–126 \(1999\)](#).
- ²¹J. Haber, X. Kong, C. Strohm, S. Willing, J. Gollwitzer, L. Bocklage, R. Ruffer, A. Pálffy, and R. Röhlberger, “Rabi oscillations of x-ray radiation between two nuclear ensembles”, [Nature Photonics **11**, 720–725 \(2017\)](#).

- ²²G. Wang, A. Chernikov, M. M. Glazov, T. F. Heinz, X. Marie, T. Amand, and B. Urbaszek, “Colloquium: Excitons in atomically thin transition metal dichalcogenides”, [Rev. Mod. Phys.](#) **90**, 021001 (2018).
- ²³J. Haber, K. S. Schulze, K. Schlage, R. Loetzsch, L. Bocklage, T. Gurieva, H. Bernhardt, H.-C. Wille, R. Ruffer, I. Uschmann, G. G. Paulus, and R. Röhlsberger, “Collective strong coupling of x-rays and nuclei in a nuclear optical lattice”, [Nature Photonics](#) **10**, 445–449 (2016).
- ²⁴A. Poddubny and E. Ivchenko, “Resonant diffraction of electromagnetic waves from solids (a review)”, [Phys. Solid State](#) **55**, 905–923 (2013).
- ²⁵A. S. Sheremet, M. I. Petrov, I. V. Iorsh, A. V. Poshakinskiy, and A. N. Poddubny, “Waveguide quantum electrodynamics: collective radiance and photon-photon correlations”, [Rev. Mod. Phys.](#) **95**, 015002 (2023).

Chapter 3

Scattering on a single emitter

In this chapter, we consider a most basic problem: interaction of propagating light at a certain frequency ω with the system, having a single optical resonance at the frequency ω_0 . The possible setup, corresponding to this model, is schematically illustrated in Fig. 3.1 — it consists of a waveguide, where photons propagate in one dimension either forward or backward, with the constant velocity c , coupled to a two-level atom. However, an actual physical realization can vary. It can involve different types of light emitters in place of the resonant system. For example, as described in the previous chapter, one can consider a plane electromagnetic wave normally incident upon a flat semiconductor quantum well. The equations describing light reflection in such a setup would be the same up to the change of notation.

Before proceeding to the actual calculation, it is important to think what can happen with incoming light wave at the frequency ω depending on the relation ω and the system resonance frequency ω_0 . If the light is strong from the resonance, we can expect no interaction. Indeed, due to the energy conservation law, the light can not be absorbed by the emitter. On the other hand, if ω and ω_0 are close, some interaction can take place. The photon can be absorbed, and after that, it can be reemitted back into the waveguide with some probability. As a result, there is a possibility that light can be reflected backward with a certain reflection coefficient r .

Our goal will be to calculate the value of this reflection r depending on the *spectral detuning* $\omega - \omega_0$. By doing this, we will also clarify what is large and what is strong detuning, that is, at which value of $|\omega - \omega_0|$ the reflection can be neglected. Moreover, we will also show that the properties of the system change when it can interact with propagating photons. In fact, our calculation, despite being mostly based on classical Maxwell equations, will allow us to

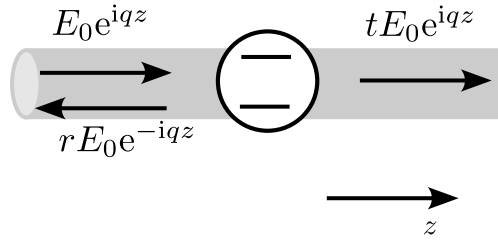


Figure 3.1: Schematics of light reflection and transmission from a resonant scatterer.

find the rate of *spontaneous emission* into the waveguide.

3.1 Brute-force approach

3.1.1 Wave equation

Let us consider a monochromatic electromagnetic wave at the frequency ω , propagating in one direction z at the frequency ω with the velocity c . It then satisfies the usual wave equation

$$\frac{d^2}{dz^2} E(z) + q^2 E(z) = 0, \quad (3.1)$$

where $q = \omega/c$ is the light wave vector. When writing Eq. (3.1) we do not write explicitly the dependence of the electromagnetic field E on two other spatial coordinates x, y . In the simplest description one can assume $\mathbf{E}(x, y, z) = E(z)\mathbf{f}(x, y)$, where $\mathbf{f}(x, y)$ describes the mode polarization and the spatial distribution in the transverse direction. We assume that those are not affected by the interaction with the emitter, so that transverse and longitudinal degrees of freedom can be separated and it suffices to consider just a single scalar equation (3.1). Now, in order to describe the light interaction with the emitter, we need to introduce external polarization $P(z)$ into the wave equation

$$\frac{d^2}{dz^2} E(z) + q^2 E(z) = -4\pi q^2 P(z). \quad (3.2)$$

Here, $P(z)$ is the electromagnetic polarization, induced in the waveguide material, due to the presence of the emitter. By definition, this polarization is in general nonzero within the emitter but quickly vanishes outside. We will now make the next approximation and assume that the emitter is small as compared to other spatial scales in the problem, namely, small as compared

to the light wavelength $\lambda = 2\pi/q$. Then, the polarization can be approximated by a δ -function

$$P(z) = p\delta(z) , \quad (3.3)$$

where we introduced the emitter dipole moment p and assumed that the emitter is placed at $z = 0$. The problem is still not quite well defined: we need to specify how to calculate the value of p . Here comes another approximation of the linear response. We say that the emitter dipole moment is nonzero only in the presence of the electric field, and that it is linearly proportional to this electric field, that is

$$p = \alpha E(0) , \quad (3.4)$$

where α is the *emitter polarizability* and $E(0)$ is the electromagnetic wave at the position of the emitter $z = 0$. The actual value of α depends on the microscopic properties of an emitter. For example, for an actual atom, it has to be calculated quantum-mechanically. Given α , the system of equations Eqs. (3.1)–(3.4) becomes complete and can be solved analytically.

3.1.2 Emitter polarizability

The goal of this book is to describe the general properties of resonant light-emitter interaction, without going into the microscopic details of the emitter. As such, we can make a following strong assumption about α : it is a complex function with a resonance at $\omega = \omega_0$,

$$\alpha(\omega) = \frac{a}{\omega_0 - \omega - i\gamma} . \quad (3.5)$$

where a and γ are two new real parameters. The parameter a characterizes the strength of the resonance. The γ characterizes the resonance damping because of some other mechanisms, unrelated to the resonant interaction with the photon mode in the waveguide. For example, such term can be related to the spontaneous emission of photons in another optical modes, or it can phenomenologically describe the dephasing because of the interaction with the modes in the environment of the emitter. The perfect emitter corresponds to the limit $\gamma \rightarrow +0$. In the simplest quantum mechanical description of a two-level atom, ω_0 corresponds to the energy difference between the levels $|1\rangle$ and $|2\rangle$, $\omega_0 = E_2 - E_1$, and $a = d^2/\hbar$, where d is the matrix element of the atom dipole moment in the direction along the electric field polarization $\boldsymbol{\sigma}$, $d^2 = e^2 |\langle 1 | (\boldsymbol{\sigma} \cdot \mathbf{r}) | 2 \rangle|^2$, and e is the electron charge. However, these details depend on the particular type of the emitter and will not be important for the following consideration.

We note, that Eq. (3.5) is valid only in the vicinity of the resonance, for ω close to ω_0 . For large detuning it is necessary to add at least one more *counter-rotating* term,

$$\alpha(\omega) = \frac{a}{\omega_0 - \omega - i\gamma} + \frac{a}{\omega_0 + \omega + i\gamma}, \quad (3.6)$$

that is maximal at $\omega = -\omega_0 - i\gamma$. However, we will neglect this term from now on, since we assume $|\omega - \omega_0| \ll \omega, \omega_0$. As an exercise, you can check that Eq. (3.6) satisfies the general Kramers-Kronig relationships for the permittivity.

Solving the wave equation

We are now in position to find light reflection coefficient r and transmission coefficient z . Let assume that an electromagnetic wave with the amplitude E_0 is incident from the left and is scattered on the emitter. Everywhere for $z \neq 0$ the right-hand side of Eq. (3.2) is absent and the solution can be presented as a superposition of right- and left-going plane waves $\exp[\pm i q z]$. This means that

$$E(z) = \begin{cases} E_0(e^{iqz} + r e^{-iqz}), & z < 0 \\ E_0 t e^{iqz}, & z > 0, \end{cases} \quad (3.7)$$

were, r and t are the light reflection and transmission coefficients. In order to find the values of r and t we need to apply the boundary conditions at the emitter position $z = 0$.

The first of these boundary conditons is the continuity of the electric field, $E(-0) = E(+0)$, that yields

$$1 + r = t. \quad (3.8)$$

The second of the boundary conditions is obtained by integrating Eq. (3.2) for z from $-\delta z$ to δz around the point $z = 0$ and then setting δz to 0. Since the right-hand side of Eq. (3.2) contains a δ -function, it will not be zero even for $\delta z = 0$. The result yields

$$\left. \frac{dE}{dz} \right|_{z=+0} - \left. \frac{dE}{dz} \right|_{z=-0} = -4\pi q^2 p \quad (3.9)$$

which means that

$$iq(t + r - 1) = -\frac{4\pi q^2 a}{\omega_0 - \omega - i\gamma}(1 + r). \quad (3.10)$$

Substituting $t = 1 + r$, we find

$$ir = -\frac{2\pi qa}{\omega_0 - \omega - i\gamma}(1 + r) \quad (3.11)$$

which results in

$$r(\omega) = \frac{i\gamma_{1D}}{\omega_0 - \omega - i(\gamma_{1D} + \gamma)}, t(\omega) = \frac{\omega_0 - \omega - i\gamma}{\omega_0 - \omega - i(\gamma_{1D} + \gamma)}. \quad (3.12)$$

with

$$\gamma_{1D} = 2\pi qa. \quad (3.13)$$

The total probability that the photon will be reflected or transmitted is given by $|r(\omega)|^2$ and $|t(\omega)|^2$, respectively. We note, that this probabilities do not in general sum up to unity:

$$|r|^2 + |t|^2 = 1 - A, \quad A = \frac{2\gamma\gamma_{1D}}{(\omega - \omega_0)^2 + (\gamma + \gamma_{1D})^2}. \quad (3.14)$$

Only for $\gamma = 0$ one has $|r|^2 + |t|^2 = 1$, which is the photon flux conservation law. In general, photon can be lost with a probability A . This allows us to better understand the physical sense of the parameter γ : it describes nonradiative losses in the emitter and emission into other photonic modes rather than into the waveguide. Reflection, transmission and absorption spectra $|r(\omega)|^2$, $|t(\omega)|^2$ and $A(\omega)$ are plotted in Fig. 3.2(a).

As expected, away from the resonance one has $r(\omega) \rightarrow 0$ and $t(\omega) \rightarrow 1$, that is, the system is transparent. At the perfect resonance condition, when $\omega = \omega_0$ and additionally $\gamma = 0$, the probability that photon is transmitted is zero, $t = 0$. At the same time, $r = -1$, that is, the photon will be reflected with 100 % probability and with a π -phase shift. This can be also seen from Fig. 3.2(b), showing real and imaginary parts of r versus ω : for $\gamma/\gamma_{1D} = 0.1$ the real part almost reaches minus unity at the resonance. The π phase shift originates from the processes of absorption and reemission by the atom.

In order to understand the physical meaning of the parameter γ_{1D} it is instructive to compare Eq. (3.12) with our starting Eq. (3.5). The original equation had a resonance at $\omega = \omega_0 - i\gamma$, and we now know γ is some damping parameter of the system (see also Appendix A). We will call it the internal decay rate. The reflection coefficient, obtained taking into account the

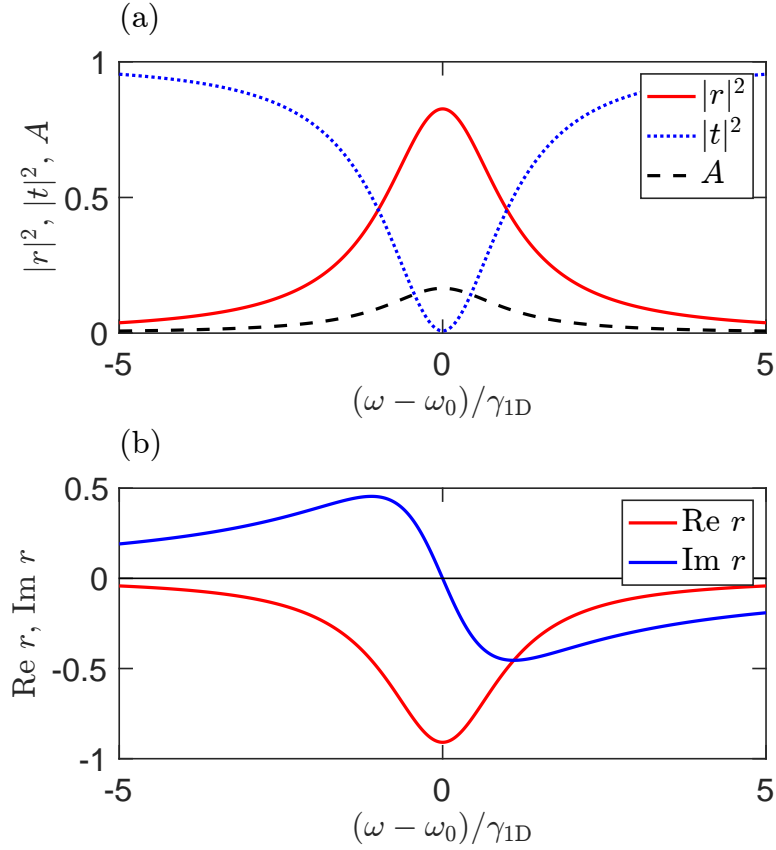


Figure 3.2: (a) Reflection, transmission and absorption spectra for a single resonant emitter. (b) Real and imaginary parts of the reflection spectrum. Calculation has been performed following Eqs. (3.12) for $\gamma/\gamma_{1D} = 0.1$.

system interaction with light, has a resonance at

$$\omega = \omega_0 - i\gamma - i\gamma_{1D} . \quad (3.15)$$

As such, γ_{1D} can be interpreted as an extra damping rate the emitter acquires due to the interaction with the waveguide photons. It turns out to be the rate of spontaneous radiative decay rate of the emitter into the waveguide. We note, that the expression Eq. (3.13) has been obtained by using an entirely classical electromagnetic calculation. The only quantumness will be encoded in the resonance strength a .

In another word, equation (3.15) can be sought as the complex resonant frequency of the emitter, renormalized by its interaction with the propagating photons. We note, that in fact γ_{1D} can depend on ω , via the factor $q = \omega/c$ in Eq. (3.13). The parameter a itself can be ω -dependent itself. However, since we are dealing with spectrally narrow resonances, one can

usually neglect this dependence and assume that

$$\gamma_{1D}(\omega) \approx \gamma(\omega_0) = 2\pi\omega_0 a(\omega_0)/c. \quad (3.16)$$

This corresponds to the so-called Markovian approximation. It is usually valid when the parameters of the medium surrounding the resonant system slowly vary with frequency on the scale of the resonance linewidth. In the following chapters, we will also consider the situations in which the emitter is strongly coupled to the cavity mode when the Markovian approximation can break down.

3.2 Green function approach

We will now find the same answer in a bit more general way, using the Green function for the Helmholtz equation, We will now use the Green function of the Helmholtz equation,

$$\frac{d^2 G(z, z')}{dz^2} + q^2 G(z, z') = -4\pi q^2 \delta(z - z'), G(z, z') = 2\pi i q e^{iq|z-z'|}, \quad (3.17)$$

that is derived in Appendix B. Using this Green function, the solution of Eq. (3.2) can be presented as

$$E(z) = E_0 e^{iqz} - 4\pi q^2 \int dz' G(z, z') P(z') = E_0 e^{iqz} - 4\pi q^2 \int dz' G(z, z') p \delta(z - z') \quad (3.18)$$

which results in

$$E(z) = E_0 e^{iqz} + 2\pi i q p e^{iq|z|} \quad (3.19)$$

where the first term in the left-hand side presents the incident wave and the second term is the wave scattered by the emitter. Given Eq. (3.4) and Eq. (3.5) we write

$$(\omega_0 - i\gamma - \omega)p = aE(0). \quad (3.20)$$

Since $E(0) = E_0 + 2\pi i q p$, we find

$$(\omega_0 - i\gamma - i\gamma_{1D} - \omega)p = aE_0, \quad (3.21)$$

3.2. GREEN FUNCTION APPROACH

where γ_{1D} is the same γ_{1D} as in Eq. (3.13). This equation allows us to find p and after substituting the result into Eq. (3.19) we obtain an electric field

$$E(z) = E_0(e^{iqz} + re^{iq|z|}), \quad r = \frac{i\gamma_{1D}}{\omega_0 - \omega - i(\gamma + \gamma_{1D})}, \quad p = \frac{aE(0)}{\omega_0 - \omega - i(\gamma + \gamma_{1D})}. \quad (3.22)$$

The answer is exactly equivalent to the one obtained in the previous section. In particular, Eq. (3.21) can be seen as the equation of motion for the emitter under the influence of the driving with the electric field E_0 . The complex frequency $\omega_0 - i\gamma - i\gamma_{1D}$, entering Eq. (3.21), is the same as (3.15) and it can be seen as the emitter resonance frequency renormalized by the interaction with light.

The advantage of our derivation using the Green function over the derivation in the previous section is that it is much more general. First, we can apply it for emitters interacting with a more complex electromagnetic environment, not just with photons in a waveguide with linear dispersion. In this case we would just need to know the Green function $G(z, z')$, solving for the electromagnetic field in the point z induced by the point dipole z' . Similarly as in this chapter, such Green function can be calculated independently beforehand and does not depend on the properties of the emitters themselves. Equation Eq. (3.21) will then become

$$[\omega_0 - i\gamma - G(0, 0) - \omega]p = aE_0, \quad (3.23)$$

where $G(0, 0)$ is the field in the origin. Second, Eq. (3.21) can be generalized for an array of N emitters with dipole moments p_m , resonance frequencies $\omega_0^{(m)}$, internal decay rates $\gamma^{(m)}$ and resonance strengths z_m . It will then become a linear system of equations

$$[\omega_0^{(m)} - i\gamma^{(m)} - \omega]p_m - \sum_{n=1}^N G(z_m, z_n)p_n = a_m E_0(z_m). \quad (3.24)$$

If we introduce the matrix $H_{mn} = \delta_{mn}(\omega_0^{(m)} - i\gamma^{(m)} - \omega) - G(z_m, z_n)$, we can rewrite Eq. (3.24) as

$$\sum_{n=1}^N H_{mn}p_n - \omega p_m = a_m E_0(z_m). \quad (3.25)$$

The matrix H_{mn} is a generalization of the complex eigenfrequency Eq. (3.15) to the emitter array. We will extensively study its properties in the following chapters, and we will show that it

can be interpreted as an effective Hamiltonian of the array, interacting with the electromagnetic environment. It is also relatively straightforward to further generalize this equation to a full 3D problem and to include the vector polarization degree of freedom of the emitters.

3.3 Summary

To summarize, in this chapter we have calculated the reflection, transmission and absorption coefficients for light, scattering on a single emitter. We have also calculated the spontaneous decay rate of an emitter into the waveguide modes. This was done in two ways: (a) by directly solving the wave equations with the resonant emitter polarizability and (b) by using the Green function approach. The latter one can be readily generalized for a more complex setting, including $N > 1$ emitters. Such a system will be considered in the next chapter.

3.4 Additional reading

Kramers-Kronig relationships and analytical properties of susceptibility: L. Landau and E. Lifshits, *Statistical physics*, Course of theoretical physics pt. 1 (Butterworth-Heinemann, 1980), SS123.

Light reflection from a quantum well: F. Tassone et al., “Quantum-well reflectivity and exciton-polariton dispersion”, [Phys. Rev. B **45**, 6023–6030 \(1992\)](#)

Light reflection from a cavity coupled to the waveguide: M. F. Yanik et al., “Stopping Light in a Waveguide with an All-Optical Analog of Electromagnetically Induced Transparency”, [Phys. Rev. Lett. **93**, 233903 \(2004\)](#)

Light reflection from an atom: A. Asenjo-Garcia et al., “Exponential improvement in photon storage fidelities using subradiance and “selective radiance” in atomic arrays”, [Phys. Rev. X **7**, 031024 \(2017\)](#)

Chapter 4

Two-dimensional arrays

In the previous chapter we have derived light reflection and transmission coefficients for a single emitter, coupled to the waveguide (3.12). In this section, we will demonstrate that similar equations can be applied for a light incident upon a square periodic array of emitters with the spacing smaller than the light wavelength. Such correspondence is valid when light diffraction is not possible, that is, when the array is periodic with the period $a < \lambda$, see Fig. 2.3. The main difference between the two-dimensional and one-dimensional cases will be the resulting expression for γ_{1D} , that will depend both on the linewidth of the individual emitter and on the lattice spacing. Also, the resonant frequency of the emitter array will be shifted from the resonance frequency of the individual emitter ω_0 .

The problem of light reflection on a planar array of scatterers is well-known in classical optics [1–3], as we have already mentioned in Chapter 2. The results in the next section apply both to natural atoms and to artificial “atoms”, such as metallic nanoparticles with plasmonic resonances [4], dielectric and semiconductor particles, e.g. made of silicon, that have the Mie optical resonances [5, 6]. The main difference of the setup based on natural atoms is the strong nonlinearity: they can change their optical response for a second photon already after absorbing a first one [7]. However, if only a single photon reflection is considered, we can still use the same equations.

4.1 Reflection calculation

We will now calculate the reflection coefficient for the light incident on a periodic array of atoms located in the points \mathbf{r}_j , forming a square lattice. We will use the discrete dipole approximation

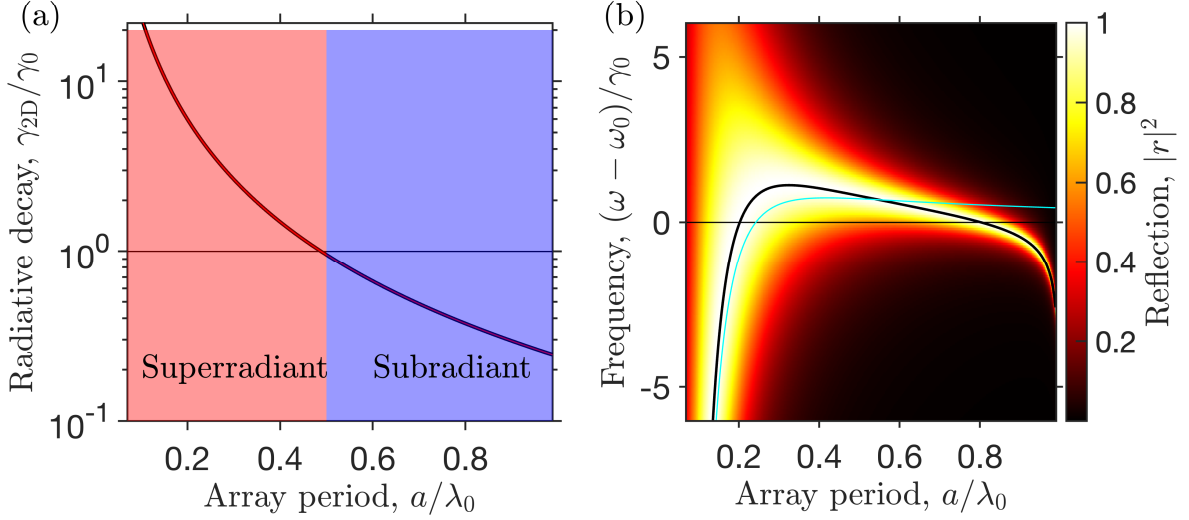


Figure 4.1: (a) Dependence of the collective radiative decay rate γ_{2D} Eq. (4.8) on the ratio of the square lattice period a to the light wavelength at the atomic resonance λ_0 . (b) Color map shows the light reflection spectra depending on the ratio a/λ_0 . Thick black line shows the collective resonance frequency $\tilde{\omega}_0$ Eq. (4.8), solid cyan line shows the analytical answer found using Eq. (4.9).

[8], that generalizes Eq. (3.24) from a scalar case to the full vector case case:

$$\mathbf{p}_j = \alpha \left[\mathbf{E}_0(\mathbf{r}_j) + \sum_{j' \neq j} G(\mathbf{r}_{j'} - \mathbf{r}_j) \mathbf{p}_{j'} \right], \quad (4.1)$$

Here, \mathbf{p}_j is the electric dipole moment of the atom number j ,

$$\alpha = \frac{3ic^3}{2\omega_0^3} \frac{\gamma_0}{\omega_0 - \omega - i(\gamma_0 + \gamma)} \quad (4.2)$$

is the single atom polarizability, characterized by the resonance frequency ω_0 , radiative decay rate γ_0 and nonradiative decay rate γ , \mathbf{E}_0 is the electric field of the incident wave and

$$G_{\mu\nu}(\mathbf{r}, \omega) = \left(\delta_{\mu\nu} + \left(\frac{c}{\omega} \right)^2 \frac{\partial^2}{\partial x_\mu \partial x_\nu} \right) \frac{e^{i\omega r/c}}{4\pi r} \quad (4.3)$$

is the electromagnetic tensor of the Green's function at the frequency ω satisfying the equation $\text{rot rot } G = (\omega/c)^2 G + \delta(\mathbf{r})$. The details on the Green function derivation are given in Appendix C and the resonant polarizability Eq. (4.2) is derived in Appendix D.

The first term in Eq. (4.1) describes the polarizability of the atom by the incident wave and the second term accounts for the sum of electric fields emitted by all other atoms. We consider for simplicity the case when light is incident in the normal direction, so that $\mathbf{E}_0(\mathbf{r}_j) \equiv \mathbf{E}_0$. Due

to translation symmetry, we then have $\mathbf{p}_j = \mathbf{p}$. In this case Eq. (4.1) is readily solved yielding

$$\mathbf{p} = \tilde{\alpha} \mathbf{E}_0, \quad \tilde{\alpha} = \frac{\alpha}{1 - C\alpha} \quad (4.4)$$

where

$$C = 4\pi \left(\frac{\omega}{c} \right)^2 \sum_{\mathbf{r} \neq 0} G_{xx}(\mathbf{r}) \quad (4.5)$$

is the so-called interaction constant describing light-induced coupling between the given atom and all the other atoms in the array. Hence, the coefficient $\tilde{\alpha}$ in Eq. (4.4) is the polarizability, renormalized by collective coupling between the atoms. The amplitude light reflection and transmission coefficients from the array r and t can be found by summing the field emitted from all the dipoles in the normal direction. The results read [9, 10]

$$r = \frac{2\pi i \omega}{ca^2} \tilde{\alpha}, \quad t = 1 + r. \quad (4.6)$$

We consider the array with $a < \lambda$, when all the diffracted waves are evanescent. In this case, the reflection and transmission coefficients reduce to

$$r = \frac{i\gamma_{2D}}{\tilde{\omega}_0 - \omega - i(\gamma + \gamma_{2D})}, \quad t = \frac{\tilde{\omega}_0 - \omega - i\gamma}{\tilde{\omega}_0 - \omega - i(\gamma + \gamma_{2D})} \quad (4.7)$$

that reminds reflection and transmission coefficients Eq. (3.12) of just one atom, coupled to a waveguide. Here, γ_{2D} is the collective radiative decay rate of the atomic array and $\tilde{\omega}_0$ is the resonance frequency modified by the collective coupling with light (that can be viewed as cooperative Lamb shift), given by

$$\tilde{\omega}_0 = \omega_0 - \frac{3\gamma_0\lambda_0^3}{16\pi^3} \text{Re } C, \quad \gamma_{2D} = \gamma_0 + \frac{3\gamma_0\lambda_0^3}{16\pi^3} \text{Im } C. \quad (4.8)$$

The explicit expression for C and the derivation details are presented in Appendix E. In the limit when the spacing between the atoms is much smaller than the light wavelength, one can show that

$$C \approx \frac{2\pi i \omega}{ca^2} + \frac{S + (\omega/c)^2 S'}{2}, \quad (4.9)$$

where $S \approx 9.03/a^3$ and $S' \approx -3.90/a$. Substituting Eq. (4.9) into Eq. (4.8) we find that [11,

12]

$$\gamma_{2D} = \gamma_0 \frac{3\lambda^2}{4\pi a^2} . \quad (4.10)$$

Hence, the decay rate of the two-dimensional array exhibits cooperative enhancement with the factor of the order of number of atoms per wavelength square: the denser the array the larger its cooperative decay rate. Figure 4.1(a) presents the dependence of the collective radiative decay rate γ_{2D} on the ratio of the array period to the light wavelength a/λ_0 . For a small period, the array exhibits a superradiant behavior, $\gamma_{2D} > \gamma_0$. The radiative linewidth quickly decays with the growth of lattice spacing and for $a/\lambda_0 > \sqrt{3/(4\pi)} \approx 0.5$ the structure becomes a subradiant one, $\gamma_{2D} < \gamma_0$. This enhancement of the collective radiative decay rate has been observed experimentally for the quantum wire arrays [12] and quantum dot arrays [2], but detailed studies of collective light-matter coupling were prevented by the strong inhomogeneous broadening. Much more experimental progress has been made for metamaterials and, recently, optical lattices of cold atoms, each individually trapped by a tweezer [13].

Figure 4.1(b) shows the light reflection spectrum depending on the array period. The spectrum exhibits a resonance at the frequency $\tilde{\omega}_0$. The resonance position is shifted from the original resonant frequency ω_0 due to the collective coupling. This shift can turn to zero at $a/\lambda_0 \approx 0.2$ and $a/\lambda_0 \approx 0.8$. The first zero is reproduced also by a semianalytical expression Eq. (4.9), as can be seen from a cyan curve in In this case the peak value of the reflection coefficient is reached at the bare atomic resonance, $\omega = \omega_0$. The possibility of high reflection from the ordered atomic array is a striking result of the collective coupling. In practice, more than 90% reflection can be achieved already for a 10×10 atomic lattice.

4.2 Additional reading

Light reflection of a square array of emitters: E. L. Ivchenko and A. V. Kavokin, “Light Reflection from Quantum Well, Quantum Wire and Quantum Dot Structures”, *Sov.Phys.Solid State* **34**, 968–971 (1992), E. Shahmoon et al., “Cooperative resonances in light scattering from two-dimensional atomic arrays”, *Phys. Rev. Lett.* **118**, 113601 (2017)

Consideration of multiple layers of emitters: E. L. Ivchenko et al., “Exciton Polaritons in Quantum-Dot Photonic Crystals”, *Phys. Solid State* **42**, 1756–1765 (2000).

References

- ¹P. de Vries, D. V. van Coevorden, and A. Lagendijk, “Point scatterers for classical waves”, *Rev. Mod. Phys.* **70**, 447–466 (1998).
- ²G. Khitrova and H. M. Gibbs, “Quantum dots: Collective radiance”, *Nat. Phys.* **3**, 84–86 (2007).
- ³N. A. Gippius and S. G. Tikhodeev, “Application of the scattering matrix method for calculating the optical properties of metamaterials”, *Physics-Uspekhi* **52**, 967–971 (2009).
- ⁴M. Decker, N. Feth, C. M. Soukoulis, S. Linden, and M. Wegener, “Retarded long-range interaction in split-ring-resonator square arrays”, *Phys. Rev. B* **84**, 085416 (2011).
- ⁵A. I. Kuznetsov, A. E. Miroshnichenko, M. L. Brongersma, Y. S. Kivshar, and B. Luk’yanchuk, “Optically resonant dielectric nanostructures”, *Science* **354**, 2472 (2016).
- ⁶Y. Kivshar, “All-dielectric meta-optics and non-linear nanophotonics”, *National Science Review* **5**, 144–158 (2018).
- ⁷K. Srakaew, P. Weckesser, S. Hollerith, D. Wei, D. Adler, I. Bloch, and J. Zeiher, “A subwavelength atomic array switched by a single Rydberg atom”, *Nature Physics*, [10.1038/s41567-023-01959-y](https://doi.org/10.1038/s41567-023-01959-y) (2023).
- ⁸B. T. Draine and P. J. Flatau, “Discrete-dipole approximation for scattering calculations”, *J. Opt. Soc. Am. A* **11**, 1491–1499 (1994).
- ⁹E. L. Ivchenko, Y. Fu, and M. Willander, “Exciton Polaritons in Quantum-Dot Photonic Crystals”, *Phys. Solid State* **42**, 1756–1765 (2000).
- ¹⁰I. A. Yugova, M. M. Glazov, E. L. Ivchenko, and A. L. Efros, “Pump-probe Faraday rotation and ellipticity in an ensemble of singly charged quantum dots”, *Phys. Rev. B* **80**, 104436 (2009).

- ¹¹E. L. Ivchenko and A. V. Kavokin, “Light Reflection from Quantum Well, Quantum Wire and Quantum Dot Structures”, *Sov.Phys.Solid State* **34**, 968–971 (1992).
- ¹²E. Ivchenko, A. Kavokin, V. Kochereshko, P. Kop’ev, and N. Ledentsov, “Exciton resonance reflection from quantum well, quantum wire and quantum dot structures”, *Superlattices and Microstructures* **12**, 317–320 (1992).
- ¹³J. Rui, D. Wei, A. Rubio-Abadal, S. Hollerith, J. Zeiher, D. M. Stamper-Kurn, C. Gross, and I. Bloch, “A subradiant optical mirror formed by a single structured atomic layer”, *Nature* **583**, 369–374 (2020).
- ¹⁴E. Shahmoon, D. S. Wild, M. D. Lukin, and S. F. Yelin, “Cooperative resonances in light scattering from two-dimensional atomic arrays”, *Phys. Rev. Lett.* **118**, 113601 (2017).

Chapter 5

Scattering on two emitters

We will now proceed to the next chapter, where we will consider light interaction with $N = 2$ resonant emitters. The fundamental questions to be answered in this chapter are as follows: How should the multiple-emitter system be treated? Will the interaction be stronger or weaker than for a single emitter? What will be the spontaneous decay rate of the emitters? Let us start with the illustrative case of $N = 2$ emitters, located at the points $z_1 = 0$ and $z_2 = d$. This problem is already rich enough to illustrate a lot of basic physics.

Let us first assume that the emitters are characterized by the resonant frequencies $\omega_0^{(1,2)}$, radiative decay rates $\gamma_{\text{ID}}^{(1,2)}$, and internal decay rates $\gamma^{(1,2)}$ that all can in general be different. How should we proceed to evaluate, say, light reflection coefficient from both emitters r_{tot} ? Based on the results in the previous chapter, we could start to decompose electric field between the emitters into plane waves, similar to Eq. (3.7). However, this will be more involved since we would now have to include 3 regions: the leftmost of the first emitter, $z < 0$, between the emitters, $0 < z < d$, and to the right of the second emitter, $z > d$. The electric field will be characterized by four complex amplitudes in total. This amplitude is to be determined by the two boundary conditions at each of the emitter positions. Such a procedure is quite tractable for a computer but rather cumbersome, especially if one has $N > 2$ emitters. It is rarely used in practice. We will now present two alternative ways to find the same answer, which are more compact and easier to generalize for larger N .

5.1 Multiple scattering approach

Following Eqs. (3.12) we can introduce reflection and transmission coefficients $r_{1,2}$, $t_{1,2}$ for each emitter. Then we calculate the reflection coefficient can be calculated as sum of multiple scattering processes as below illustrated Here, three terms correspond to light having bounced


$$r_{\text{tot}} = r_1 + t_1^2 r_1 e^{2i\varphi} + t_1^2 r_1 r_2 e^{2i\varphi} + \dots$$


Figure 5.1: Illustration of the geometric series to calculate light reflection coefficient from the two emitters.

zero, once and twice between the emitters, respectively, before being reflected back. At each roundtrip, the reflection amplitude gets a factor $r_1 r_2 \exp(2i\varphi)$ where $\varphi = \omega d/c$ is the light phase while propagating between the two emitters. As a result, we obtain a geometric series, that can be summed analytically:

$$r_{\text{tot}} = r_1 + \frac{t_1^2 r_2 e^{2i\varphi}}{1 - r_1 r_2 e^{2i\varphi}}. \quad (5.1)$$

In a similar fashion one can also obtain a transmission coefficient through both emitters

$$t_{\text{tot}} = \frac{t_1 t_2 e^{i\varphi}}{1 - r_1 r_2 e^{2i\varphi}}. \quad (5.2)$$

Interestingly, the reflection coefficient Eq. (5.1) is not symmetric with respect to first and second emitter, while the transmission coefficient Eq. (5.2) is symmetric. This is not a coincidence but a result of a general principle of *time-reversal invariance*, also related to *Lorentz reciprocity*. This principle, when applied to our one-dimensional setup, states that while reflection coefficients for light incident from the left and from the right of the structure can be different, the amplitude transmission coefficients from the left to the right and from the right to the left are the same. Swapping the two emitters is equivalent to swapping the direction the light is incident from. Such symmetry holds in the linear optics regime unless an external magnetic field is applied.

The multiple scattering procedure can be, in principle, readily generalized for an arbitrary number of emitters, but it is still slightly inconvenient. Thus, we will consider two more approaches later in this chapter.

Figure 5.2 shows the reflection spectra dependence on the distance between the emitters,

encoded by the phase $\varphi = \omega_0 d/c$. It is clear that the distance matters much. For $\varphi = 0, \pi, 2\pi$, corresponding to $d = 0, \lambda_0/2, \lambda_0$ (λ_0 is the light wavelength at the emitter resonance frequency), the spectrum has a single Lorentzian peak. The half-width at half-maximum for this peak is equal to $2\gamma_{1D}$, twice larger than for a single emitter; compare Fig. 3.2(a) and Fig. 5.2(a). For intermediate values of $0 < \varphi < \pi$ the peak is in general asymmetric. The value of $\varphi = \pi/2$ corresponds to a single symmetric peak with significantly lower spectral width than for $\varphi = 0, \pi$. This overall behavior can be understood from a basic argument of constructive and destructive interference for light exhibiting multiple scattering events; see Fig. 5.1. For φ being an integer number of π , all the waves going from emitter 1 to emitter 2 and back interfere constructively with each other. Hence, the overall reflection is enhanced as compared to that for one emitter. This is the essence of the collective enhancement effect. For $\varphi = \pi/2$, the interference is destructive, and the reflection is suppressed.

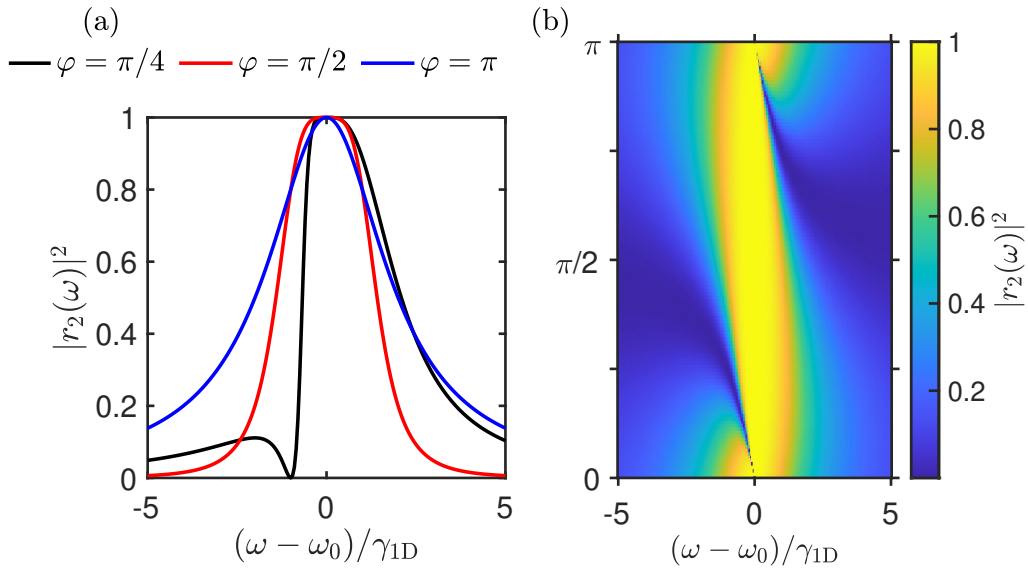


Figure 5.2: Reflection spectra for three specific values of $\varphi = \omega_0 d/c$ and the dependence of the reflection spectra on φ . Calculation has been performed for $\gamma = 0$ and identical emitters.

There are also sharp, narrow dips in the reflection spectrum when φ is close to 0 or π , but not exactly equal. To understand them better, in the next chapter we will develop a more involved technique of eigenmode decomposition for the reflection and transmission coefficients.

5.2 Non-Hermitian Hamiltonian method

We will now present in detail the Non-Hermitian Hamiltonian method that was already briefly mentioned in the previous chapter. To this end, we generalize Eqs. (3.2)–(3.4) for our system:

$$\frac{d^2}{dz^2}E(z) + q^2 E(z) = -4\pi q^2 \sum_{n=1}^N \delta(z - z_n) p_n, \quad (5.3)$$

where

$$p_n = \frac{a^{(n)}}{\omega_0^{(n)} - \omega - i\gamma^{(n)}} E(z_n) \quad (5.4)$$

are the corresponding dipole moments. Similarly to Eq. (3.18) we find

$$E(z) = E_0 e^{iqz} + \sum_{n=1}^N G(z, z_n) p_n, \quad (5.5)$$

Substituting Eq. (5.5) into Eq. (5.4) we obtain

$$\sum_{n=1}^N H_{mn} p_n - \omega p_m = a_m E_0 e^{iqz_m}. \quad (5.6)$$

with

$$\begin{aligned} H_{mn} &= (\omega_0^{(m)} - i\gamma^{(m)}) \delta_{mn} - a_m G(z_m, z_n) \\ &\equiv (\omega_0^{(m)} - i\gamma^{(m)}) \delta_{mn} - \gamma_{1D}^{(m)} e^{iq|z_m - z_n|}, \end{aligned} \quad (5.7)$$

being the effective Hamiltonian matrix. We stress, that the matrix Eq. (5.7) is (i) non-Hermitian, (ii) symmetric and (iii) in general depends on the light frequency ω via the wave vector $q = \omega/c$. We will further discuss its properties in the following chapter 5.3.

Now, the dipole moments p_m can be found from the linear system of equations (5.6). It is instructive to introduce the matrix *Green function* of the emitter array, defined as an inverse of the matrix in the left hand-side of (5.6)

$$\mathcal{G}_{mn}(\omega) = \left[(H(\omega) - \omega \hat{1})^{-1} \right]_{mn} \quad (5.8)$$

($\hat{1}$ is the $N \times N$ identity matrix). With the help of the Green function we write

$$p_m = \sum_{n=1}^N G_{mn} a_n E_0 e^{iqz_m}. \quad (5.9)$$

In order to find light reflection and transmission coefficients r_{tot} and t_{tot} , one substitutes Eqs. (5.9) into Eq. (5.5) and takes the limits $z < z_1$ or $z > z_2$, respectively. Thus,

$$E \Big|_{z < z_1} = E_0 e^{iqz} + r_{\text{tot}} E_0 e^{iqz}, \quad (5.10)$$

$$E \Big|_{z > z_2} = t_{\text{tot}} E_0 e^{iqz}, \quad (5.11)$$

with

$$r_{\text{tot}} = \sum_{n,m=1}^N e^{iq(z_m+z_n)} \frac{\gamma_{1D}^{(m)}}{2\pi q} \mathcal{G}_{mn}(\omega), \quad t_{\text{tot}} = 1 + \sum_{n,m=1}^N e^{iq(z_m-z_n)} \frac{\gamma_{1D}^{(m)}}{2\pi q} \mathcal{G}_{mn}(\omega). \quad (5.12)$$

Equations (5.12) are valid for arbitrary N . We leave it as an exercise to prove, that for particular case of $N = 2$ they reduce to Eq. (5.1) and Eq. (5.2).

5.3 Complex eigenmodes

As has been mentioned in the previous chapter, the effective non-Hermitian Hamiltonian (5.7) does in general depend on the light frequency. This dependence comes from several places. First, as has been already mentioned in Chapter 3, even the coefficients a , γ_{1D} and γ can depend on ω . Typically, they change much only when ω changes by large value on the order of c/R , where R is the characteristic emitter size. There is an exception of so-called *giant atoms*, that are essentially superconducting qubits with the size on the order of the wavelength. There the $\gamma_{1D}(\omega)$ dependence is fast [1]. However, usually it is slow and can be neglected. The second place, where H_{mn} depends on ω , is the phase factor $\exp[i\omega|z_m - z_n|/c] \equiv \exp(i\omega d/c)$ for the considered case of $N = 2$ emitters. This factor changes when the ω variation is on the order of c/d , that is inverse flight time of light between the two emitters. Typically, for small emitters $\delta z \ll d$, so $c/d \gg c/R$ and the dependence of this factor on ω is more important. Still, due to the large light velocity typically $R/c \ll \gamma_{1D}$, the flight time is much smaller than the spontaneous emission time. Equivalently, one can say that the scale at which $\exp(i\omega d/c)$ changes is much larger than the resonance linewidth γ_{1D} . For example, for superconducting

qubits coupled to the waveguide one has $\gamma_{1D} \sim 10 \text{ MHz} \times 2\pi$ and $\omega_0 \sim 10 \text{ GHz} \times 2\pi \gg \gamma_{1D}$. Even if the spacing between the qubits is on the order of the light wavelength $\lambda = 2\pi c/\omega_0$ at the qubit resonance frequency, the photon flight time will be on the order of $2\pi/\omega_0$ and much shorter than $2\pi/\gamma_{1D}$, see e.g. Ref. [2]. As such, one can safely neglect the frequency dependence of $\exp(i\omega d/c)$ and set

$$H_{mn}(\omega) \rightarrow H_{mn}(\omega_0) , \quad (5.13)$$

where ω_0 is the emitter resonance frequency. By doing this we also assume that the spread of the resonance frequencies is small, $|\omega_0^{(1)} - \omega_0^{(2)}| \ll \omega_0^{(1,2)}$, so it does not matter which exactly ω_0 we choose in Eq. (3.16). Equation (3.16) is termed Markovian approximation. It is very general, and it means that the photon (or general reservoir) dynamics is much faster than the dynamics of the emitters that we are interested in. We will now show that the Markovian approximation considerably simplifies the analysis. Later on, in Sec. 5.6, we will also look beyond this approximation.

Once the Markovian approximation is done, the system Eq. (5.6) can be solved by expanding p_n over the *collective eigenmodes* of the frequency-independent Hamiltonian H_{mn} . There is, however, one important caveat. The Hamiltonian Eq. (5.7) is non-Hermitian, but it is still complex-symmetric. We will introduce the eigenvectors $\psi_n^{(\nu)}$ and eigenfrequencies $\omega^{(\nu)}$ in the conventional way:

$$\sum_{n=1}^N H_{mn} \psi_n^{(\nu)} = \omega^{(\nu)} \psi_m^{(\nu)} , \quad (5.14)$$

but the caveat will reveal itself in the *unconjugated orthogonality* condition [3]:

$$\sum_{n=1}^N \psi_n^{(\nu)} \psi_n^{(\mu)} = \delta_{\mu\nu} . \quad (5.15)$$

The condition (5.15) for the Hamiltonian with the property $H_{mn} = H_{nm}$ is different from the usual condition

$$\sum_{n=1}^N \psi_n^{(\nu)*} \psi_n^{(\mu)} = \delta_{\mu\nu} . \quad (5.16)$$

for the usual Hermitian Hamiltonian, $H_{mn} = H_{nm}^*$. It can be still derived by exactly the same

way. Multiplying Eq. (5.14) by ψ_m^μ and summing over m we find

$$\sum_{n,m=1}^N H_{mn} \psi_n^{(\nu)} \psi_n^{(\mu)} = \omega^{(\nu)} \sum_{n=1}^N \psi_n^{(\nu)} \psi_n^{(\mu)} , \quad (5.17)$$

On the other hand, if we write

$$\sum_{n=1}^N H_{mn} \psi_n^{(\nu)} = \omega^{(\nu)} \psi_m^{(\nu)} , \quad (5.18)$$

multiply by ψ_m^ν and summing over m we find

$$\sum_{n,m=1}^N H_{mn} \psi_n^{(\mu)} \psi_n^{(\nu)} = \omega^{(\mu)} \sum_{n=1}^N \psi_n^{(\nu)} \psi_n^{(\mu)} . \quad (5.19)$$

Subtracting Eq. (5.19) from Eq. (5.17) we find

$$\sum_{n=1}^N \psi_n^{(\nu)*} \psi_n^{(\mu)} (\omega^{(\mu)} - \omega^{(\nu)}) = 0 . \quad (5.20)$$

which leads to Eq. (5.20): the modes are orthogonal once their eigenfrequencies are different.

Given the condition Eq. (5.15) we can expand the solution of Eq. (5.6) in the usual way:

$$p_n = E_0 \sum_{\nu=1}^N \frac{\psi_n^{(\nu)} \langle \nu | q \rangle}{\omega^{(\nu)} - \omega} , \quad \langle \nu | a | q \rangle \equiv \sum_{n=1}^N \psi_n^{(\nu)} a_n e^{iqz_m} . \quad (5.21)$$

where we have introduced an unconjugated scalar product notation $\langle \nu | \mu \rangle$ for the left-hand-side of Eq. (5.15) and also for the overlap $\langle \nu | a | q \rangle$ of the incident plane wave $\exp(iqz_m)$ with the mode ν weighted by the emitter radiative decay rates. This allows us to express the reflection and transmission coefficients in terms of eigenmodes. Equations (5.12) then acquire an especially simple form if all decay rates are the same, $\gamma_{1D}^{(m)} \equiv \gamma_{1D}$:

$$r_{\text{tot}}(\omega) = i \sum_{\nu=1}^N \frac{\gamma_{1D} \langle q | \nu \rangle \langle \nu | q \rangle}{\omega^{(\nu)} - \omega} , \quad t_{\text{tot}}(\omega) = 1 + i \sum_{\nu=1}^N \frac{\gamma_{1D} \langle -q | \nu \rangle \langle \nu | q \rangle}{\omega^{(\nu)} - \omega} . \quad (5.22)$$

The advantage of Eqs. (5.22) is that they clearly show that the reflection and transmission spectra have resonances at the collective eigenmode frequencies. To be more precise, the spectra $|r_{\text{tot}}(\omega)|^2, |t_{\text{tot}}(\omega)|^2$ will have resonances at ω close to $\text{Re } \omega^\nu$ with linewidths of $|\text{Im } \omega^\nu|$.

The states with low $|\operatorname{Im} \omega_\nu|$ will be manifested as sharp resonances.

5.4 Purcell enhancement

Before considering the case of two identical emitters, it is instructive to look closer first into two different emitters, with different resonant frequencies and different values of γ_{1D} . The effective Hamiltonian Eq. (5.7) then becomes

$$H = \begin{pmatrix} \omega_0^{(1)} - i\gamma_{1D}^{(1)} & -i\gamma_{1D}e^{i\varphi} \\ -i\gamma_{1D}e^{i\varphi} & \omega_0^{(2)} - i\gamma_{1D}\gamma_{1D}^{(2)} \end{pmatrix}, \quad (5.23)$$

For simplicity we set $\gamma = 0$ in this chapter. Let us assume that the spectral detuning between the two resonance frequencies is large, or, to be more precise,

$$|\omega_0^{(1)} - \omega_0^{(2)} - i\gamma_{1D}^{(1)} + i\gamma_{1D}^{(2)}| \gg \gamma_{1D}^{(1,2)}.$$

Then we can expect that the effects of the collective interaction between the two emitters are weak. Formally, this means that the eigenfrequencies of Eq. (5.23) can be found using the second-order quantum mechanical perturbation theory. In particular, the complex resonance frequency of the first emitter, slightly renormalized due to the interaction with the second one, can be written as

$$\tilde{\omega}_0^{(1)} = \omega_0^{(1)} - i\gamma_{1D}^{(1)} + \frac{\gamma_{1D}^{(1)}\gamma_{1D}^{(2)}e^{2i\varphi}}{\omega_0^{(1)} - \omega_0^{(2)} - i\gamma_{1D}^{(1)} + i\gamma_{1D}^{(2)}}, \quad (5.24)$$

Equation (5.24) is quite instructive. It tells us that both the radiative decay rate $-\operatorname{Im} \omega$ and the resonance frequency are changed by the interaction. The first effect, radiative correction to the resonance frequency has analogy to the *Lamb shift* in vacuum quantum electrodynamics. The second effect is the correction to the decay rate of the emitter in the presence of another one,

$$\frac{-\operatorname{Im} \tilde{\omega}_0^{(1)}}{\gamma_{1D}^{(1)}} = 1 + \operatorname{Im} \frac{\gamma_{1D}^{(2)}e^{2i\varphi}}{\omega_0^{(1)} - \omega_0^{(2)} - i\gamma_{1D}^{(1)} + i\gamma_{1D}^{(2)}} \approx 1 + \operatorname{Re}[r_2(\omega_0^{(1)})e^{2i\varphi}] \quad (5.25)$$

where

$$r_2(\omega) = \frac{i\gamma_{1D}^{(2)}}{\omega_0^{(2)} - \omega - i\gamma_{1D}^{(2)}}. \quad (5.26)$$

is the reflection coefficient of the second emitter. The factor in the right-hand side of Eq. (5.25) is the ratio of the decay rates of the first emitter in the presence of the second one and without

the second one. It can be termed as a generalized *Purcell factor*. In his seminal work [4] Purcell understood that the spontaneous decay rate is different for an emitter in vacuum and in a cavity. Now the term Purcell factor is used to describe the modification of the spontaneous decay rate in any structured electromagnetic environment. In this paragraph, the environment is provided by the second emitter. However, in principle the second part of Eq. (5.24) is valid for emitter near any mirror. For example, in Ref. [5] the authors have measured the modification of the radiative lifetime the presence of a planar dielectric mirror.

The answer Eq. (5.24) can be also recovered without involving the concept of non-Hermitian Hamiltonian, directly from the resonances of the reflection coefficient of the two emitters. The central idea here is that the collective eigenmodes correspond to the complex poles of the collective linear response function, for example, of the reflection or transmission coefficient for the two emitters. We see from Eq. (5.2) that the resonance condition for the reflection or transmission of light through two emitters is given just by

$$1 - r_1 r_2 \exp(2i\varphi) = 0. \quad (5.27)$$

Equation (5.27) is just the usual condition for the Fabry-Pérot resonance in the cavity, made of two mirrors with the reflection coefficients r_1 and r_2 . However, if we take into account that in our case the mirrors are resonant, we will also find “for free” the collective eigenmode frequencies. Indeed, if we substitute

$$r_1 = \frac{i\gamma_{1D}^{(1)}}{\omega_0^{(1)} - \omega - i\gamma_{1D}^{(1)}} \quad (5.28)$$

into Eq. (5.27) and solve for ω for fixed r_2 , we recover

$$\omega = \omega_0 - i\gamma_{1D}^{(1)}(1 + r_2 e^{2i\varphi}), \quad (5.29)$$

in exact agreement with Eq. (5.24), Eq. (5.25).

It is also instructive to plot reflection spectra for two unidentical emitters, with $\gamma_{1D}^{(2)} \gg \gamma_{1D}^{(1)}$ as function of their spectral detuning $\omega_0^{(1)} - \omega_0^{(2)}$. This is done in Fig. 5.3. Since $\gamma_{1D}^{(2)} \gg \gamma_{1D}^{(1)}$, away from the first emitter resonance it does not contribute much to the reflection and one has $r_{\text{tot}} \approx r_2$. Closer to the resonance the presence of the first emitter is manifested as a spectrally

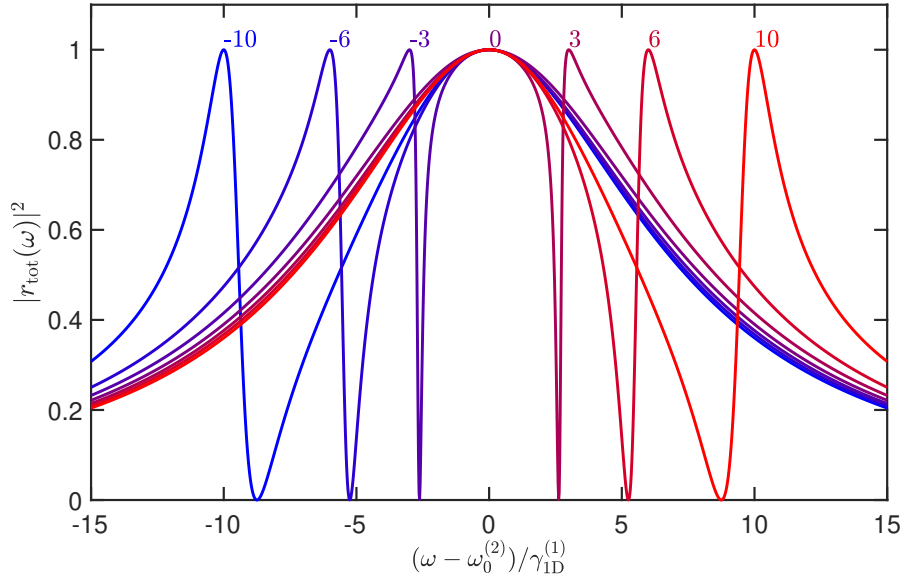


Figure 5.3: Reflection spectra for two unidentical emitters with $\gamma_{1D}^{(2)} = 7\gamma_{1D}^{(1)}$. Different curves correspond to different values of $(\omega_0^{(1)} - \omega_0^{(2)})/\gamma_{1D}^{(1)}$, indicated on graph on top of the curves. Calculation has been performed following Eqs. (3.12) for $\gamma = 0$, $\varphi = 0$.

narrow resonant feature. This feature is, in general, asymmetric and its shape depends on the detuning. Such asymmetric spectral lines are very typical when there exist several resonances with different spectral linewidths in the system and is termed as *Fano resonance*. This follows original work of Ugo Fano on interference of different ionization processes in atomic physics [6] but is now often used in a much broad (maybe, too broad), context. More details on Fano resonances in optical settings can be found in Ref. [7].

5.5 Super- and subradiant modes for $N = 2$

We will now illustrate the non-Hermitian Hamiltonian approach above for two identical coupled emitters. Since their eigenfrequencies will be the same, the interaction effects will be even stronger than in the previous section. They can no longer be treated perturbatively. To find the eigenmodes we will diagonalize of the effective non-Hermitian Hamiltonian matrix Eq. (5.7), that assumes the form

$$H = \begin{pmatrix} \omega_0 - i(\gamma_{1D} + \gamma) & -i\gamma_{1D}e^{i\varphi} \\ -i\gamma_{1D}e^{i\varphi} & \omega_0 - i(\gamma_{1D} + \gamma) \end{pmatrix}. \quad (5.30)$$

We remind that $\varphi = \omega_0 d/c$ is the phase gained by light between the two emitters and plays the role of the dimensionless distance. The eigenfrequencies are given by

$$\omega_{\pm} = \omega_0 - i\gamma - i(\gamma_{1D} \pm \gamma_{1D}e^{i\varphi}) . \quad (5.31)$$

and the eigenvectors correspond to symmetric and antisymmetric excitation, $[1, \pm 1]/\sqrt{2}$. Equations (5.31) show, that both the real and imaginary parts of the two decay rates are renormalized by the interaction:

$$\text{Re } \omega_{\pm} = \omega_0 \pm \gamma_{1D} \sin \varphi , \quad -\text{Im } \omega_{\pm} = \gamma \pm \gamma_{1D}(1 \pm \cos \varphi) . \quad (5.32)$$

Figure 5.4 shows how the real and imaginary parts of the eigenfrequencies depend on the distance between the emitters. Clearly, they exhibit an oscillating behavior. Indeed, the complex off-diagonal terms in Eq. (5.30) have both real and imaginary part. These parts correspond to *dispersive* (also called *exchange*) coupling and *dissipative* coupling, that tend to split real and imaginary parts of the eigenfrequencies, respectively. Such type of oscillating behavior of collective modes has been first observed in Ref. [8] for two trapped ions. Similarly to the case of a single emitter, we interpret the terms $\gamma_{1D}(1 \pm \cos \varphi)$ as the radiative decay rates of the two coupled emitters. As a sanity check, we see that the decay rates state positive. In other words, $\text{Im } \omega_{\pm} < 0$, which means that the eigenexcitations of the system, $\propto \exp(-i\omega_{\pm}t)$, decay in time. The special case, similar to Fig. 5.2 is when $\varphi = 0$ ($\varphi = \pi$). In this case the decay rate for the symmetric (antisymmetric) mode ω_+ (ω_-) is equal to $2\gamma_{1D}$, twice larger than for an individual emitter. This mode can be called a collective *superradiant* mode of the two emitters: constructive interference between radiation of the two emitters leads to twice large radiative decay rate. The concept of superradiance has been initially put forward by Dicke [9] in a broader context of N emitters and many photon excitations, we will encounter it many times in this book. The antisymmetric mode for $\varphi = 0$ (symmetric mode for $\varphi = \pi$) is completely dark, that is, its radiative decay is zero. When the distance between the emitters is changed, and deviates from an exact value of $0, \pi, 2\pi$, the dark states stops being completely dark and becomes subradiant:

$$-\text{Im } \omega_- = \gamma + \frac{\varphi^2}{2}\gamma_{1D} \text{ for } \varphi \ll 1 . \quad (5.33)$$

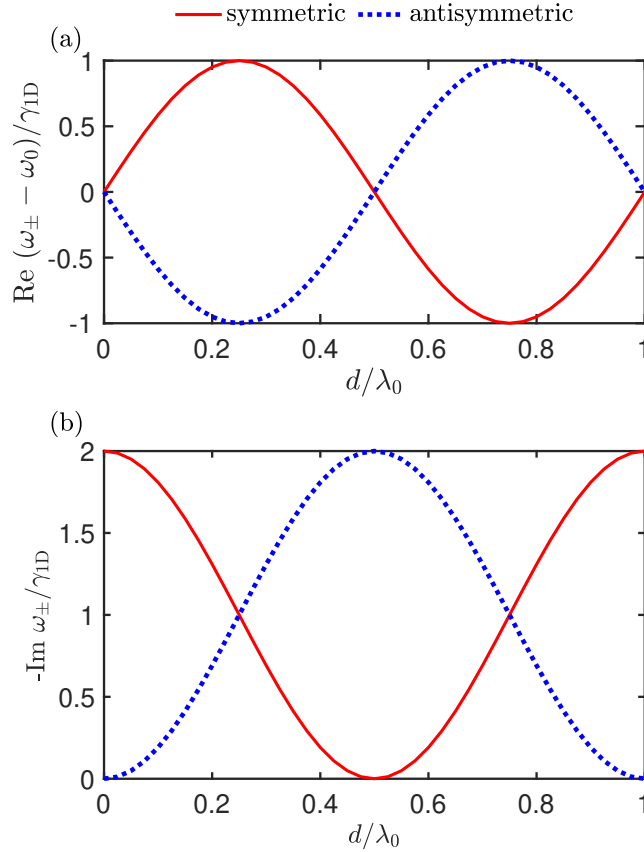


Figure 5.4: Real (a) and imaginary (b) parts of the eigenmodes of two coupled emitters. Calculated following Eqs. (5.31) for $\gamma = 0$.

If the other decay channels are weak $\gamma \ll \gamma_{1D}$, one has $|\text{Im } \omega_-| \ll \gamma_{1D}$ and, according to Eq. (5.22), the mode will be seen as a sharp resonance in the reflection spectrum. It is this subradiant state resonance that is behind the narrow dips in the reflection spectra in Fig. 5.2(a) for φ close to $0, \pi$.

For those more used to quantum mechanics description of the spontaneous emission, there is another simple way to explain collective enhancement or suppression of light emission. Let us use the Fermi Golden rule to calculate the radiative decay rate:

$$-2 \text{Im } \omega^{(\nu)} = \frac{2\pi}{\hbar} \int_{-\infty}^{\infty} \frac{dk}{2\pi} |M_k^{(\nu)}|^2 \delta(\hbar\omega_0 - \hbar c|k|) \quad (5.34)$$

Here, M_k is the matrix element for the interaction of the plain electromagnetic wave $\exp(ikz)$ with the given mode. That, Eq. (5.34) represents the sum of the probabilities of emission of waveguide photons. For simplicity we also in Eq. (5.34) assume $\gamma = 0$. The reason of the factor 2 in the left-hand-side is that the emission rate is twice the imaginary part of the

eigenmode frequency: if $\psi \propto \exp(-i\omega^{(\nu)}t)$, then $|\psi|^2 \propto \exp(-2 \operatorname{Im} \omega^{(\nu)}t)$. In order to actually use Eq. (5.34) we also need to calculate $M_k^{(\nu)}$. We define it as

$$M_k^{(\nu)} = \hbar g \sum_{m=1}^N e^{ikdm} \psi_m^{(\nu)}, \quad (5.35)$$

where $\hbar g$ is the photon-emitter interaction strength. Since we know that for the two emitters $\psi^{(\pm)} = [1, \pm 1]/\sqrt{2}$ we get

$$M_k^{(\pm)} = \frac{\hbar g}{\sqrt{2}} (1 \pm e^{ikd}). \quad (5.36)$$

and

$$-2 \operatorname{Im} \omega^{(\nu)} = \frac{2g^2}{c} \left(1 \pm \cos \frac{\omega_0 d}{c} \right). \quad (5.37)$$

If we identify

$$\gamma_{1D} = g^2/c \quad (5.38)$$

as a spontaneous decay rate of a single emitter in the waveguide, we recover exactly the radiative decay rates from Eq. (5.32).

5.6 Non-Markovian effects

In this section, we will go beyond the Markovian approximation usually used in this book. Namely, we will solve Eq. (5.27) for the collective modes of the two emitters without assuming that they are closed to each other:

$$1 - r^2 \exp(2i\omega d/c) = 0. \quad (5.39)$$

Here, we explicitly write $\varphi = \omega d/c$ and we are going to take the dependence of φ on ω into account. For simplicity, we assume both emitters to be the same and we remind that $r = i\gamma_{1D}/[\omega_0 - \omega - i(\gamma + \gamma_{1D})]$. Substituting explicit expressions for $r(\omega)$ into Eq. (5.39) we find

$$\omega_{\pm} = \omega_0 - i\gamma - i\gamma_{1D} \mp i\gamma_{1D} \exp(i\omega_{\pm} d/c). \quad (5.40)$$

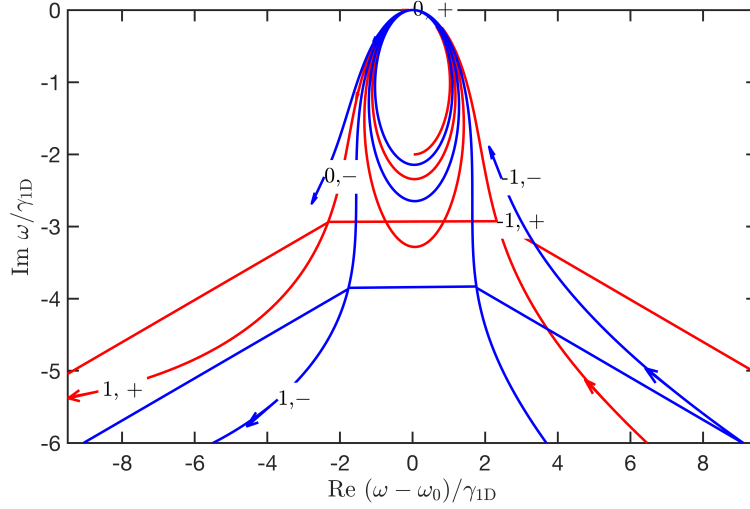


Figure 5.5: Eigenmodes (5.41) of two coupled oscillators beyond the Markovian approximation. Calculated for $\gamma_{1D}/\omega_0 = 0.02$, $\gamma = 0$ and varying $\omega_0 d/c = 0 \dots 7\pi$. Arrows indicate the direction of increasing d the values of ν and mode parity sign \pm are indicated near each curve.

Compared to Eq. (5.31), these are now transcendental equations to solve for complex ω_{\pm} . The solution can be formally written as

$$\omega_{\pm}^{\nu} = \tilde{\omega}_0 + i \frac{c}{d} W_{\nu} \left[\mp \frac{\gamma_{1D} d}{c} \exp \left(i \frac{\tilde{\omega}_0 d}{c} \right) \right], \quad \tilde{\omega}_0 \equiv \omega_0 - i\gamma - i\gamma_{1D}. \quad (5.41)$$

Here, $W_{\nu}(z)$ is the so-called Lambert W-function, found as solution of $W(z) \exp[W(z)] = z$. Importantly, it is a multibranch function, characterized by the integer index ν . Thus, there are infinite eigenmode solutions for two oscillators! Where do the additional modes come from? The answer is simple — the extra modes are just the Fabry-Pérot modes in the cavity, formed by two emitters, acting as resonant mirrors. There is, in principle, an infinite amount of such modes, so we should not be surprised much. Indeed, at larger $|\nu| \gg z$ the main term in $W_{\nu}(z)$ asymptotic expression is $2\pi i\nu$. Being substituted in Eq. (5.41) this gives a set of Fabry Pérot modes separated by $2\pi c/d$.

At small spacing d , when photon flight time d/c is much less than the spontaneous emission lifetime $1/\gamma_{1D}$, the argument of the Lambert functions is small, and one can use the approximate expression $W_0(x) \approx x$. Both solutions of Eq. (5.41) then reduce to

$$\omega_{\pm}^{\nu} \approx \tilde{\omega}_0 + i \frac{c}{d} \left[\mp \frac{\gamma_{1D} d}{c} \exp \left(i \frac{\tilde{\omega}_0 d}{c} \right) \right] \approx \tilde{\omega}_0 \pm i\gamma_{1D} e^{i\varphi}. \quad (5.42)$$

This is equivalent to the usual Markovian approximation answer Eq. (5.31). For $\nu \neq 0$ and

$d \ll c/\gamma_{1D}$ the rest of the solutions will be strongly detuned from ω_0 by the frequency $\sim c/d$.

The complex spectrum of eigenmodes plotted for varying d following Eqs. (5.41) is shown in Fig. 5.5. For low values of d , when $\gamma_{1D}d/c \ll 1$, there only two eigenmodes in the spectra vicinity of the resoance $|\omega - \omega_0| \lesssim \gamma_{1D}$, which are just the usual solutions Eq. (5.31). When the phase $\omega_0 d/c \equiv \varphi$ changes, the imaginary and real parts of these two modes oscillate and they rotate around the point $\omega_0 - i\gamma_{1D}$, just as shown in Fig. 5.4. This is manifested by spirals in the middle of Fig. 5.5. For large values of d , however, additional Fabry-Pérot modes appear “from infinity”, and the eigenspectrum becomes much more complex. Thus, even the seemingly simple problem of two coupled oscillators becomes quite involved beyond the Markovian approximation!

More details on the complex energy spectrum and Fabry-Pérot modes of a finite-size slab can be found in [10].

5.7 Summary

To summarize, we have seen that the problem of light scattering on just two emitters is surprisingly rich. The reason behind this is multiple scattering of light from the emitters with constructive or destructive interference. Depending on the distance of the emitters, the difference between their resonant frequencies, and their radiative decay rates, one can realize totally different regimes of interaction. The two-emitter problem can illustrate a large part of the collective interaction effects. We will, however, see in the next chapter that there are also some effects that are uncovered for larger arrays with $N > 2$.

5.8 Additional reading

Fano-like resonance for cavity side coupled to a waveguide: S. Fan, “Sharp asymmetric line shapes in side-coupled waveguide-cavity systems”, [Appl. Phys. Lett.](#) **80**, 908 (2002)

Fano resonances in photonics: M. F. Limonov et al., “Fano resonances in photonics”, [Nat. Photonics](#) **11**, 543–554 (2017).

A detailed discussion of original Purcell work [4] on spontaneous emission: M. Glazov et al., “Purcell Factor in Small Metallic Cavities”, [Phys. Solid State](#) **53**, 1753 (2011)

References

- ¹A. Frisk Kockum, “Quantum optics with giant atoms—the first five years”, in [International symposium on mathematics, quantum theory, and cryptography](#), edited by T. Takagi, M. Wakayama, K. Tanaka, N. Kunihiro, K. Kimoto, and Y. Ikematsu (2021), pp. 125–146.
- ²E. S. Redchenko, A. V. Poshakinskiy, R. Sett, M. ?emli?ka, A. N. Poddubny, and J. M. Fink, “Tunable directional photon scattering from a pair of superconducting qubits”, [Nature Communications](#) **14**, [10.1038/s41467-023-38761-6](#) (2023).
- ³V. A. Kosobukin and A. N. Poddubny, “Exciton-polariton absorption in periodic and disordered quantum-well chains”, [Physics of the Solid State](#) **49**, 1977–1987 (2007).
- ⁴E. M. Purcell, “Spontaneous Emission Probabilities at Radio Frequencies”, [Phys. Rev.](#) **69**, 681 (1946).
- ⁵H. H. Fang, B. Han, C. Robert, M. A. Semina, D. Lagarde, E. Courtade, T. Taniguchi, K. Watanabe, T. Amand, B. Urbaszek, M. M. Glazov, and X. Marie, “Control of the exciton radiative lifetime in van der Waals heterostructures”, [Phys. Rev. Lett.](#) **123**, 067401 (2019).
- ⁶U. Fano, “Effects of Configuration Interaction on Intensities and Phase Shifts”, [Phys. Rev.](#) **124**, 1866–1878 (1961).
- ⁷M. F. Limonov, M. V. Rybin, A. N. Poddubny, and Y. S. Kivshar, “Fano resonances in photonics”, [Nat. Photonics](#) **11**, 543–554 (2017).
- ⁸R. G. DeVoe and R. G. Brewer, “Observation of superradiant and subradiant spontaneous emission of two trapped ions”, [Phys. Rev. Lett.](#) **76**, 2049–2052 (1996).
- ⁹R. H. Dicke, “Coherence in Spontaneous Radiation Processes”, [Phys. Rev.](#) **93**, 99 (1954).
- ¹⁰L. J. Armitage, M. Doost, W. Langbein, and E. Muljarov, “Resonant-state expansion applied to planar waveguides”, [Physical Review A](#) **89**, 053832 (2014).

- ¹¹S. Fan, “Sharp asymmetric line shapes in side-coupled waveguide-cavity systems”, [Appl. Phys. Lett. **80**, 908 \(2002\)](#).
- ¹²M. Glazov, E. Ivchenko, A. Poddubny, and G. Khitrova, “Purcell Factor in Small Metallic Cavities”, [Phys. Solid State **53**, 1753 \(2011\)](#).

REFERENCES

Chapter 6

2×2 non-Hermitian Hamiltonian

In the previous chapter, we have seen, that non-Hermitian effective Hamiltonians H_{mn} naturally arise when considering a problem of emitters coupled by light, i.e. by the processes, when photon is emitted by an atom n and reabsorbed by an atom m . The goal of this chapter will be to study the properties of the non-Hermitian Hamiltonians in a bit more detail, without the focus on the particular setup of a one-dimensional emitter array. We will consider the generic situation, where two emitters, that can in principle be different, are coupled to exactly the same electromagnetic mode. This can be realized, for example, when emitters are located in resonance with the same photonic mode of a cavity. As illustrated in Fig. 6.1, this mode will induce both *collective dissipation* for the emitters, when energy is emitted in the far field, and dispersive coupling, when a photon emitted from the first emitter will be reabsorbed by the second one and vice versa.

6.1 Derivation of the Hamiltonian

Let us again rewrite the general equation (5.7) for $N = 2$, assuming that the Green function $G(z_m, z_n) \equiv G$, i.e. it does not depend on the emitter positions. This can be realized when for example emitters are placed close to each other, or in the different antinodes of the standing wave.

$$\begin{pmatrix} \omega_0^{(1)} - a_1 G & -a_1 G \\ a_2 G & \omega_0^{(2)} - a_2 G \end{pmatrix} \begin{pmatrix} p_1 \\ p_2 \end{pmatrix} = \omega \begin{pmatrix} p_1 \\ p_2 \end{pmatrix}. \quad (6.1)$$

Here, we assumed that the only decay mechanism comes from the emission of photons into the mode, so we have set internal decay rates γ to zero. It is instructive to symmetrize the problem

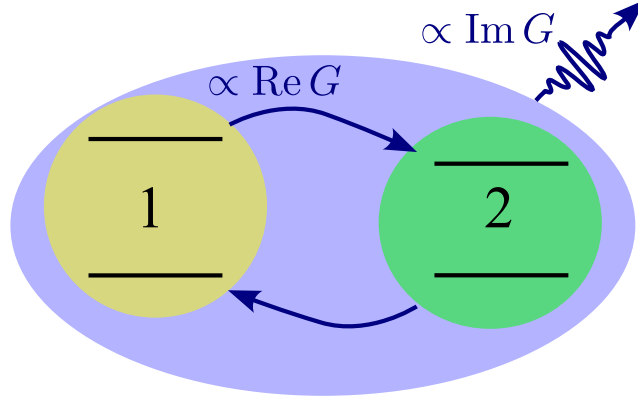


Figure 6.1: Schematic illustration of two emitters coupled to the same electromagnetic environment. Real part of the electromagnetic Green function $\text{Re } G$ is responsible for the dispersive coupling, imaginary part $\text{Im } G$ is responsible for the collective dissipation.

Eq. (6.1) by changing the unknowns to $\psi_{1,2} = p_{1,2}/\sqrt{a_{1,2}}$. For a two-level atom emitters, these amplitudes $\psi_{1,2}$ describe the coherences between the ground and excited states. We also explicitly The system Eq. (6.1) is then transformed to

$$H\psi = \omega\psi, \quad H = \begin{pmatrix} \omega_1 - i\gamma_1 & g - i\sqrt{\gamma_1\gamma_2} \\ g - i\sqrt{\gamma_1\gamma_2} & \omega_2 - i\gamma_2 \end{pmatrix}, \quad (6.2)$$

where $\omega_{1,2} = \omega_0^{(1,2)} - a_{1,2} \text{Re } G$ are the resonant frequencies of two coupled emitters (both are real), shifted due to their interaction with photons by $a_{1,2} \text{Re } G$. The parameter $g = -\sqrt{a_1 a_2} \text{Re } G$ describes the dispersive part of the coupling and the real parameters $\gamma_{1,2} = -a_{1,2} \text{Im } G$ describe the dissipation. The form Eq. (6.2) makes the distinction between the dispersive (exchange) and dissipative parts of the effective non-Hermitian Hamiltonian especially clear. We can write

$$H = H_{\text{exch}} + H_{\text{diss}}, \quad H_{\text{exch}} = \begin{pmatrix} \omega_1 & g \\ g & \omega_2 \end{pmatrix}, \quad H_{\text{diss}} = -i \begin{pmatrix} \sqrt{\gamma_1} \\ \sqrt{\gamma_2} \end{pmatrix} \begin{pmatrix} \sqrt{\gamma_1} \\ \sqrt{\gamma_2} \end{pmatrix}^T. \quad (6.3)$$

The dissipative part is a rank-1 matrix, which is a direct consequence of the fact that the dissipation is due to the emission into a single photonic mode. In a more general case, the number of terms in the expansion of the dissipative part of the effective Hamiltonian is equal to the number of independent decay channels [1].

6.2 Exceptional points. Strong and weak coupling

The eigenfrequencies ω_{\pm} of Eq. (6.2) are given by

$$\omega_{\pm} = \frac{\omega_1 + \omega_2}{2} - i\frac{\gamma_1 + \gamma_2}{2} \pm \sqrt{D}, \quad D = \left(\frac{\omega_1 - \omega_2 - i\gamma_1 + i\gamma_2}{2} \right)^2 + (g - i\sqrt{\gamma_1\gamma_2})^2. \quad (6.4)$$

Figure 6.2 plots the dependence of the real (a) and imaginary parts (b) of the eigenfrequencies on the dispersive coupling strength g for the case of zero detuning, when $\omega_1 = \omega_2$. We have also chosen $\gamma_2 = 0$, which means that the dissipative part of the coupling matrix element $g - i\sqrt{\gamma_1\gamma_2}$ in Eq. (6.2) is exactly zero. Even then, the problem is not trivial and there are two qualitatively different coupling regimes. For $|g| < \gamma_1/2 = 1$, the coupling is weaker than the half-difference between the imaginary parts of the complex eigenfrequencies. As a result, the coupling leads to the renormalization of the decay rates, $\text{Im}\omega_{\pm}$ in Fig. 6.2(b), but the real parts stay equal to zero. As a sanity check we see that $\text{Im}\omega_{\pm} < 0$: the eigenexcitations of the system, $\propto \exp(-i\omega_{\pm}t)$, decay in time. In the opposite case, $|g| > \gamma_1/2 = 1$, the real parts of the eigenfrequencies are split and imaginary stay the same. This regime of large dispersive coupling is similar to usual avoided crossing of levels in Hermitian problems. In the case when both decay rate and dispersive coupling are present, the parameter range when the coupling is stronger than the decay rates is called strong coupling regimes. It means that the excitations can be coherently transferred between the emitters, and the transfer rate is faster, then the rate of dissipation. The opposite case of small g is called the weak coupling regime. In the very strong coupling regime, one can think of the eigenstates of the non-Hermitian Hamiltonian as hybridized even and odd combinations of the excitations of first and second emitter, $[\psi_1, \psi_2] = [1, \pm 1]/\sqrt{2}$. In the weak coupling regime with $g \ll \gamma_{1,2}$ it is easier to think of the eigenstates as independent modes, $[1, 0]$ and $[0, 1]$.

The transition between the strong and weak coupling regimes goes through the exceptional point, that is seen as square-root singularities in Fig. 6.2 at $g = \pm 1$. Not only two eigenvalues are the same at the exceptional point, but also the eigenvectors coalesce and the Hamiltonian matrix becomes degenerate.

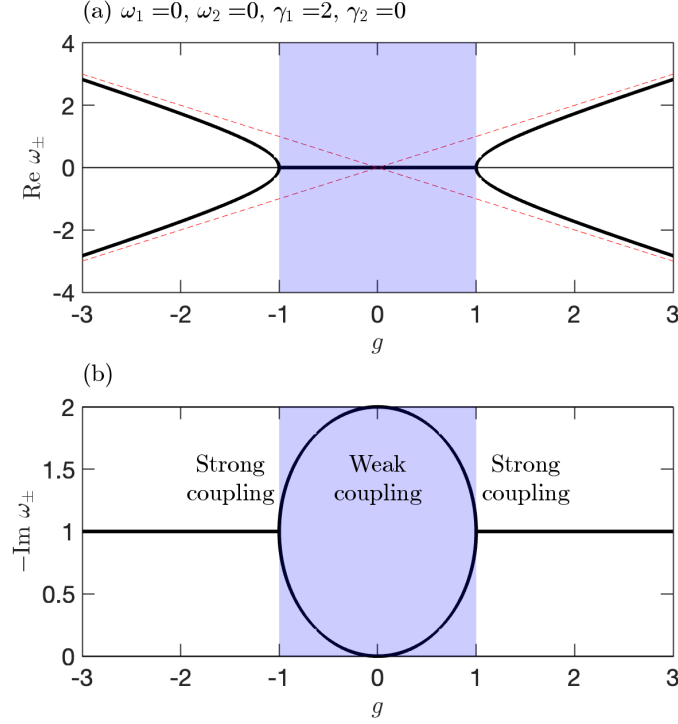


Figure 6.2: Real (a) and imaginary (b) parts of the eigenfrequencies (6.4) depending on the coupling strength g . Calculation has been performed for zero detuning, $\tilde{\omega}_0^{(1)} = \tilde{\omega}_0^{(2)}$ and for $\gamma_2 = 0$. Dashed red lines in (a) show the asymptotic description in the strong dispersive coupling limit, $\omega_{\pm} = \pm g$. Blue shading indicates the weak coupling regime. Other calculation parameters are indicated on graph.

6.3 Friedrich-Wintgen condition

Figure 6.3 shows the dependence of the complex eigenfrequencies ω_{\pm} on g in a slightly more general scenario. Not only the eigenfrequencies ω_1 and ω_2 are detuned from each other, but also $\gamma_2 > 0$, so that there is an extra off-diagonal dissipative coupling term $\sqrt{\gamma_1\gamma_2}$ in Eq. (6.2). One can then see in Fig. 6.3 that there is a special point when one of the imaginary parts of one of the eigenvalues turns to zero. This point can also be found analytically from Eq. (6.4). If we denote $\sqrt{D} = x + iy$, we need $y = (\gamma_1 + \gamma_2)/2$ to have real-valued solution. This yields to the condition

$$\operatorname{Re} D = x^2 - y^2, \quad \operatorname{Im} D = 2xy, \quad \text{with } y = \frac{\gamma_1 + \gamma_2}{2}. \quad (6.5)$$

Finding x from the first equation and substituting in the second one, we find

$$\operatorname{Re} D - (x^2 - y^2) \propto \left(g - \frac{\sqrt{\gamma_1\gamma_2}(\omega_1 - \omega_2)}{\gamma_1 - \gamma_2} \right)^2 \quad (6.6)$$

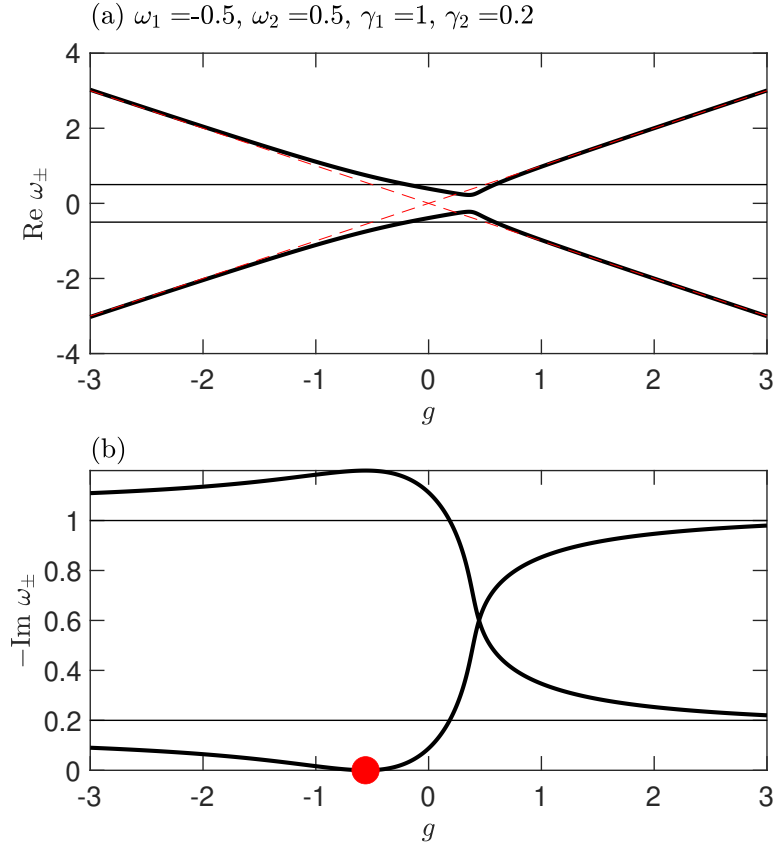


Figure 6.3: Real (a) and imaginary (b) parts of the eigenfrequencies (6.4) depending on the coupling strength g . Calculation has been performed in the detuned case, $|\tilde{\omega}_0^{(1)} - \tilde{\omega}_0^{(2)}| = 1$. Red dot indicates the Friedrich-Wintgen condition Eq. (6.7), where the imaginary part of one of the eigenmodes is exactly zero. Dashed red lines in (a) show the asymptotic description in the strong dispersive coupling limit, $\omega_{\pm} = \pm g$. Thin horizontal lines show the eigenfrequencies assuming no coupling between the emitters. Other calculation parameters are indicated on graph.

which leads to

$$\sqrt{\gamma_1 \gamma_2}(\omega_1 - \omega_2) = g(\gamma_1 - \gamma_2). \quad (6.7)$$

This is a so-called Friedrich-Wintgen condition, named after the authors of Ref. [2]. Currently, it is often used in the context of so-called bound states in continuum in photonic structures [3], where it describes destructive interference of decay via two different decay channels. In the previous chapter, discussing two emitters coupled to the same waveguide mode, we have already encountered such points with $\text{Im } \omega_{\pm} = 0$ and associated them with dark states see Fig. 5.4 for $d = 0, \lambda/2, \lambda$. There we considered identical emitters with no detuning, $\omega_1 = \omega_2$ and $\gamma_1 = \gamma_2$. The Friedrich-Wintgen condition then reduces to just $g = 0$, zero dispersive coupling. This is exactly the case for $d = 0, \lambda/2, \lambda$, when the Green function $\propto i \exp(2\pi i \varphi) \equiv i \exp(2\pi i d/\lambda)$ is purely imaginary. Thus, the dark states present a particular realization of the Friedrich-Wintgen

condition.

6.4 Summary

To summarize, in this chapter, we have learned that even the seemingly simple problem of two emitters coupled to the same electromagnetic environment can be nontrivial. Depending on the spectral detuning between the emitter resonances, their decay rates, and the dispersive coupling strength, one can realize both strong coupling regimes when excitations of both emitters can be hybridized by hopping from one emitter to another and back, and the weak coupling regimes, when the excitations dissipate faster than hopping and thus stay localized. Transitions between the two regimes goes through exceptional points. There are also special cases, when the decay rate of one of the modes becomes exactly zero, i.e. the mode is dark and does not dissipate in the environment.

6.5 Additional reading

More on symmetry of 2×2 non-Hermitian Hamiltonians in optics [4].

Discussion of non-Hermitian Hamiltonian for a general system: W. Suh et al., “Temporal coupled-mode theory and the presence of non-orthogonal modes in lossless multimode cavities”, *IEEE Journal of Quantum Electronics* **40**, 1511–1518 (2004).

References

- ¹W. Suh, Z. Wang, and S. Fan, “Temporal coupled-mode theory and the presence of non-orthogonal modes in lossless multimode cavities”, *IEEE Journal of Quantum Electronics* **40**, 1511–1518 (2004).
- ²H. Friedrich and D. Wintgen, “Interfering resonances and bound states in the continuum”, *Phys. Rev. A* **32**, 3231–3242 (1985).
- ³C. W. Hsu, B. Zhen, A. D. Stone, J. D. Joannopoulos, and M. Soljačić, “Bound states in the continuum”, *Nature Reviews Materials* **1**, 16048 (2016).
- ⁴G. Arwas, S. Gadas, I. Gershenzon, A. Friesem, N. Davidson, and O. Raz, “Anyonic-parity-time symmetry in complex-coupled lasers”, *Science Advances* **8**, 10.1126/sciadv.abm7454 (2022).

REFERENCES

Chapter 7

Light interaction with $N > 2$ periodically spaced emitters.

The goal of this chapter will be to study the collective light interaction with $N > 2$ emitters, arranged in the periodic array and coupled to the waveguide mode, see Fig. ???. Some of the phenomena, such as the formation of collective super- and sub-radiant eigenmodes, will be essentially the same as in the case of $N = 2$. The super-radiant modes will just get brighter, and the subradiant modes will just be darker for a larger number of emitters N . However, there will also be new phenomena for long periodic arrays. We will show, that light can see a long periodic array of emitters either as an effective medium, where the interaction will be averaged over all the emitters, or as a resonant periodic photonic crystal. In the first case the whole array can be described by some effective permittivity, in the second case, the photonic *band gap* will form, similarly to band gaps for electrons in usual crystals. The description of such interaction of light with arrays will require different theoretical tools.

7.1 Collective super- and subradiant modes for N emitters

Let us again look for the eigenstates Eq. (5.7) in the case of the periodic array, when $\omega_0 z_m / c \equiv \varphi m$, and $\varphi = \omega_0 d / c$ is still the phase gained by light between the two emitters.

$$\omega_0 p_m - i\gamma_{1D} \sum_{n=1}^N e^{i\varphi|m-n|} p_n = \omega p_m, \quad m = 1, 2 \dots N, \quad (7.1)$$

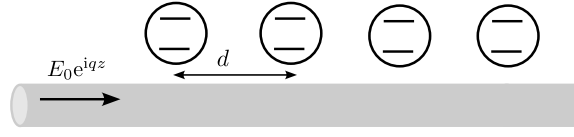


Figure 7.1: Periodic array of resonant scatterers coupled to the waveguide.

where $\varphi = 2\pi d/\lambda$ is the phase gained by light propagating between the two neighboring emitters. In this chapter, we will focus on specific case of the Bragg-spaced array. when $d = \lambda/2$, so $\varphi = \pi$.

We start by rewriting the coupled equations using the fact that $\varphi = \pi$:

$$\omega_0 p_m - i\gamma_{1D} \sum_{n=1}^N (-1)^{m+n} p_n = \omega p_m, \quad m = 1, 2 \dots N, \quad (7.2)$$

Next, we make the substitution $(-1)^m p_m = \chi_m$ which leads to

$$\omega_0 \chi_m - i\gamma_{1D} \sum_{n=1}^N \chi_n \equiv -i\gamma_{1D} \Lambda = \omega \chi_m, \quad m = 1, 2 \dots N, \quad \Lambda = \sum_{n=1}^N \chi_n. \quad (7.3)$$

The same equations describe the systems with $d = 0, \lambda, 2\lambda \dots$. Next, we can sum the equation (7.3) over m :

$$(\omega + i\gamma_{1D}N - \omega_0)\Lambda = 0. \quad (7.4)$$

From this we find that if $\Lambda \neq 0$ than $\omega = \omega_0 - i\gamma_{1D}N$. For the solution with $\omega = \omega_0 - i\gamma_{1D}N$ we find from Eq. (7.3) that all χ_m are the same. For the solution with $\Lambda = 0$ Eq. (7.3) means that $\omega = 0$. Hence, there is a symmetric solution of Eqs. (7.3) with

$$\chi_1 = \chi_2 = \dots \chi_N, \text{ and } \omega = \omega_0 - iN\gamma_{1D} \quad (7.5)$$

and $N - 1$ solutions with eigenfrequency $\omega = \omega_0$, where eigenvectors satisfying the condition

$$\sum_{n=1}^N \chi_n = 0, \text{ and } \omega = \omega_0. \quad (7.6)$$

The first solution demonstrates collective enhancement of the spontaneous emission rate, $-\text{Im } \omega = N\gamma_{1D}$. This is a Dicke superradiant mode: the radiative decay rate $N\gamma_{1D}$ for this mode grows proportionally to the number of emitters N . Such collective enhancement of the

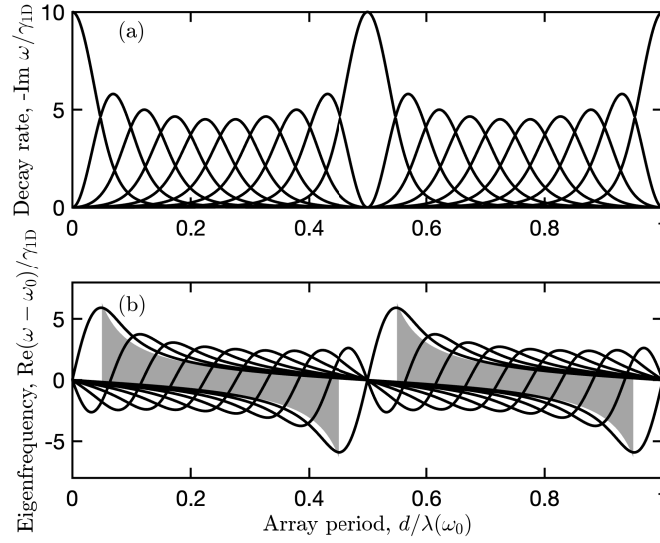


Figure 7.2: From Ref. [1]. Imaginary (a) and real (b) parts of the complex eigenfrequencies of the array of $N = 10$ atoms coupled to a waveguide depending on the period of the array d . Shaded areas (b) show the edges of the polariton band gaps. Each value of d/λ corresponds to $N = 10$ eigenvalues.

spontaneous decay rate is the most basic effect of dissipative interaction in the emitter arrays. All the other modes Eq. (7.6) have zero decay rates, and hence can be termed as dark modes. These super- and sub-radiant modes can be seen as generalization of the modes (5.32) for $N = 2$ emitters for the particular case of $\varphi = \pi$.

We now consider a more general case of arbitrary spacing. We plot in Fig. 7.2 the complex eigenfrequencies of Eq. (7.2) for $N = 10$. As already expected after examining the two-emitter case in Fig. 5.4, the eigenfrequencies for an array oscillate with the array period d . At $d = 0, \lambda_0/2, \lambda_0$ there is one superradiant state and $N - 1$ dark states. When the period is detuned from this condition, the dark states acquire nonzero decay rates.

How does this picture depend on N ? For the superradiant state, the answer is already known and trivial, $\omega = \omega_0 - iN\gamma_{1D}$. The scaling of the decay rates for subradiant states with N is less trivial. The answer can be found using the Fermi Golden rule, similar to the case of $N = 2$ emitters, considered in Sec. 5.5:

$$-2 \operatorname{Im} \omega = 2\pi \int_{-\infty}^{\infty} \frac{dk}{2\pi} |M_k|^2 \delta(\omega_0 - c|k|), \quad M_k = g \sum_{m=1}^N e^{ikdm} \psi_m. \quad (7.7)$$

Here, M_k is the matrix element of the interaction of the state ψ_m with photon with wave vector k , ω_0 is the emitter resonance frequency, d is the array period, g is the coupling constant. We



Figure 7.3: Schematics of the spatial profile of the most superradiant (left) and most subradiant modes (right).

can also rewrite the decay rate as

$$-2 \operatorname{Im} \omega = \frac{1}{c} M_0^2, \quad M_0 = g \sum_{m=1}^N e^{i\varphi m} \psi_m, \quad \varphi = \omega_0 d/c. \quad (7.8)$$

Let us now calculate the decay rate for the states with

$$\psi_m = \frac{1}{\sqrt{N}} \quad (\text{superradiant state}), \quad (7.9)$$

$$\psi_m = \sqrt{\frac{2}{N}} (-1)^m \sin \frac{\pi(m-1/2)}{N} \quad (\text{most subradiant state for } \omega_0 d/c \ll 1) \quad (7.10)$$

Here, we assume that $N \gg 1$. The states are illustrated in the Fig. 7.3. We have already proved that Eq. (7.9) is the eigenstate. We give here Eq. (7.10) for the subradiant state without proof. The derivation can be found in Ref. [2] and it can be also easily checked numerically that is the darkest state. It is also easy to see that Eq. (7.10) satisfies the condition $\sum_{m=1}^N \psi_m = 0$. The sign oscillations, described by the factor $(-1)^m$, lead to the destructive interference of the photon emission from different emitters and suppress the overall decay rate. We will present another qualitative argument for the solution Eq. (7.10) later in this chapter, when we will analyze the polariton dispersion in the periodic arrays. For the Dicke superradiant state, the decay rate calculation is trivial and yields $M_0 = g\sqrt{N}$ and $-2 \operatorname{Im} \omega = 2N\gamma_{1D}$. As expected, the radiative decay rate is enhanced $\propto N$ because of the constructive interference of the waves from different emitters. For the subradiant states, the calculation is slightly more involved: We first find

$$M_0 = -\frac{\sqrt{2} (e^{i\varphi} + e^{i\varphi(N+1)} - e^{iN\varphi} - 1)}{\sqrt{N} (e^{2i\varphi} + 2 \cos \frac{\pi}{N} e^{i\varphi} + 1)} \sin \frac{\pi}{2N}, \quad (7.11)$$

and then we expand this answer up to the linear terms in the small parameter φ . The result reads

$$M_0 = -\frac{ig\sqrt{2}\varphi}{4N^{3/2}}, \quad (7.12)$$

which results in the decay rate

$$-2 \operatorname{Im} \omega = \frac{\pi^2 (\omega_0 d/c)^2}{8N^3} \gamma_{1D} \text{ (most subradiant state) }, \quad (7.13)$$

where $\gamma_{1D} = g^2/c$. This answer can also be found in Ref. [2]. It means that the subradiant state becomes darker for larger N very quickly. The reason for such a quick suppression can be intuitively understood as follows. First, the state Eq. (7.10) oscillates with a π -phase difference between neighboring sites, which suppresses the light-matter coupling matrix element M_0 . Second, it is also close to zero at the border of the structure, see Fig. 7.3. Since the radiative decay goes through the edges of the array, this state kind of stays away from the edges, which gives an extra power of N in denominator. One can quickly check this by calculating the decay rate for example for a simpler trial function of $\psi_n = (-1)^n/\sqrt{N}$, that will be parametrically larger. It has been proved in Ref. [3] that such $1/N^3$ scaling of the radiative decay rate is universal. In special cases of arrays with tailored dispersion, the decay rate can decrease with N even faster; see the review [1] and references therein.

7.2 Transfer matrix method

7.2.1 General approach

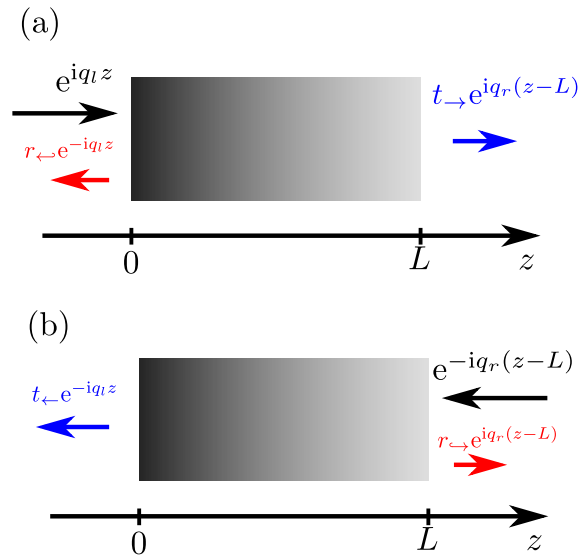


Figure 7.4: Definition of reflection coefficients r_{\leftarrow} , r_{\rightarrow} and transmission coefficients t_{\rightarrow} , t_{\leftarrow} of light, incident upon the scatterer with length L from left (a) and right (b) half-spaces, respectively.

The approaches, presented above, were suitable either for just several emitters, or for periodic arrays. It is instructive to present one more method, the transfer matrix method, that

is suitable for both periodic and nonperiodic structures of arbitrary length. It also allows for a very efficient numerical implementation.

Let us consider the scattering of light on a general object, see Fig. 7.4. The electric field to the left and to the right of the object can be presented as a linear combination of right-propagating (E_{\rightarrow}) and left-propagating (E_{\leftarrow}) waves:

$$E(z) = \begin{cases} E_{\text{left},\rightarrow}^+ e^{iq_l z} + E_{\text{left},\leftarrow}^- e^{-iq_l z} & (z < 0) \\ E_{\text{right},\rightarrow}^+ e^{iq_r(z-L)} + E_{\text{right},\leftarrow}^- e^{-iq_r(z-L)} & (z > L) \end{cases}, \quad (7.14)$$

where $q_{r,l}$ are light wave vectors from the left and from the right of the scatterer. Now we introduce the 2×2 matrix T , that relates the plane wave amplitudes by

$$\begin{pmatrix} E_{\text{right},\rightarrow} \\ E_{\text{right},\leftarrow} \end{pmatrix} = T \begin{pmatrix} E_{\text{left},\rightarrow} \\ E_{\text{left},\leftarrow} \end{pmatrix}. \quad (7.15)$$

The beauty of the transfer matrix method is the easiness with which it can be applied to an array of scatterers $1, 2, \dots, N$, characterised by their individual transfer matrices $T_1 \dots T_N$. Equation (7.15) can be just applied in a cascaded way: we express the field after the N -th scatterer via the field between scatterers N and $N-1$, the field between scatterers N and $N-1$ via the field between scatterers $N-1$ and $N-2$ and so on until the field before the first scatterer. Formally, this just means the product of the transfer matrices:

$$T_{\text{tot}} = T_N T_{N-1} \dots T_2 T_1, \quad (7.16)$$

the matrix through the whole array is given by a product of the matrices of the individual scatterers, taken in reverse order, from the last one to the first one. So we are now in position to find this total transfer matrix T . How do we use it for something useful, such as reflection and transmission coefficients through the structure?

To this end, we just rewrite the transfer matrix definition. If the wave with unitary amplitude is incident from the left and propagates to the right, so that $E_{\text{left},\rightarrow} = 1$ and $E_{\text{left},\leftarrow} = 0$, we have

$$T \begin{pmatrix} 1 \\ r_{\leftarrow} \end{pmatrix} = \begin{pmatrix} t_{\rightarrow} \\ 0 \end{pmatrix}, \quad (7.17)$$

where r_{\leftarrow} is the reflection coefficient and t_{\rightarrow} is the left-to-right (or forward) transmission coefficient. At the same time, for the wave incident from the right, and propagating to the left, we find

$$T \begin{pmatrix} 0 \\ t_{\rightarrow} \end{pmatrix} = \begin{pmatrix} r_{\leftarrow} \\ 1 \end{pmatrix}. \quad (7.18)$$

where r_{\leftarrow} and t_{\rightarrow} are the corresponding reflection and transmission coefficients. It is straightforward to check, that the conditions Eq. (7.35), Eq. (7.18) are satisfied by the transfer matrix

$$T = \frac{1}{t_{\leftarrow}} \begin{pmatrix} t_{\rightarrow}t_{\leftarrow} - r_{\leftarrow}r_{\rightarrow} & r_{\leftarrow} \\ -r_{\leftarrow} & 1 \end{pmatrix}. \quad (7.19)$$

We note here, that in mirror-symmetric structure $r_{\leftarrow} = r_{\rightarrow}$. Moreover, as has been already mentioned in Sec. 5.1, when time-reversal symmetry holds (which is even in the presence of nonradiative losses), one has $t_{\rightarrow} = t_{\leftarrow}$. In this case, the transfer matrix is unimodular, $T = 1$.

In turn, this allows us to find reflection and transmission coefficients given the transfer matrix:

$$r_{\leftarrow} = -\frac{T_{2,1}}{T_{2,2}}, \quad t_{\rightarrow} = \frac{1}{T_{2,2}}. \quad (7.20)$$

We will now demonstrate the transfer matrix method's strength for the emitters array. To this end, we will need two ingredients, the matrix that describes the propagation between the emitters for a distance d and the matrix that describes the scattering. The free propagation matrix is given by

$$T_{\text{free}} = \begin{pmatrix} e^{iqd} & 0 \\ 0 & e^{-iqd} \end{pmatrix} \quad (7.21)$$

is the transfer matrix for the free waveguide propagation in the basis of propagating waves, where $q = \omega/c$. It is diagonal, so there is no wave scattering, and the right- and left-going waves acquire the same phase qd , see also Eqs. (7.15). In order to describe scattering on a single emitter, we use the reflection and transmission coefficients from Eq. (3.12) in Eq. (7.19); $r_{\leftarrow} = r_{\rightarrow} = r$ and $t_{\rightarrow} = t_{\leftarrow} = t$. The result reads

$$T_{\text{res}} = \frac{1}{t} \begin{pmatrix} t^2 - r^2 & r \\ -r & 1 \end{pmatrix}, \quad r = \frac{i\gamma_{\text{1D}}}{\omega_0 - \omega - i(\gamma_{\text{1D}} + \gamma)}, \quad t = 1 + r. \quad (7.22)$$

is the resonant matrix of a scatterer. Armed with Eq. (7.22), Eq. (7.21), the cascaded product

rule Eq. (7.16), we can now calculate the transfer matrix through the arbitrary array and then find its reflection and transmission coefficients from Eq. (7.20). In periodic arrays, this calculation can also be done analytically, as we will show in the next section.

7.3 Polariton dispersion

In a periodic array of emitters, the scattering on each unit cell will be characterized by the transfer matrix

$$T = T_{\text{free}} T_{\text{res}} \quad (7.23)$$

where T_{free} and T_{res} were derived in the previous section and are given by Eq. (7.21) and Eq. (7.22). In particular, this means that the waves before and after the n -th emitter are related by

$$\begin{pmatrix} E_{n+1}^+ \\ E_{n+1}^- \end{pmatrix} = T \begin{pmatrix} E_n^+ \\ E_n^- \end{pmatrix}. \quad (7.24)$$

On the other hand, we can use the Floquet-Bloch theorem, that states that in translationally periodic structure the eigenstates are periodic with the lattice spacing up to the phase factor:

$$\begin{pmatrix} E_{n+1}^+ \\ E_{n+1}^- \end{pmatrix} = \exp(iK) \begin{pmatrix} E_n^+ \\ E_n^- \end{pmatrix}, \quad (7.25)$$

where K is the quasimomentum. For simplicity, we have absorbed the period of the structure into the definition of K . Hence, the $\exp(iK)$ is the eigenstate of the transfer matrix and we can find it from the characteristic equation

$$\det \begin{pmatrix} T_{11} - e^{iK} & T_{12} \\ T_{21} & T_{22} - e^{iK} \end{pmatrix} = 0 \quad (7.26)$$

This yields a quadratic equation

$$e^{2iK} - 2e^{iK} \text{Tr } T + \det T = 0, \quad (7.27)$$

which, given that $\det T = 1$, can be rewritten as

$$\cos K = \frac{1}{2} \text{Tr } T. \quad (7.28)$$

For the periodic array of emitters we can use Eq. (7.22) and Eq. (7.21) to find

$$\cos K = \cos qd - \frac{\sin qd \gamma_{1D}}{\omega_0 - \omega - i\gamma}. \quad (7.29)$$

This answer has been obtained in [4] for the array of quantum wells. Equation (7.29) has an interesting property: the radiative decay rate, present in the resonant denominators in Eq. (7.22), has disappeared from the denominator in the second term. In another words, for $\gamma = 0$ the right-hand side of Eq. (7.29) is purely real, there is no radiative decay term! This has a deep physical meaning: there is no radiative decay in the infinite array of emitters in the infinite periodic waveguide. In a finite array, the radiative decay occurs through the emission through the edges. However, an infinite array has no edge! Every emitted photon will eventually be reabsorbed, the emitted again by another emitter, and so on. Such a cascade of emission and reabsorption events lead to a formation of a hybrid polariton wave, that in the ideal periodic structure does not exhibit any radiative decay. This result is known since the beginning of the XX-th century as the Ewald-Oseen cancellaton theorem (it means cancellation of the radiative decay) [5]. Here we encountered a particular manifestation of this theorem for resonant one-dimensional structures.

The dispersion law Eq. (7.29) can also be obtained strtaight from Eqs. (7.1), without resorting to the transfer matrix method. Because of the translational symmetry, we can look for the solution of Eqs. (7.1) for $N \rightarrow \infty$ in the form

$$\psi_m = \psi_0 e^{iKm}. \quad (7.30)$$

Next, we set $m = 0$, $\psi_0 = 1$ and obtain the equation

$$(\omega_0 - \omega) - i\gamma_{1D} \sum_{n=-\infty}^{\infty} e^{i\varphi|n|+iKn} = 0. \quad (7.31)$$

The series can be evaluated as

$$\sum_{n=-\infty}^{\infty} e^{i\varphi|n|+iKn} = \left(\sum_{n=0}^{\infty} + \sum_{n=-\infty}^{-1} \right) e^{i\varphi|n|+iKn} = \frac{1}{1 - \exp[i(\varphi + K)]} + \frac{\exp[i(\varphi - K)]}{1 - \exp[i(\varphi - K)]}.$$

Substituting the result into Eq. (7.31) we can recover Eq. (7.29).

We have plotted the dispersion law $K(\omega)$ in Fig. 7.5. Thick curves present two polariton

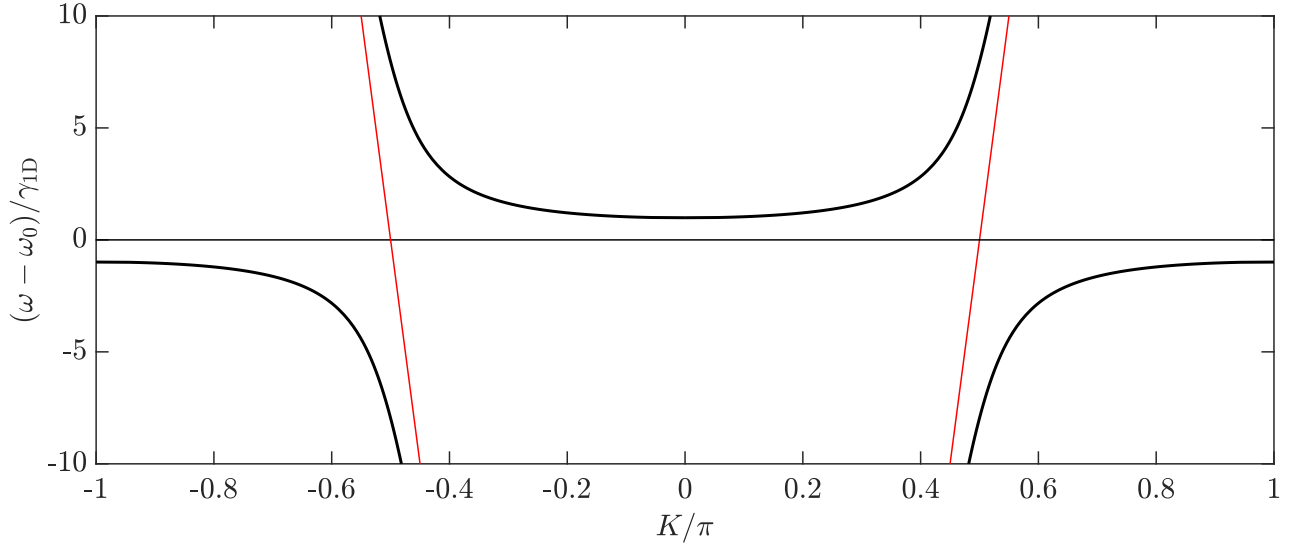


Figure 7.5: Dispersion law in the array of emitters. Calculation has been performed for $\varphi = 0.15\pi$ and $\gamma_{1D}/\omega_0 = 10^{-2}$.

dispersion branches, the upper one and the lower one, that are separated by the avoided crossings at $K = \pm\varphi \equiv \pm\omega_0 d/c$. This avoided crossings occur between the light dispersion curve (shown by thin red lines) and the atomic resonance at $\omega = \omega_0$. They lead to the formation of the polariton band gap between the upper and lower dispersion branches: this is the spectral region without solutions with real K , corresponding to $(\omega - \omega_0)/\gamma_{1D} = [0 \dots 4]$ for the parameters of Fig. 7.5. Any wave, incident upon the infinite array in this spectral range, will be fully reflected. In X-ray physics, this region is also termed as Reststrahlenband. The now-familiar Markovian approximation would mean disregarding the frequency dependence of the phase factors qd in Eq. (7.29); $qd \rightarrow q_0 d = \varphi \equiv \omega_0 d/c$. In this approximation the light dispersion lines in Fig. 7.5 would be vertical, since this it corresponds to assuming infinite slope, given by the speed of light.

Equation Eq. (7.29) can be further simplified when the emitters are close to each other, so that the phase factors $K \ll 1$, $qd = \omega d/c \ll 1$ are small. We can then approximate $\cos K$ as $1 - K^2/2$ and $\sin qd$ as qd . The result assumes the form

$$K^2 = \left(\frac{\omega d}{c} \right)^2 \varepsilon_{\text{eff}}(\omega) \quad (7.32)$$

where

$$\varepsilon_{\text{eff}}(\omega) = 1 + \frac{2\gamma_{1D}}{(\omega_0 - \omega)} \frac{c}{\omega d}. \quad (7.33)$$

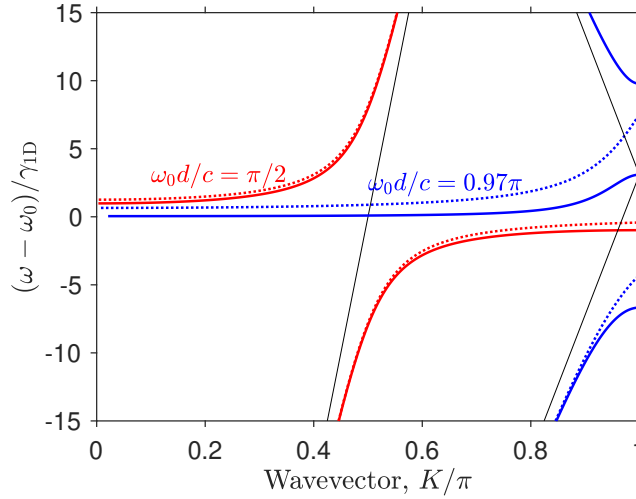


Figure 7.6: Dispersion law in the array of emitters. Calculation has been performed for $\omega_0 d/c = 0.5\pi$ and $\omega_0 d/c = 0.97\pi$ (take $\gamma_{1D}/\omega_0 = 10^{-2}$).

The form of Eq. (7.32) is the same as the form of the light dispersion law in the homogeneous structure with the permittivity $\varepsilon_{\text{eff}}(\omega)$. Thus, the function $\varepsilon_{\text{eff}}(\omega)$ is termed as an effective permittivity. The second resonant factor in the permittivity is proportional to λ/d , that is, it is enhanced with the density of emitters in the array. Similarly to the original dispersion equation, the effective permittivity does not contain γ_{1D} term in the resonant denominator.

We compare in Fig. 7.6 the dispersion curves calculated from Eq. (7.29) and in the effective medium approximation for two values of the array period. Surprisingly, the effective medium approximation works well even for a large period $\omega_0 d/c = 0.5\pi$, see the red curves. However, it fails to a close-to-Bragg period, $\omega_0 d/c = 0.97\pi$. The solid dispersion curves show an additional band gap that is missed in the effective medium approximation. The effective medium approximation also allows us to estimate the transmission coefficient through the structure as $|t_N|^2 \propto \exp -2N \text{Im } K$. We can evaluate $\text{Im } K$ from Eq. (7.32) and Eq. (7.33) assuming that the second term in Eq. (7.33) is much smaller than unity. The result is

$$|t_N(\omega)|^2 = e^{-\text{OD}}, \quad \text{OD} = \frac{2N\gamma\gamma_{1D}}{(\omega - \omega_0)^2 + \gamma^2}. \quad (7.34)$$

where OD is the so-called optical density. The spectral dependence of the OD is just a Lorentzian, centered at the resonance frequency. Importantly, the linewidth of the Lorentzian is determined solely by the nonradiative decay.

Figure 7.7 compares the transmission coefficient calculated numerically (solid curves) and analytically following Eq. (7.34) (dashed curves). One can see that the effective medium

approximation works well for large values of γ (panel b), but fails for $\gamma \ll \gamma_{1D}$.

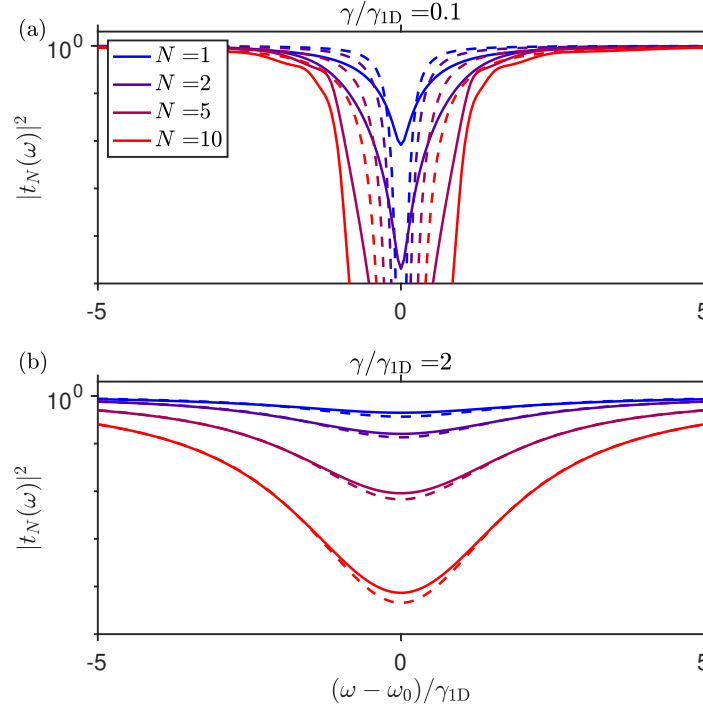


Figure 7.7: Transmission spectra from the periodic structure for different values of N . Calculation has been performed for the spacing $\omega_0 d/c = \pi$, $\gamma_0/\omega_0 = 2 \times 10^{-2}$ and $\gamma/\gamma_{1D} = 0.1$ (a), $\gamma/\gamma_{1D} = 2$ (b). Solid lines have been calculated exactly, dotted lines correspond to the optical density approximation, Eq. (7.34). The calculation demonstrates that the OD approximation works well for a large ratio γ/γ_{1D} .

7.3.1 Reflection and transmission from a periodic structure

In the previous section we found the light dispersion in a periodic array. Now, we can also find analytically reflection and transmission coefficients for a periodic array. We start again with the transfer matrix through one period of the structure, written in the form

$$T = \frac{1}{t_1} \begin{pmatrix} t_1^2 - r_1^2 & r_1 \\ -r_1 & 1 \end{pmatrix}, \quad (7.35)$$

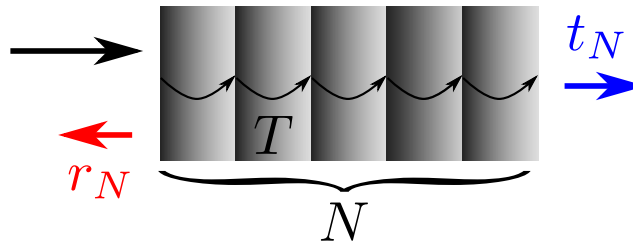


Figure 7.8: Schematics of light reflection and transmission from a structure with N scatterers.

(see also (7.22)). The eigenvalues of the transfer matrix are given by $\exp(\pm iK)$ with $2 \cos K = \text{Tr } T$. Now we will also need the the eigenvectors of the transfer matrix $C_{1,2}$ that are defined as $TC_{1,2} = e^{\pm iK}C_{1,2}$. Using the explicit transfer matrix definition we find

$$C_{1,2} = \begin{pmatrix} 1 \\ a_{1,2} \end{pmatrix}, \quad a_{1,2} = \frac{r}{1 - te^{\pm iK}}. \quad (7.36)$$

Next, we use the boundary conditions. On the left of the structure, the field amplitudes are given by $E_L = \begin{pmatrix} 1 \\ r_N \end{pmatrix}$ and on the right side the field amplitudes are $E_R = \begin{pmatrix} t_N \\ 0 \end{pmatrix}$. The transfer matrix connects fields on the left and on the right

$$T^N E_L = E_R. \quad (7.37)$$

In order to calculate T^N we expand the electric field in terms of the eigenvectors $C_{1,2}$,

$$E_L = C_1 f_1 + C_2 f_2, \quad f_1 = -\frac{a_2 - r_N}{a_1 - a_2}, \quad f_2 = \frac{a_1 - r_N}{a_1 - a_2}. \quad (7.38)$$

Next, we can write

$$E_R = T^N E_L = C_1 e^{iKN} f_1 + C_2 e^{-iKN} f_2. \quad (7.39)$$

Since $E_R = \begin{pmatrix} t_N \\ 0 \end{pmatrix}$ we find

$$f_1 = -\frac{a_2 t_N e^{-iKN}}{a_1 - a_2}, \quad f_2 = \frac{a_1 t_N e^{iKN}}{a_1 - a_2}. \quad (7.40)$$

Combining Eq. (7.40) and Eq. (7.38) and solving them for r_N , t_N we obtain analytical expressions for the reflection and transmission coefficients.

$$r_N = \frac{r_1 \sin(NK)}{\sin(NK) - t_1 \sin[(N-1)K]}, \quad t_N = \frac{t_1 \sin K}{\sin(NK) - t_1 \sin[(N-1)K]}. \quad (7.41)$$

7.4 Bragg-spaced arrays

When analysing Fig. 7.6 in the previous section, we have already seen that the effective medium approximation fails for $\omega_0 d/c$ close to π (or, in another words, period d close to $\lambda(\omega_0)/2$). Indeed, the situation when the atomic resonance frequency and array period d satisfy or are

close to the resonant Bragg condition,

$$d = \frac{m}{2}\lambda(\omega_0), \quad m = 1, 2, \dots, \quad (7.42)$$

deserves a special attention. In this case, the incident wave exhibits not only resonant reflection from each individual atom, but also the Bragg diffraction: waves reflected from different atoms interfere constructively.

Bragg diffraction in arrays of resonant scatterers has been studied in very different setups. Probably, historically the first platform is presented by natural crystals, such as iron, where sharp resonances with the widths on the order of neV exist for γ -rays ($\hbar\omega \approx 14$ keV) exhibiting Mössbauer scattering on the nuclei. Such crystals are experimentally studied since the 1960s, see the reviews Refs. [6, 7]. One has also considered artificial Bragg lattices for γ -rays, made from alternating layers of different isotopes [8]. This field has recently experienced a lot of progress [9–12] with the advent of high-brilliance synchrotron radiation sources, see also a review [13]. While initially the researchers have mainly studied the angular dependence of the reflectivity instead of its spectral properties [8], modern technologies have enabled high-resolution spectroscopic demonstration of Bragg reflection from nuclear multilayers [14]. In the 1990s, it has been independently proposed to use Bragg-spaced lattices of semiconductor quantum wells [15, 16] and optical lattices of cold atoms [17] for light. Some other examples of Bragg-spaced lattices with resonant scatterers include ring resonators [18], metallic gratings with plasmonic resonances [19] and dielectric cylinders with Mie resonances [20]. A detailed comparison between cold atom systems, semiconductor lattices and Mössbauer isotopes can be found in the review [21]. It has also been theoretically suggested to consider Bragg lattices of atoms [22] and superconducting qubits coupled to the waveguide [23]. The modification of Bragg conditions for scattering of light from an array of atoms into the guided modes of a waveguide has been analyzed in Ref. [24]. Large Bragg reflection from atomic arrays trapped near a one-dimensional waveguide have already been demonstrated experimentally in the groups of J. Laurat [25] and E. Polzik [26].

In order to see the enhancement of the reflection under the Bragg condition, we plot in Fig. 7.9 the reflection spectra depending on the ratio $d/\lambda(\omega_0)$. The calculation shows two ranges with large reflection coefficient, corresponding to the two band gaps, where the reflection coefficient is large (these are the same band gaps as in Fig. 7.6 and in Fig. 7.10). As expected,

the band gap width increases when the array period approaches the resonant Bragg condition Eq. (7.42).

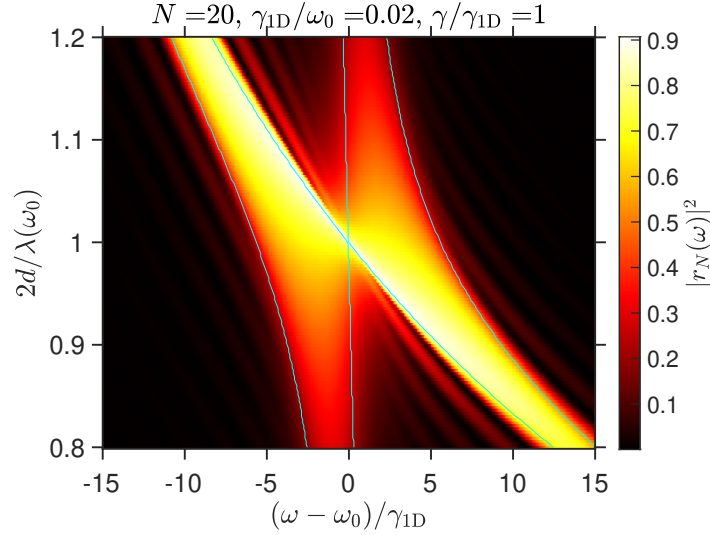


Figure 7.9: Reflection coefficient from a resonant periodic structure vs period. Calculated for $N = 20$, $\gamma_{1D}/\omega_0 = 10^{-2}$, $\gamma = \gamma_{1D}$.

To gain more quantitative insight, we examine the polariton dispersion law in the close-to-Bragg regime in Fig. 7.10. Figures 7.10(a),(b),(c) present the polariton dispersion law $\omega(K)$ calculated for the periods close to the Bragg value for $m = 1$. The first panel corresponds to the situation when the period is smaller than the Bragg value. The dispersion features two band gaps: the polariton band gap below the atomic resonance (we have already seen in the effective medium approximation), and the photonic band gap at the frequency satisfying the Bragg condition $\omega d/c = \pi$. Figure 7.10(c) presents an opposite scenario where the Bragg band gap is located below the polariton one. In the Bragg case, illustrated in Fig. 7.10(b), the two band gaps fuse with each other and form a wide Bragg polariton band gap around the atomic resonance.

The polariton dispersion law Eq. (7.29) in the vicinity of the resonance can be approximately described by the following equation

$$\frac{Kd}{\pi} - 1 = \pm \sqrt{\left(\frac{\omega - \omega_0}{\omega_0}\right)^2 - \left(\frac{\Delta_{\text{Bragg}}}{\omega_0}\right)^2}, \quad (7.43)$$

where Δ_{Bragg} is the half-width of the polariton band gap

$$\Delta_{\text{Bragg}} = \sqrt{\frac{2\gamma_{1D}\omega_0}{\pi}}. \quad (7.44)$$

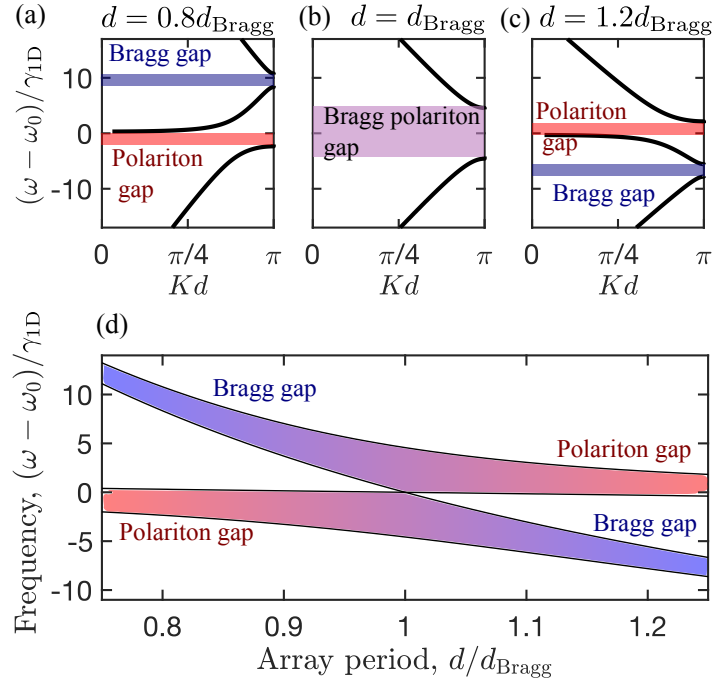


Figure 7.10: Reproduced from [1]. Polaron dispersion in the atomic arrays with different periods. Panels (a,b,c) correspond to three different values of d/d_{Bragg} , indicated in the graph. Bragg and polariton band gaps are indicated. Panel (d) shows the dependence of the band gap positions on the period of the array. Calculation has been performed for $\gamma_{1D}/\omega_0 = 0.03$ and $\gamma = 0$.

The gap half-width Δ_{Bragg} exceeds the radiative linewidth of the atomic resonance of γ_{1D} by the large factor $\sim \sqrt{\omega_0/\gamma_{1D}}$. Hence, the light incident upon the Bragg-spaced array will exhibit a strong reflection in the wide spectral range $\omega_0 - \Delta_{\text{Bragg}} < \omega < \omega_0 + \Delta_{\text{Bragg}}$. However, this Bragg band gap will be manifested in reflection only if the number of atoms of the array is large enough, exceeding

$$N^* \sim \frac{1}{m} \sqrt{\omega_0/\gamma_{1D}}. \quad (7.45)$$

Indeed, the phase gained by light between two atoms in the Bragg-spaced array is an integer multiple of π . So, at the first glance, the distance does not matter and the Bragg-spaced array is equivalent to the array with $d = 0$. This results in the reflection coefficient

$$r_N(\omega) = \frac{iN\gamma_{1D}}{\omega_0 - \omega - i(\gamma + N\gamma_{1D})}, \quad (7.46)$$

with the collectively enhanced radiative decay rate $N\gamma_{1D}$. Equation (7.46) could be formally obtained from (7.41) replacing $\sin(N-1)K/\sin K$ by $-(N-1)/N$, which is valid for $K \approx \pi$. Such approximation corresponds to a single collective superradiant mode contributing to the light reflection. However, such superradiant approximation assumes the validity of the

Markovian approximation when the time of flight of photons through the array Nd/c is smaller than the inverse lifetime of the superradiant mode $1/(N\gamma_{1D})$. When the total length of the structure exceeds the wavelength in $\sim \sqrt{\omega_0/\gamma_{1D}}/m$ times, as specified by Eq. (7.45), the time of flight of photons can no longer be ignored [27] and the waveguide-mediated interaction between the atoms stops being instantaneous. Namely, for $N \gg \frac{1}{m}\sqrt{\omega_0/\gamma_{1D}}$ the reflection coefficient is close to unity inside the Bragg band gap and quickly decays outside the gap, see Fig. 7.11.

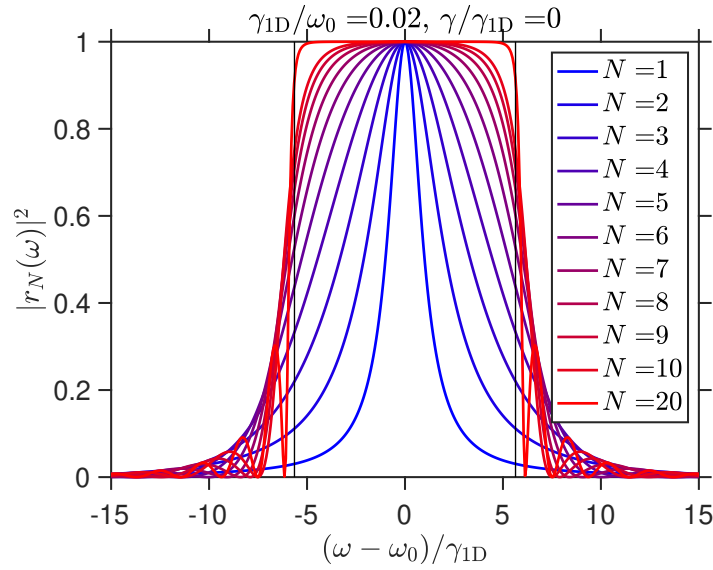


Figure 7.11: Reflection spectra for a resonant periodic structure for different values of N . Vertical lines show the edges of the polariton band gap $\omega - \omega_0 = \pm \sqrt{2\gamma_0\omega_0/\pi}$.

7.5 Borrmann effect

It is instructive to consider light propagation through thick absorbing Bragg structures, with large N and $\gamma \gg \gamma_{1D} \gg \Delta_{\text{Bragg}}$. Figure 7.12 compares transmission, reflection and absorption spectrum. We also plot in Fig. 7.12(a) by dashed curves the effective medium result Eq. (7.34). Surprisingly, the effective medium approximation works quite well despite the large spacing between the emitters. It correctly predicts the Lorentzian dip in the transmission coefficient. However, it fails to grasp the sharp transmission peak, centered at ω_0 . The same peak is also manifested by a sharp dip in the absorption spectrum in Fig. 7.12(c). Thus, right at the resonance, the Bragg structure transmits light better and absorbs light less than what could be expected from the naive effective medium approximation.

The origin of this phenomenon is the so-called Borrmann effect, first discovered experi-

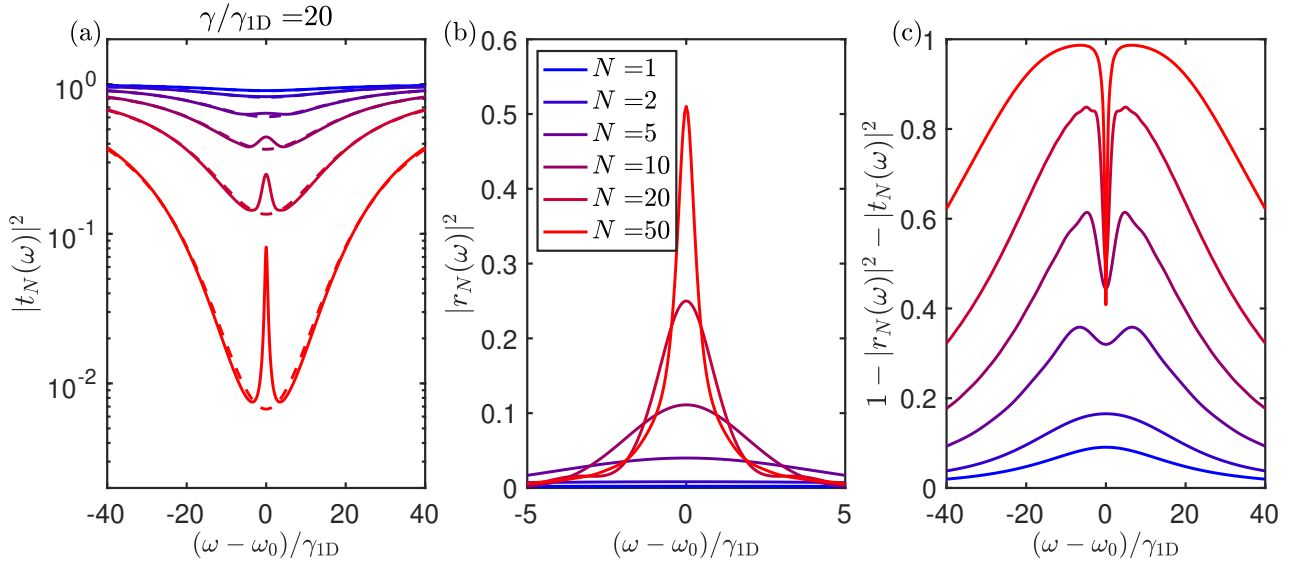


Figure 7.12: Transmission (a), reflection (b) and absorption (c) spectra for a resonant periodic structure for different values of N . Calculation has been performed for $\gamma/\gamma_{1D} = 20$ and $\gamma_{1D}/\omega_0 = 2 \times 10^{-2}$.

mentally as anomalously high transmission of X-rays through natural crystals [28]. In the considered system, right at the frequency ω_0 the light forms a standing wave, and the nodes of this wave are centered at the emitter position [29]. As such, there is less incident field at the emitters, and hence there is less light absorption and more transmission. To demonstrate this, we plot in Fig. 7.13 the electric field distribution at resonance (a) and off-resonance (b) for the wave, incident from the left. The calculation has been done by the transfer matrix method:

$$E(z_n < z < z_{n+1}) = E_{n+1}^+ e^{iq(z-z_n)} + E_{n+1}^- e^{-iq(z-z_n)}, \quad \begin{pmatrix} E_{n+1}^+ \\ E_{n+1}^- \end{pmatrix} = T^n \begin{pmatrix} 1 \\ r_N(\omega) \end{pmatrix}. \quad (7.47)$$

It is clear, that in the resonant case (a) the standing wave is formed, that decays with distance much slower. The Borrmann effect can be seen as one of the first experimental confirmations of the *dynamical diffraction theory*, that predicts the standing wave formation. The detailed analysis and closed-form analytical expressions for the absorption dip in the emitter array due to the Borrmann effect could be found in [30].

Such an anomalous transmission effect also exists in nonresonant systems, for example, a stack of layers ABABAB... with different refractive indices. It is most prominent if the layers A are much thinner than the layers B, and if only layers A are absorbing. Then there will be a characteristic peak in the transmission spectrum at the edge of the photonic band gap, where the field nodes are centered in the layers A.

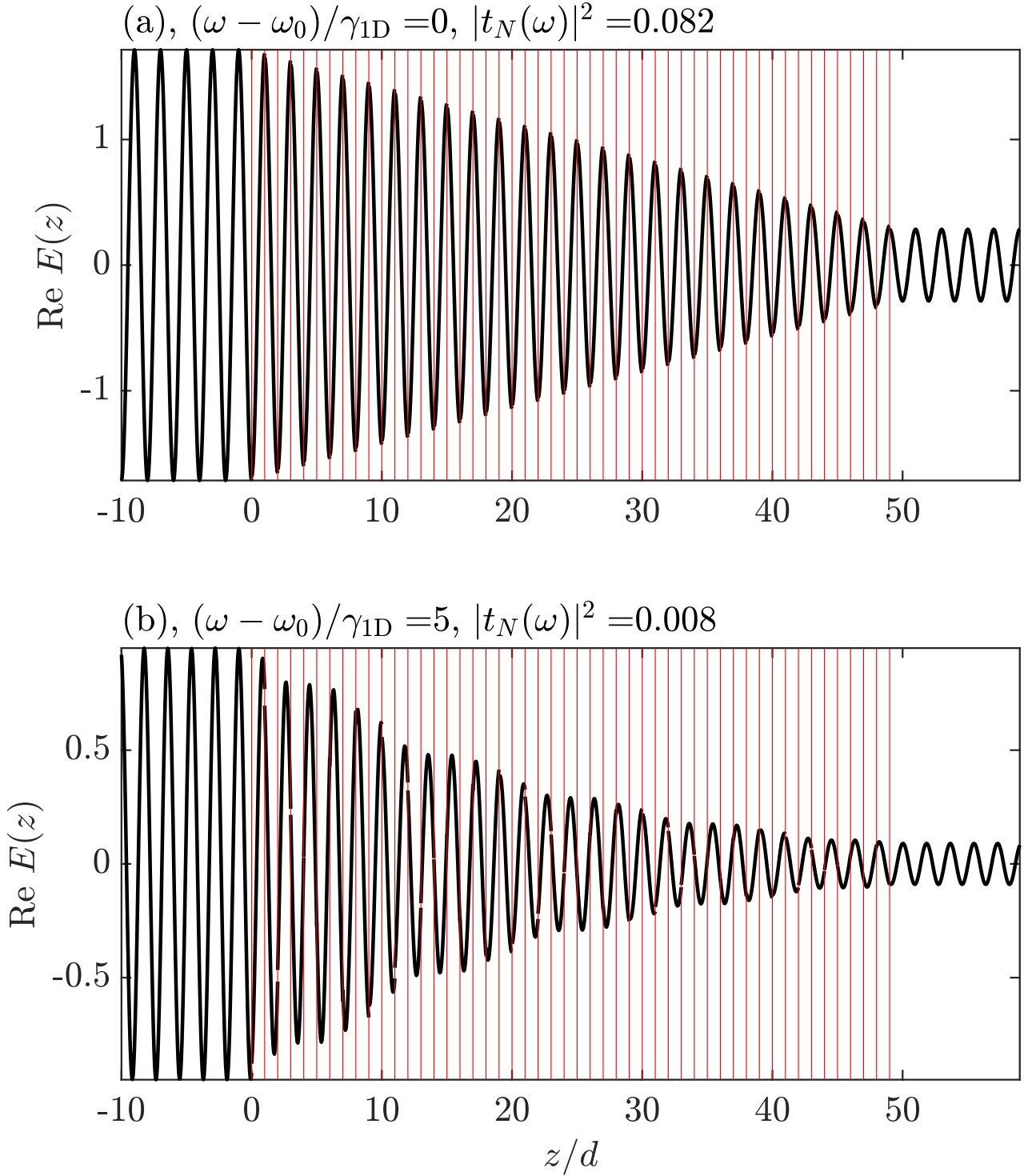


Figure 7.13: Electric field distribution at resonance (a) and off-resonance (b), showcasing the Borrmann effect. The frequencies and field transmission coefficients are indicated on the plot. Thin vertical lines show the emitter positions. Calculation has been performed for $N = 50$, $\gamma/\gamma_{1D} = 20$ and $\gamma_{1D}/\omega_0 = 2 \times 10^{-2}$.

7.6 Summary

To summarize, in this chapter we have learned about collective super- and sub-radiate modes of the arrays with multiple emitters and we have also learned how to calculate their reflection

and transmission coefficients. Another important concept we introduced has been the dispersion of the collective polaritonic modes $K(\omega)$: the band gaps of the dispersion correspond to the maxima of the reflection coefficient. The band gaps can arise due to the resonance at the atomic resonance frequency, due to the Bragg diffraction in a periodic lattice, and due to the interplay of these two effects as well. The latter happens in periodic resonant Bragg structures, where the Bragg condition is satisfied at the resonant frequencies of the emitters. Bragg structures show especially strong reflection and also non-Markovian features in their collective eigenmodes.

7.7 Additional reading

Photonic crystals: J. D. Joannopoulos et al., *Photonic crystals. Molding the flow of light*. (Princeton University Press, 2008).

Review on periodic Bragg-spaced structures: A. Poddubny and E. Ivchenko, “Resonant diffraction of electromagnetic waves from solids (a review)”, [Phys. Solid State](#) **55**, 905–923 (2013).

Analytical results for subradiant states in emitter arrays M. R. Vladimirova et al., “Exciton polaritons in long-period quantum-well structures”, *Semiconductors* **32**, 90–95 (1998).

Subradiant states in arrays of emitters: Y.-X. Zhang and K. Mølmer, “Theory of subradiant states of a one-dimensional two-level atom chain”, [Phys. Rev. Lett.](#) **122**, 203605 (2019)

Proposal of subradiant states for quantum memory: A. Asenjo-Garcia et al., “Exponential improvement in photon storage fidelities using subradiance and “selective radiance” in atomic arrays”, [Phys. Rev. X](#) **7**, 031024 (2017)

Non-Markovian effects and Borrmann effect in resonant Bragg structures A. V. Poshakinskiy and A. N. Poddubny, “Quantum Borrmann effect for dissipation-immune photon-photon correlations”, [Phys. Rev. A](#) **103**, 043718 (2021).

References

- ¹A. S. Sheremet, M. I. Petrov, I. V. Iorsh, A. V. Poshakinskiy, and A. N. Poddubny, “Waveguide quantum electrodynamics: collective radiance and photon-photon correlations”, [Rev. Mod. Phys.](#) **95**, 015002 (2023).
- ²Y.-X. Zhang and K. Mølmer, “Theory of subradiant states of a one-dimensional two-level atom chain”, [Phys. Rev. Lett.](#) **122**, 203605 (2019).
- ³Y.-X. Zhang and K. Mølmer, “Subradiant emission from regular atomic arrays: universal scaling of decay rates from the generalized bloch theorem”, [Phys. Rev. Lett.](#) **125**, 253601 (2020).
- ⁴E. L. Ivchenko, “Excitonic polaritons in periodic quantum-well structures”, *Sov. Phys. Sol. State* **33**, 1344–1346 (1991).
- ⁵M. Born and E. Wolf, *Principles of optics: electromagnetic theory of propagation, interference and diffraction of light* (Elsevier, 2013).

- ⁶Y. Kagan, “Theory of coherent phenomena and fundamentals in nuclear resonant scattering”, *Hyperfine Interactions* **123**, 83–126 (1999).
- ⁷J. Hannon and G. Trammell, “Coherent γ -ray optics”, *Hyperfine Interactions* **123**, 127–274 (1999).
- ⁸A. I. Chumakov, G. V. Smirnov, A. Q. R. Baron, J. Arthur, D. E. Brown, S. L. Ruby, G. S. Brown, and N. N. Salashchenko, “Resonant diffraction of synchrotron radiation by a nuclear multilayer”, *Phys. Rev. Lett.* **71**, 2489–2492 (1993).
- ⁹R. Röhlsberger, K. Schlage, B. Sahoo, S. Couet, and R. Rüffer, “Collective lamb shift in single-photon superradiance”, *Science* **328**, 1248–1251 (2010).
- ¹⁰R. Röhlsberger, H.-C. Wille, K. Schlage, and B. Sahoo, “Electromagnetically induced transparency with resonant nuclei in a cavity”, *Nature* **482**, 199–203 (2012).
- ¹¹J. Haber, X. Kong, C. Strohm, S. Willing, J. Gollwitzer, L. Bocklage, R. Rüffer, A. Pálffy, and R. Röhlsberger, “Rabi oscillations of x-ray radiation between two nuclear ensembles”, *Nature Photonics* **11**, 720–725 (2017).
- ¹²J. Haber, J. Gollwitzer, S. Francoual, M. Tolkiehn, J. Stremper, and R. Röhlsberger, “Spectral control of an x-ray L -edge transition via a thin-film cavity”, *Phys. Rev. Lett.* **122**, 123608 (2019).
- ¹³R. Röhlsberger and J. Evers, “Quantum optical phenomena in nuclear resonant scattering”, in *Topics in applied physics* (Springer Singapore, 2021), pp. 105–171.
- ¹⁴J. Haber, K. S. Schulze, K. Schlage, R. Loetzsch, L. Bocklage, T. Gurieva, H. Bernhardt, H.-C. Wille, R. Rüffer, I. Uschmann, G. G. Paulus, and R. Röhlsberger, “Collective strong coupling of x-rays and nuclei in a nuclear optical lattice”, *Nature Photonics* **10**, 445–449 (2016).
- ¹⁵E. L. Ivchenko, A. I. Nesvizhskii, and S. Jorda, “Bragg reflection of light from quantum-well structures”, *Phys. Solid State* **36**, 1156–1161 (1994).
- ¹⁶E. Ivchenko, A. Nesvizhskii, and S. Jorda, “Resonant bragg reflection from quantum-well structures”, *Superlattices and Microstructures* **16**, 17–20 (1994).
- ¹⁷I. H. Deutsch, R. J. C. Spreeuw, S. L. Rolston, and W. D. Phillips, “Photonic band gaps in optical lattices”, *Phys. Rev. A* **52**, 1394–1410 (1995).
- ¹⁸M. F. Yanik, W. Suh, Z. Wang, and S. Fan, “Stopping Light in a Waveguide with an All-Optical Analog of Electromagnetically Induced Transparency”, *Phys. Rev. Lett.* **93**, 233903 (2004).

- ¹⁹R. Taubert, D. Dregely, T. Stroucken, A. Christ, and H. Giessen, “Octave-wide photonic band gap in three-dimensional plasmonic Bragg structures and limitations of radiative coupling”, [Nat. Comm. **3**, 691 \(2012\)](#).
- ²⁰M. V. Rybin, D. S. Filonov, K. B. Samusev, P. A. Belov, Y. S. Kivshar, and M. F. Limonov, “Phase diagram for the transition from photonic crystals to dielectric metamaterials”, [Nature Communications **6**, 10102 \(2015\)](#).
- ²¹A. Poddubny and E. Ivchenko, “Resonant diffraction of electromagnetic waves from solids (a review)”, [Phys. Solid State **55**, 905–923 \(2013\)](#).
- ²²H. R. Haakh, S. Faez, and V. Sandoghdar, “Polaritonic normal-mode splitting and light localization in a one-dimensional nanoguide”, [Phys. Rev. A **94**, 053840 \(2016\)](#).
- ²³Y. S. Greenberg, A. A. Shtygashev, and A. G. Moiseev, “Waveguide band-gap N -qubit array with a tunable transparency resonance”, [Phys. Rev. A **103**, 023508 \(2021\)](#).
- ²⁴B. Olmos, C. Liedl, I. Lesanovsky, and P. Schneeweiss, “Bragg condition for scattering into a guided optical mode”, [Phys. Rev. A **104**, 043517 \(2021\)](#).
- ²⁵N. V. Corzo, B. Gouraud, A. Chandra, A. Goban, A. S. Sheremet, D. V. Kupriyanov, and J. Laurat, “Large Bragg reflection from one-dimensional chains of trapped atoms near a nanoscale waveguide”, [Phys. Rev. Lett. **117**, 133603 \(2016\)](#).
- ²⁶H. L. Sørensen, J.-B. Béguin, K. W. Kluge, I. Iakoupov, A. S. Sørensen, J. H. Müller, E. S. Polzik, and J. Appel, “Coherent backscattering of light off one-dimensional atomic strings”, [Phys. Rev. Lett. **117**, 133604 \(2016\)](#).
- ²⁷A. V. Poshakinskiy, A. N. Poddubny, and S. A. Tarasenko, “Reflection of short polarized optical pulses from periodic and aperiodic multiple quantum well structures”, [Phys. Rev. B **86**, 205304 \(2012\)](#).
- ²⁸G. Borrmann, “Die Absorption von Röntgenstrahlen im Fall der Interferenz”, [Zeitschrift für Physik **127**, 297–323 \(1950\)](#).
- ²⁹A. V. Poshakinskiy and A. N. Poddubny, “Quantum Borrmann effect for dissipation-immune photon-photon correlations”, [Phys. Rev. A **103**, 043718 \(2021\)](#).
- ³⁰M. M. Voronov, E. L. Ivchenko, V. A. Kosobukin, and A. N. Poddubny, “Specific features in reflectance and absorbance spectra of one-dimensional resonant photonic crystals”, [Physics of the Solid State **49**, 1792–1802 \(2007\)](#).
- ³¹J. D. Joannopoulos, S. G. Johnson, J. N. Winn, and R. D. Meade, *Photonic crystals. Molding the flow of light*. (Princeton University Press, 2008).

REFERENCES

- ³²M. R. Vladimirova, E. L. Ivchenko, and A. V. Kavokin, “Exciton polaritons in long-period quantum-well structures”, *Semiconductors* **32**, 90–95 (1998).
- ³³A. Asenjo-Garcia, M. Moreno-Cardoner, A. Albrecht, H. J. Kimble, and D. E. Chang, “Exponential improvement in photon storage fidelities using subradiance and “selective radiance” in atomic arrays”, *Phys. Rev. X* **7**, 031024 (2017).

Chapter 8

Chiral light-matter interaction

So far, we have considered a symmetric situation, where an excited atom can emit a photon to the left into the waveguide and to the right into the waveguide with an equal rate of $\gamma_{\rightarrow} = \gamma_{\leftarrow} = \gamma_{1D}/2$. The transmission coefficients of right- and left-going photons, t_{\rightarrow} and t_{\leftarrow} , have also been the same. The condition $t_{\rightarrow} = t_{\leftarrow}$ is related to the time-reversal symmetry. This symmetry holds in the linear optics regime, and if no magnetic field is applied to the system. In this chapter we will consider a chiral waveguide situation, when the symmetry is broken by the external static magnetic field \mathbf{B} that is transverse to the waveguide. The first implication will be the preferential emission in one of the directions, either to the left or to the right, depending on the sign of the magnetic field, $\gamma_{\rightarrow} \neq \gamma_{\leftarrow}$, as illustrated in Fig. 8.1 and the second implication will be asymmetric transmission, $t_{\rightarrow} \neq t_{\leftarrow}$. We will first illustrate the microscopic origin of this directionality, and then we will consider collective effects in the chiral regime.

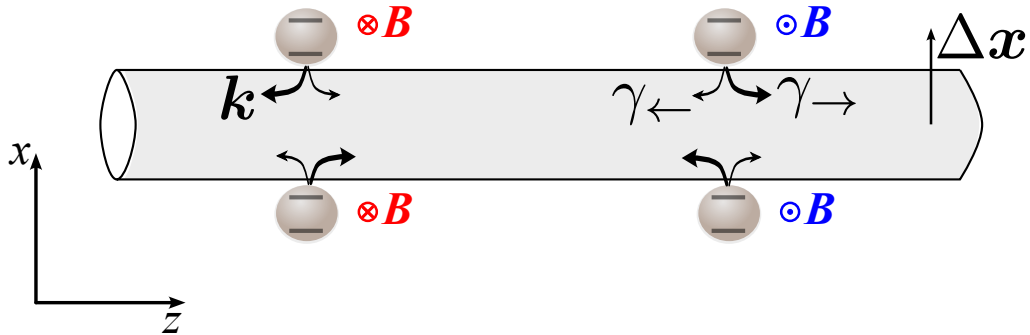


Figure 8.1: Directional light emission from an atom above and below the waveguide, controlled by the direction of the transverse magnetic field \mathbf{B} .

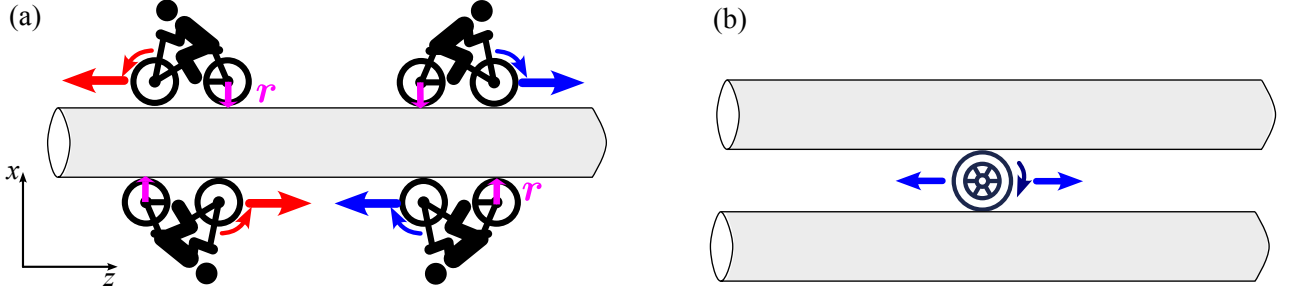


Figure 8.2: (a) Bicycle analogy to Fig. 8.1: Illustration of connection between rotation and parallel motion by cyclists, going in different direction (b) the wheel is jammed and can not move if upper and lower surfaces are exactly the same, so that inversion symmetry $z \rightarrow -z$ holds.

8.1 Spin-momentum locking: photonic bicycles

The directionality of the emission and transmission, announced above, relies on peculiar polarization properties of the electromagnetic field, that propagates in the waveguide. This field travels freely along the waveguide direction z , $\mathbf{E}(x, z) \propto \exp(ik_z z)$, but decays outside the waveguide $\mathbf{E}(x, z) \propto \exp(-\kappa|x|)$, where $\kappa > 0$. As a result, the electric field of the electromagnetic mode can be written as

$$\mathbf{E}(x, z) \propto \mathbf{e}_0(k_z) \exp(ik_z z - \kappa|x|), \quad (8.1)$$

where the polarization vector \mathbf{e}_0 depends on the sign of k_z . It turns out that one can make meaningful conclusions about the wave polarization based just on one property: electromagnetic wave has to be a transverse one, $\text{div } \mathbf{E} = 0$. Due to the $y \rightarrow -y$ reflection symmetry of the problem, we can distinguish between the two independent types of waves polarization: those with $e_{0,z} = e_{0,x} = 0, e_{0,y} \neq 0$ (odd with respect to the reflection) and those with $e_y = 0$ (even with respect to the reflection). We are only interested in the latter waves, which have nonzero electric field components both along the propagation direction and in the direction perpendicular to the waveguide. For planar waveguides, these are termed as TM- or p-polarized waves [1].

Substituting Eq. (8.1) into the condition $\text{div } \mathbf{E} = 0$ we find

$$ik_z e_{0,z} - \kappa \text{sign } |x| e_{0,x} = 0 \text{ or } \frac{e_{0,x}}{e_{0,z}} = i \frac{k_z}{\kappa} \text{sign } x. \quad (8.2)$$

The condition Eq. (8.2) is very important due to the presence of the factor of i . It means, that

the wave has, in general, an elliptical polarization in the xz plane, containing the propagation wave vector. The sign of ellipticity depends both on the propagation direction (sign of k_z) and on the point of observation (above or below the waveguide, sign of x). Above the waveguide for the right-going wave field is rotating **counter-clockwise**, and the left-going field is rotating clockwise in the xz plane; and below the waveguide, it is the opposite situation.

This peculiar “transverse circular” polarization is a feature of all general vector surface waves with transverse polarization, that propagate in one direction and decay in another one. For example, it also applies to surface plasmon polaritons [2, 3], elastic waves or to the waves on the surface of the sea. I can recommend trying the following experiment: if you float horizontally on the sea surface close to the shore and look at the sea bottom, you will notice that the water waves incoming into the shore do not just move you up and down, but actually carry you along the ellipse (the experiment of course should be done by competent enough swimmers). Transverse circular polarization should be distinguished from a true circular polarization of plane waves in free space. If the wave propagates along z , the transverse means electric field rotation in the xz plane, containing the propagation direction and the usual one means that field rotates in the xy plane. In yet another reformulation, the surface waves carry transverse angular momentum, and the usual circularly polarized waves carry longitudinal angular momentum [4]. The connection of the rotation sign to the propagation direction is termed spin-momentum locking.

The essence of spin-momentum locking could be understood from a simple bicycle analogy, as shown in Fig. 8.2(a). The bicycle moves because the wheel rotation on a surface is converted to parallel motion. Namely, the motion velocity \mathbf{v} can be written as

$$\mathbf{v} = \mathbf{r} \times \boldsymbol{\Omega} \quad (8.3)$$

where \mathbf{r} is the vector connecting the wheel center to the ground and $\boldsymbol{\Omega}$ is the pseudovector of the angular velocity. The velocity in Eq. (8.3) flips sign when the wheel rotation direction is changed, $\boldsymbol{\Omega} \rightarrow -\boldsymbol{\Omega}$ and when the sign of \mathbf{r} changes, that is, the bicycle is riding on the ceiling rather than on the floor (do not try to repeat this experiment!). The “normal” circularly polarized waves, when the wave carries angular momentum along its propagation direction, would be described as a propeller, not a bicycle. Notable, the propeller can work in free space, while the bicycle requires a ground (or a ceiling) to move. If the symmetry between the ground

and the ceiling is not broken, that is, if the situation is symmetric with respect to the $z \rightarrow -z$ reflection, the wheel of our bicycle will be jammed. The wheel that experiences an equal friction with the floor and the surface will not go anywhere, see Fig. 8.2(b). So symmetry breaking, implied by $\mathbf{r} \neq 0$ in Eq. (8.3), is essential for a bicycle effect.

This bicycle analogy has an exact one-to-one correspondence with the atom emission in Fig. 8.1, with the difference that wheel rotation $\boldsymbol{\Omega}$ is replaced by the magnetic field \mathbf{B} . In order to understand that we would need to know some basics of dipole emission: the intensity of emission of a dipole \mathbf{d} into the mode with the electric field \mathbf{E} at the dipole point is proportional to

$$I(k_z) \propto |\mathbf{d} \cdot \mathbf{E}^*(k_z)|^2. \quad (8.4)$$

The origin of the conjugation in Eq. (8.4) can be understood by those familiar with quantum mechanics: the radiation leads to creation of a photon, which means that it involves \mathbf{E}^\dagger component of the quantized electric field operator, containing \mathbf{E}^* . In the presence of a transverse magnetic field $\mathbf{B} \parallel y$ the energy levels of the atom are split by the project of angular momentum on the y axis. As such, the dipole moment \mathbf{d} (technically, the matrix element of the dipole momentum operator, calculated between the ground and excited states), will be elliptically polarized, $d_z/d_x = i\xi \text{sign } B_y$. Substituting the field (8.1),(8.2) into Eq. (8.4) we find immediately, that the emission will be directional,

$$I(k_z) - I(-k_z) \propto \xi \text{sign } B_y k_z \text{sign } x. \quad (8.5)$$

Equation Eq. (8.5) can be written in a symmetric form

$$\mathbf{k} \propto \mathbf{B} \times \Delta \mathbf{x} \quad (8.6)$$

where $\Delta \mathbf{x} \parallel x$ is the shift of the atoms in the vertical direction, with respect to the waveguide center (see Fig. 8.1). Equation (8.6) is a complete analogy to our bicycle equation (8.3). For a example, an atom located just at the center of a symmetric waveguide would not emit directionally, just like the symmetrically jammed wheel in Fig. 8.2(b) will not go anywhere. Thus, we just proved that the spontaneous emission to the left and to the right directions, γ_{\leftarrow} and γ_{\rightarrow} , would be different. This is the essence of the chiral quantum optics [5]. In the next section, we will analyze how this affects the light transmission coefficients through an array of

atoms, coupled to the waveguide.

8.2 Chiral atom-light interaction

In order to calculate the transmission and reflection coefficient for a light through a waveguide, chirally coupled to an atom, we can generalize the Green function methods, Eq. (3.21), Eq. (3.22). Let us assume that the atomic wavefunction is given by $|\psi\rangle \equiv |g\rangle + \psi|e\rangle$ and $\mathbf{d}_{ge} = \langle g|\hat{\mathbf{d}}|e\rangle$ is the corresponding matrix element of the dipole momentum operator. In the dipole approximation, the interaction with the electric field is described by the Hamiltonian

$$H_{\text{int}} = -\mathbf{d} \cdot \mathbf{E}_0. \quad (8.7)$$

We write the incident electric field amplitude \mathbf{E}_0 at the position of an atom as a superposition of left- and right- going waves with the amplitudes E_{\leftarrow} and E_{\rightarrow}

$$\mathbf{E}_0 = \mathbf{e}_0(-k_z)E_{\leftarrow}e^{-i\omega t} + \mathbf{e}_0(k_z)E_{\rightarrow}e^{-i\omega t}. \quad (8.8)$$

The equation of motion for the excited state wavefunction is then given by

$$[\omega_0 - \omega - i\gamma_{1D} - i\gamma]\psi = [\mathbf{d}_{eg} \cdot \mathbf{e}_0(-k_z)E_{\rightarrow} + \mathbf{d}_{eg} \cdot \mathbf{e}_0(+k_z)E_{\leftarrow}] \quad (8.9)$$

When writing Eq. (8.9) we included into the left-hand side the total radiative decay γ_{1D} and the phenomenological damping γ . Without these terms, this is just a Schrödinger equation for the excited state amplitude ψ , transition energy $\omega_0 \equiv E_e - E_g$ and the interaction Hamiltonian given by Eqs. (8.7), (8.8). The emitted electric field is given, in turn, by

$$\mathbf{E}_{\text{tot}} = \mathbf{E}_0 + \mathbf{E}_{\text{scat}}, \quad \mathbf{E}_{\text{scat}} = 2\pi i q \mathbf{e}_0(k_z)[\mathbf{d}_{ge} \cdot \mathbf{e}_0(k_z)]e^{iqz}\theta(z) + 2\pi i q \mathbf{e}_0(-k_z)[\mathbf{d}_{ge} \cdot \mathbf{e}_0(-k_z)]e^{-iqz}\theta(-z), \quad (8.10)$$

where $\theta(z)$ is the Heaviside step function. Compared with Eq. (3.22), we needed to take into account different amplitudes of emission into the forward and backward directions. We now obtain the value of ψ from Eq. (8.9) and substitute it into Eq. (8.10) and find the reflection and transmission coefficients,

$$r_{\leftarrow} = \frac{\mathbf{e}_0(-k_z) \cdot \mathbf{E}_{\text{scat}}}{E_{\rightarrow}}, \quad t_{\rightarrow} = 1 + \frac{\mathbf{e}_0(k_z) \cdot \mathbf{E}_{\text{scat}}}{E_{\rightarrow}}, \quad (8.11)$$

that are given by

$$r_{\leftarrow} = \frac{i\sqrt{\gamma_{\rightarrow}\gamma_{\leftarrow}}}{\omega_0 - \omega - i(\gamma_{1D} + \gamma)} \quad (8.12)$$

$$t_{\rightarrow} = \frac{\omega_0 - \omega + i\frac{1}{2}(\gamma_{\rightarrow} - \gamma_{\leftarrow}) - i\gamma}{\omega_0 - \omega - i(\gamma_{1D} + \gamma)} . \quad (8.13)$$

The radiative decay rate is given by $\gamma_{1D} = (\gamma_{\rightarrow} + \gamma_{\leftarrow})/2$. In the nonchiral case, when $\gamma_{\rightarrow} = \gamma_{\leftarrow} = \gamma_{1D}$, these expressions reduce to Eq. (3.12). When the wave is incident upon the structure from the left, the reflection coefficient stays the same,

$$r_{\leftrightarrow} = r_{\leftarrow} \quad (8.14)$$

but the transmission coefficient becomes different ,

$$t_{\leftarrow} = \frac{\omega_0 - \omega - i\frac{1}{2}(\gamma_{\rightarrow} - \gamma_{\leftarrow}) - i\gamma}{\omega_0 - \omega - i(\gamma_{1D} + \gamma)} \neq t_{\rightarrow} . \quad (8.15)$$

The reflection coefficient through an array of emitters can now be readily calculated by using the transfer matrix method. It assumes an especially simple form in the totally chiral structure, where

$$t_{\text{total},\rightarrow} = t_{1,\rightarrow} t_{2,\rightarrow} \dots t_{N,\rightarrow} , \quad (8.16)$$

where $t_{j,\rightarrow}$ is the transmission coefficient through the j -th emitter. That is, in the absence of backreflection, $\gamma_{\leftarrow} = 0$, the transmission coefficient is given just by a product of individual emitter transmission coefficients. Interestingly, this expression is the same as the effective medium approximation, Eq. (7.34). Indeed, the effective medium approximation assumes that the light averages out the inhomogeneities of the system, and does not experience any backreflection. In the chiral case, the effective medium answer becomes exact.

Since Eq. (8.16) describes an independent transmission of light through multiple emitters, the collective coupled modes of the multiple emitters, are not formed in the totally chiral case. This can also be seen when comparing Eq. (8.16) for $N = 2$ with Eq. (5.2) we obtained for in the nonchiral case. There, the collective super- and sub-radiant modes were found as poles of the denominator of the transmission coefficient, see Eq. (5.27), $1 - r_1 r_2 \exp(2i\varphi)$. In the chiral case, this denominator is absent, $r_1 = r_2 = 0$. In other words, the formation of collective modes is a result of multiple scattering of light between the emitters, and in the chiral case, this is not

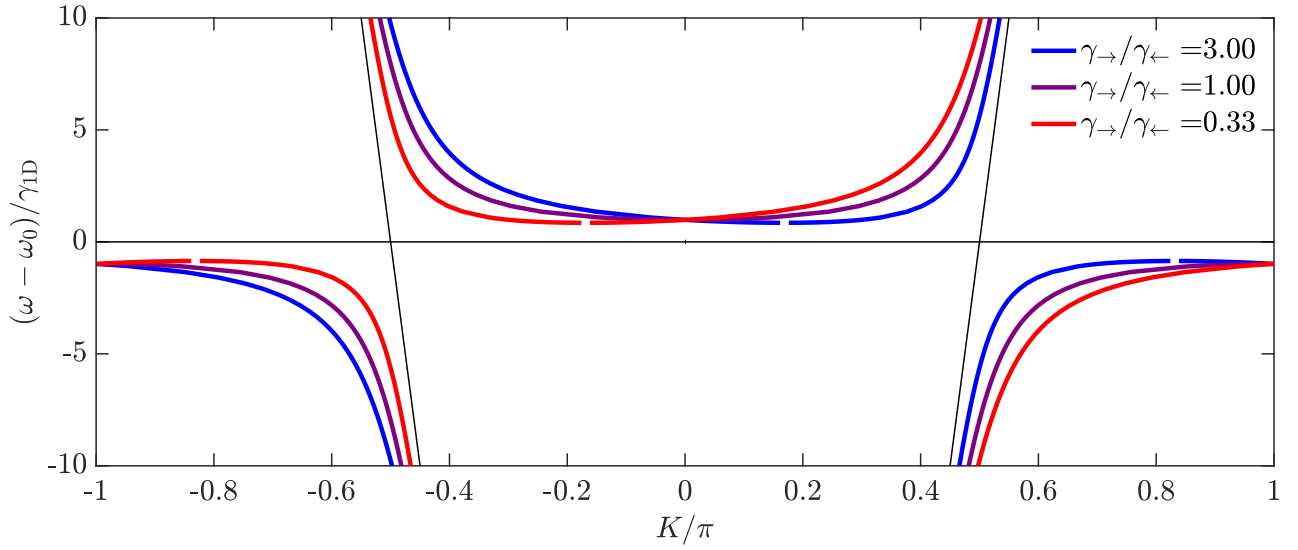


Figure 8.3: Dispersion law in chiral arrays depending on the ratio $\gamma_{\rightarrow}/\gamma_{\leftarrow}$. Calculated for $\gamma_{1D}/\omega_0 = 10^{-2}$ and $\omega_0 d/c = \pi/2$.

possible. Interestingly, however, as we will see later in this book, there exist collective effects in chiral structures that appear in the quantum nonlinear regime.

Let us now calculate the dispersion law of the waves, propagating in the periodic chiral array. To this end, we substitute Eq. (8.12)–(8.15) for the reflection and transmission coefficient into general expression for the transfer matrix Eq. (7.19) and then we solve Eq. (7.26) for $\det[T - \exp(iK)] = 0$. We note, that the simpler equation, $\cos K = \text{Tr } T/2$, is inapplicable in this case, since $t_{\rightarrow} \neq t_{\leftarrow}$ in a chiral structure, so that $\det T \neq 1$. The results reads

$$\omega(K) = \omega_0 + \gamma_{1D} \frac{\sin \varphi + \chi \sin K}{\cos K - \cos \varphi}, \text{ where } \chi = \frac{1 - \xi}{1 + \xi} \text{ and } \varphi = \omega d/c. \quad (8.17)$$

We plot in Fig. 8.3 the result of numerical solution of Eq. (8.17) for the three following cases: $\gamma_{\rightarrow} > \gamma_{\leftarrow}$, $\gamma_{\rightarrow} < \gamma_{\leftarrow}$ and $\gamma_{\rightarrow} \neq \gamma_{\leftarrow}$. The calculation demonstrates that in the chiral case the two avoided crossings for forward and backward going polaritons become unequal. In the extreme limiting cases $\gamma_{\leftarrow}/\gamma_{\rightarrow} \rightarrow 0$ or $\gamma_{\rightarrow}/\gamma_{\leftarrow} \rightarrow 0$ only one of these avoided crossings survives.

8.3 Summary

In this chapter we learned that electric field of the waves, propagating in a waveguide, has a peculiar chiral polarization when this waves leak outside the waveguide: the electric field rotates in the direction containing the normal to the waveguide and the propagation direction. Such “transverse circular” polarization is very different from the usual circular polarization

8.3. SUMMARY

for free-space plane waves, and it can lead to a directional light-matter interaction when a magnetic field is applied to the structure. Collective effects in the strongly chiral regime are suppressed due to the absence of light multiple scattering on different atoms.

8.4 Additional reading

Review on chiral light-matter interaction: A. Aiello et al., “From transverse angular momentum to photonic wheels”, [Nature Photonics](#) **9**, 789–795 (2015)

Review on chiral quantum optics: P. Lodahl et al., “Chiral quantum optics”, [Nature](#) **541**, 473–480 (2017)

Details on collective light-matter interaction in an array of atoms, chirally coupled to a waveguide: D. F. Kornovan et al., “Transport and collective radiance in a basic quantum chiral optical model”, [Phys. Rev. B](#) **96**, 115162 (2017).

References

- ¹M. Born and E. Wolf, *Principles of optics: electromagnetic theory of propagation, interference and diffraction of light* (Elsevier, 2013).
- ²F. J. Rodriguez-Fortuno, G. Marino, P. Ginzburg, D. O’Connor, A. Martinez, G. A. Wurtz, and A. V. Zayats, “Near-field interference for the unidirectional excitation of electromagnetic guided modes”, [Science](#) **340**, 328–330 (2013).
- ³F. Spitzer et al., “Routing the emission of a near-surface light source by a magnetic field”, [Nature Physics](#) **14**, 1043–1048 (2018).
- ⁴A. Aiello, P. Banzer, M. Neugebauer, and G. Leuchs, “From transverse angular momentum to photonic wheels”, [Nature Photonics](#) **9**, 789–795 (2015).
- ⁵P. Lodahl, S. Mahmoodian, S. Stobbe, A. Rauschenbeutel, P. Schneeweiss, J. Volz, H. Pichler, and P. Zoller, “Chiral quantum optics”, [Nature](#) **541**, 473–480 (2017).
- ⁶D. F. Kornovan, M. I. Petrov, and I. V. Iorsh, “Transport and collective radiance in a basic quantum chiral optical model”, [Phys. Rev. B](#) **96**, 115162 (2017).

REFERENCES

Chapter 9

Arrays in a cavity

So far in this book, we have considered the interaction of emitter arrays with the travelling photons. This chapter will be devoted to arrays interacting with a single confined photon mode, trapped in a cavity. Since photons will be confined in all three spatial dimensions instead of just two, the light-matter coupling strength can become even larger. In particular, it becomes possible to realize the strong coupling regime, previously considered in Chapter 6. Our goal will be to examine how the transition between the strong and weak coupling regimes depends on the parameters of the cavity (such as the quality factor) and on the parameters of the emitter array. In particular, we will show that the light-matter coupling strength in a cavity can also be collectively enhanced.

9.1 Empty cavity response

9.1.1 Reflection, transmission and Fabry-Pérot modes

Let us start by analyzing the light transmission and reflection through an empty Fabry-Pérot cavity that is formed by two identical mirrors with reflection coefficient r_{mirror} and transmission coefficient t_{mirror} , separated by a distance d . For simplicity, we also assume that mirrors are symmetric, that is, their reflection and transmission coefficients are the same for the light

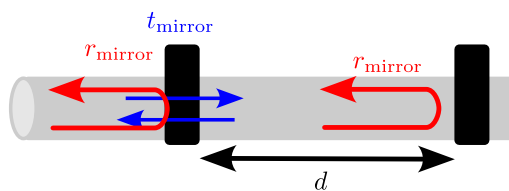


Figure 9.1: Schematics of light reflection from a double-sided cavity.

incident from the left and from the right. We have already learned in Chapter 5, how to calculate the reflection and transmission coefficient through two scatterers by summing all the multiple scattering amplitudes. In the considered case the scatterers are just cavity mirrors, and the results for reflection and transmission coefficients Eq. (5.1), Eq. (5.2) assume a simple form

$$r_{\text{tot}} = r_{\text{mirror}} + \frac{t_{\text{mirror}}^2 r_{\text{mirror}} e^{2i\varphi}}{1 - r_{\text{mirror}}^2 e^{2i\varphi}}, \quad t_{\text{tot}} = \frac{t_{\text{mirror}}^2 e^{i\varphi}}{1 - r_{\text{mirror}}^2 e^{2i\varphi}}, \quad (9.1)$$

where $\varphi = \omega d/c$ is the phase gained by light between the two mirrors. We plot the reflection and transmission spectra $|r_{\text{tot}}|^2$ and $|t_{\text{tot}}|^2$ vs frequency in Fig. 9.2. When calculating the spectra in Fig. 9.2 one needs to take care that the reflection and transmission coefficients r_{mirror} and t_{mirror} are not independent. First, if there is no loss in the mirrors, their absolute amplitudes are related by the flux conservation condition, $|r_{\text{mirror}}|^2 + |t_{\text{mirror}}|^2 = 1$. Second, a general lossless centrosymmetric scatterer satisfies a more subtle condition

$$\text{Re} \left(\frac{r_{\text{mirror}}}{t_{\text{mirror}}^*} \right) = 0. \quad (9.2)$$

This condition can be easily verified either numerically or analytically. For example, it is clear that the reflection coefficients for a single resonant emitter Eq. (3.12) satisfy this condition for $\gamma = 0$. Thus, in our calculation in Fig. 9.2 we assumed that r_{mirror} is real and $t_{\text{mirror}} = i\sqrt{1 - r_{\text{mirror}}^2}$, which automatically satisfies Eqs. (9.2).

The results demonstrate, that when the mirrors get better ($|r_{\text{mirror}}| \rightarrow 1$ and $t_{\text{mirror}} \rightarrow 0$) the spectra consist just of series of sharp peaks and dips at the frequencies of the Fabry-Pérot modes ω_m , corresponding to the condition

$$\frac{\omega_m d}{c} = m\pi, \quad m = 1, 2, 3 \quad (9.3)$$

Away from the mode resonance almost all the light gets reflected and nothing gets through the cavity. However, exactly at the mode resonance frequency, if the mirrors are lossless, $|r_{\text{mirror}}|^2 + |t_{\text{mirror}}|^2 = 1$, there is a possibility of 100-% transmission of light through the structure with zero reflection. This might seem counterintuitive, since two mirrors should transmit less light than one. However, the possibility of a stopover in the middle and multiple roundtrips with constructive interference results in a 100-% transmission probability. Nevertheless, the width of the transmission peak decreases as the mirrors improve.

One can obtain the following approximate expressions for Eqs. (9.1) in the vicinity of each resonance Eq. (9.3) that read

$$t_{\text{tot}} \approx \frac{i\gamma_{\text{cav}}^{(m)}}{\omega_m - i\gamma_{\text{cav}}^{(m)} - \omega}, r_{\text{tot}} = 1 + t_{\text{tot}} \approx \frac{\omega_m + i\gamma_{\text{cav}}^{(m)} - \omega}{\omega_m - i\gamma_{\text{cav}}^{(m)} - \omega} \quad (9.4)$$

where the parameter

$$\gamma_{\text{cav}}^{(m)} = \frac{\omega_m(1 - |r^2|)}{2m} \equiv \frac{\omega_m}{2Q_m} \quad (9.5)$$

determines the half-width of the resonant reflection dip or transmission peak. It can be interpreted as the decay rate of the cavity mode, that is finite due to the photon escape through the mirrors, where Q_m is the mode quality factor.

We note, that expressions Eq. (9.4) have a striking similarity to the reflection and transmission coefficient of a resonant emitter, coupled to a cavity, Eqs. (3.12). The only difference is that reflection and transmission coefficients are swapped: for a cavity, far away from resonance there is 100-% reflection and no transmission, and for the resonant emitter the situation is reversed. In both cases the coefficient have a resonance in the complex plane, and the imaginary part of the complex resonance frequency describes the rate of the mode decay.

9.1.2 Empty cavity Green function

We have learned in chapter Sec. 5, that in order to describe the interaction of an array of emitters with an electromagnetic field it is convenient to use the electromagnetic Green function. Thus, it is instructive to find the Green function for a cavity, which will enable us to consider light-emitter interaction in the next section. We will again assume that the cavity is formed by two identical mirrors, characterized by the amplitude reflection coefficients r_{mirror} and located at $z = \pm d/2$. We already know, that without the mirrors, for $r_{\text{mirror}} = 0$, the Green function is given by Eq. (B.6)

$$G_0 = 2\pi i q e^{iq|z-z'|}, \quad (9.6)$$

where $q = \omega/c$ is the light wave vector at the frequency ω . Now we are interested to find the Green function in the presence of the mirrors.

We will look for solution in the form

$$G(z, z') = G_0 + f_{\rightarrow}(z')e^{iqz} + f_{\leftarrow}(z')e^{-iqz'} \quad (9.7)$$

where G_0 is given by Eq. (9.6) and $G_R(z, z')$ describes the effect of the mirrors. The G_R term will include the contribution of waves reflected from the mirrors and making a number of roundtrips inside the cavity. In order to find this term, we will write the boundary conditions at the mirrors. At the right mirror, $z = +d/2$ we find

$$r_{\text{mirror}}(f_{\rightarrow}e^{iqd/2} + e^{iq(d/2-z')}) = f_{\leftarrow}e^{-iqd/2}. \quad (9.8)$$

In the left-hand side, we have r times the amplitude of the waves propagating towards the mirror. The first term, $e^{iqd/2}$, stems from G_R and the second term stems from $e^{iq|z-z'|}$ in Eq. (9.6). Similarly, in the left-hand side we have the amplitude of the wave reflected from the mirror and propagating to the right.

In a similar fashion, the boundary conditions at the left mirror, $z = -d/2$, are:

$$r_{\text{mirror}}(f_{\leftarrow}e^{iqd/2} + e^{iq(d/2+z')}) = f_{\rightarrow}e^{-iqd/2}. \quad (9.9)$$

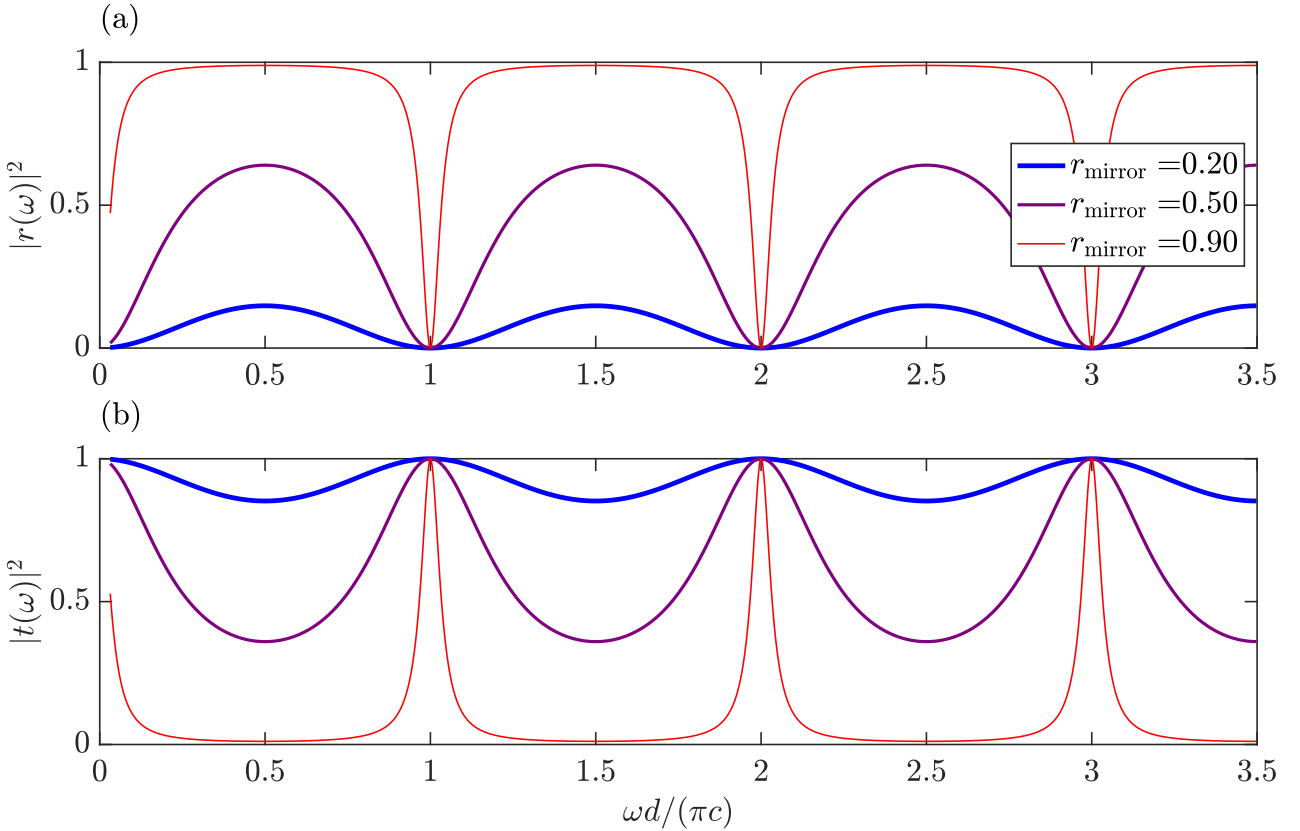


Figure 9.2: Light reflection (a) and transmission (b) spectra through a Fabry-Pérot cavity, calculate for different mirror reflection coefficients, indicated on graph.

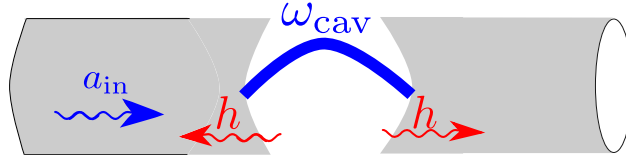


Figure 9.3: Schematics of a two-sided cavity coupled to the propagating photons

The system of two linear equations Eq. (9.8) and Eq. (9.9) yields the amplitudes $f_{\rightarrow/\leftarrow}$. Substituting them into Eq. (9.7), we obtain the answer for the total Green function:

$$G(z, z') = 2\pi i q \left[e^{iq|z-z'|} + \frac{2\tilde{r}}{1-\tilde{r}^2} [\cos q(z+z') + \tilde{r} \cos q(z-z')] \right], \quad \tilde{r} = r_{\text{mirror}} e^{iqd}. \quad (9.10)$$

Now we are prepared to describe an array of emitters in the cavity, which will be done in the next section.

It is also instructive to simplifying the general expression for the Green function Eq. (9.10) when ω is in the spectral vicinity of the given cavity mode ω_m . To this end, we expand $1/G(0, 0)$ in Taylor series around the resonance at $\omega = \omega_m$, which result in

$$G(z, z') = 2\pi q \frac{2\omega_m}{\omega_m - \omega - i\gamma_{\text{cav}}^{(m)}} \times \begin{cases} \cos q_m z \cos q_m z', & m = 1, 3, 5, \dots, \\ \sin q_m z \sin q_m z', & m = 2, 4, 6, \dots \end{cases} \quad (9.11)$$

9.1.3 Input-output theory for an empty cavity

It is instructive to present a bit more quantum description of a cavity mode coupled to the environment. The derivation below is essentially the quantum input-output theory developed by Gardiner and Colett [1]. But at the moment we try to focus less on the quantum properties of light and more on the general properties of a system losing energy to the reservoir.

Let us consider a cavity mode with the frequency ω_{cav} that interacts with a reservoir of photons with continuous spectrum $\omega_k = c|k|$, see Fig. 9.3. The coupling to the reservoir is described by the coefficient h that is proportional to the amplitude transmission coefficient of the cavity mirrors. The Hamiltonian of the problem reads

$$H = \omega_{\text{cav}} a_0^\dagger a_0 + \sum_k \omega_k a_k^\dagger a_k + \frac{1}{\sqrt{L}} \sum_k (h_k^* a_k^\dagger c + h_k a_k c^\dagger), \quad (9.12)$$

For simplicity, the Planck constant \hbar is set to unity, L is the normalization length $\omega_k = ck$ is

the frequency of the photon with the wave vector k , c is the mode velocity in the reservoir, $\sum_k \equiv L \int_{-\infty}^{\infty} dk / (2\pi)$. Here, ω_{cav} is the cavity resonance frequency, a_0 is the cavity photon annihilation operator, a_k is annihilation operator of the reservoir photon with the wave vector k , and we also assume $t \ll \omega_{\text{cav}}$ so that we can use rotating wave approximation. One of the reservoir modes is pumped with the frequency $\omega_{\text{in}} = ck_{\text{in}}$ and the amplitude a_{in} , $a_k(t) = \delta_{k,|\omega_{\text{in}}|/c} e^{-i\omega_{\text{in}}t} a_{\text{in}}$. Our goal is to obtain the equations for the amplitude of the field inside the cavity, and for the field scattered from the cavity.

We start with the Heisenberg equations of motion for the operators a_0 and a_k :

$$\frac{da_0}{dt} = -i\omega_{\text{cav}}a_0 - i\frac{1}{\sqrt{L}}h \sum_k a_k, \quad (9.13)$$

$$\frac{da_k}{dt} = -i\omega_k a_k - i\frac{1}{\sqrt{L}}h_k^* a_0. \quad (9.14)$$

In what follows, we are interested only in the classical properties of the field, so we assume that the operators a_0 , a_k can be replaced by complex numbers. The main problem with these equations is that they deal with a continuum of modes outside the cavity. However, since photons outside of the cavity do not scatter and exhibit a linear spectrum, the dependence on k can be hidded into the already known Green function of photons in free space.

We start by doing the Fourier transform and introducing the frequency and position dependent amplitudes of the field outside the cavity:

$$a(z, t) = \sum_k e^{ikz} a_k(t) = \sum_k e^{ikz} \int_{-\infty}^{\infty} \frac{d\omega}{2\pi} a_k(\omega) e^{-i\omega t}. \quad (9.15)$$

Without the cavity, the field is given by

$$a_{\text{in}}(z, t) = \sum_k e^{ikz} \delta_{k,|\omega_{\text{in}}|/c} e^{-i\omega_{\text{in}}t} a_{\text{in}} = a_{\text{in}} e^{ik_{\text{in}}(z-ct)}. \quad (9.16)$$

The Fourier transform of Heisenberg equation (9.14) for the field outside the cavity reads

$$(\omega - c|k|)a_k(\omega) = \frac{1}{\sqrt{L}}h_k^* a_0(\omega). \quad (9.17)$$

We solve it as

$$a_k(\omega) = -\frac{1}{\sqrt{L}} \frac{1}{\omega_k - \omega} h_k^* a_0(\omega) + \delta_{k,|\omega_{\text{in}}|/c} 2\pi \delta(\omega - \omega_{\text{in}}) a_{\text{in}}. \quad (9.18)$$

Here, we have added the second term by taking into account that without the field emitted into the reservoir from the cavity the field amplitude should be given just by Eq. (9.16). Since $\omega_{\text{in}} - ck_{\text{in}} = 0$, the second term in Eq. (9.18) does not change the left-hand-side of Eq. (9.17) and Eq. (9.18) still remains a solution. We can now use Eq. (9.16) and calculate the field in the real space:

$$a(z, \omega) = -\frac{1}{\sqrt{L}} \sum_k \frac{e^{ikz}}{\omega_k - \omega} h_k^* a_0(\omega) + 2\pi\delta(\omega - \omega_{\text{in}}) a_{\text{in}} e^{ik_{\text{in}} z}. \quad (9.19)$$

Next, we are going to assume that the coupling coefficients weakly depend on the photon wave vector, $h_k \approx h$. This approximation is valid when a reservoir has a linear spectrum and the transmission coefficient through the mirrors varies with frequency slowly, on the frequency scale smaller than the cavity linewidth. Essentially, this is the same Markovian approximation for the coupling to the reservoir. In this approximation, we can express the sum over k via the photon Green function

$$\mathcal{G}(z, \omega) \equiv \frac{1}{L} \sum_k \frac{e^{ikz}}{\omega_k - \omega} = \frac{i}{c} e^{i\omega|z|/c}. \quad (9.20)$$

that has been introduced in Appendix B:

$$a(z, \omega) = -\sqrt{L}\mathcal{G}(z, \omega)h^*a_0(\omega) + 2\pi\delta(\omega - \omega_{\text{in}})a_{\text{in}}e^{ik_{\text{in}}z}, \quad (9.21)$$

see in particular Eq. (B.12).

In a similar way, we transform the equation (9.13) for the amplitude of the field inside the cavity into the frequency domain:

$$(\omega - \omega_{\text{cav}})a_0(\omega) = \frac{1}{\sqrt{L}}ha(z=0, \omega). \quad (9.22)$$

Next, we express $a(z=0, \omega)$ via Eq. (9.21) and obtain

$$(\omega - \omega_{\text{cav}})a_0(\omega) = -|h|^2\mathcal{G}(z=0, \omega)a_0(\omega) + \frac{1}{\sqrt{L}}h2\pi\delta(\omega - \omega_{\text{in}})a_{\text{in}}. \quad (9.23)$$

We now use the Markovian approximation once again and assume that the Green function varies slowly with the frequency:

$$\mathcal{G}(z=0, \omega) \approx \mathcal{G}(z=0, \omega_{\text{cav}}), \quad (9.24)$$

which allows us to rewrite Eq. (9.23) as

$$(\omega - \omega_{\text{cav}} + i\gamma_{\text{cav}})a_0(\omega) = \frac{1}{\sqrt{L}}h2\pi\delta(\omega - \omega_{\text{in}})a_{\text{in}}, \quad (9.25)$$

where

$$\gamma_{\text{cav}} = |h|^2 \text{Im} \mathcal{G}(z = 0, \omega_{\text{cav}}) = \frac{|h|^2}{c} \quad (9.26)$$

is the cavity decay rate. Comparing with Eq. (9.5) for $m = 1$, we can establish the connection between the amplitude h and the mirror transmission coefficients, $h = \sqrt{2\omega_{\text{cav}}c}|t_{\text{mirror}}|$ (we used $|t_{\text{mirror}}|^2 = 1 - |r_{\text{mirror}}|^2$).

There is also an alternative way to calculate γ_{cav} . We can use the Fermi Golden Rule as the rate of photon escape from the cavity due to the coupling to the reservoir,

$$\begin{aligned} 2\gamma_{\text{cav}} \equiv \frac{1}{\tau} &= 2\pi \sum_k \frac{1}{L} |h|^2 \delta(\omega_{\text{cav}} - c|k|) \equiv 2\pi |h|^2 \int_{-\infty}^{\infty} \frac{dk}{2\pi} \delta(c|k| - \omega_{\text{cav}}) \\ &= |h|^2 \int_{-\infty}^{\infty} dk \delta(c|k| - \omega_{\text{cav}}) = \frac{2|h|^2}{c}. \end{aligned} \quad (9.27)$$

Transforming Eq. (??) back into the time domain we find

$$i \frac{da_0}{dt} = (\omega_{\text{cav}} - i\gamma_{\text{cav}})a_0 + \sqrt{\frac{c}{L}}\gamma_{\text{cav}}a_{\text{in}}(t). \quad (9.28)$$

The field outside the cavity in the time domain is found from Eq. (9.21):

$$a(z, t) = -i\sqrt{\frac{L}{c}}e^{i\omega|z|/c - i\omega t}h^*a_0(t) + a_{\text{in}}e^{ik_{\text{in}}z - i\omega_{\text{in}}t}. \quad (9.29)$$

We now also choose the gauge where $h = h^*$ is real and also rescale the amplitude of the field inside the cavity as $\tilde{a}_0 = -a_0\sqrt{L/c}$. The transformed equations for the field inside and outside the cavity become

$$i \frac{d\tilde{a}_0}{dt} = (\omega_{\text{cav}} - i\gamma_{\text{cav}})\tilde{a}_0 - \sqrt{\gamma_{\text{cav}}}a_{\text{in}}(t) \quad (9.30)$$

$$a(z, t) = i\sqrt{\gamma_{\text{cav}}}e^{i\omega|z|/c - i\omega t}\tilde{a}_0(t) + a_{\text{in}}e^{ik_{\text{in}}z - i\omega_{\text{in}}t}. \quad (9.31)$$

The system of equations Eq. (9.30), Eq. (9.31) allows us to solve the scattering problem without explicitly dealing with the continuous spectrum of the modes outside the cavity. In particular, for the monochromatic input field $a_{\text{in}}(t) \equiv a_{\text{in}} \exp(-i\omega_{\text{in}}t)$ we readily find the field

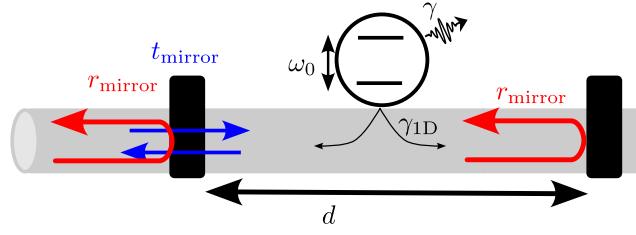


Figure 9.4: Schematics of light reflection from a two-level atom inside a cavity.

inside

$$a_0 = a_{\text{in}} \frac{\sqrt{\gamma_{\text{cav}}}}{\omega_{\text{cav}} - i\gamma_{\text{cav}} - \omega_{\text{in}}} \quad (9.32)$$

and then Eq. (9.31) yields the reflection and transmission coefficients,

$$r = \frac{i\gamma_{\text{cav}}}{\omega_{\text{cav}} - \omega_{\text{in}} - i\gamma_{\text{cav}}}, t = 1 + r \quad (9.33)$$

that are equivalent to Eqs. (3.12).

9.2 Purcell factor in a cavity

Let us now consider a more complicated problem of an emitter in a cavity. In particular, we are going to place an emitter in the center of a symmetric cavity, see Fig. 9.4. The emitter has a resonance frequency ω_0 and decay rate γ_{1D} . Our goal is to demonstrate, that the emitter interaction with the cavity mode changes both the frequency and the decay rate, or, in a more fancy words, they are renormalized by the light-matter interaction. The phenomenon of the modification of the radiative decay rate is termed as Purcell effect [2].

How to address this problem? We are going to use an approach we already established in the previous chapters, in particular, when we considered emitter near a single mirror. Resonance frequencies of a coupled system can be found as poles of the response function. In particular, let us calculate the reflection coefficient of the emitter in a cavity. We already know, that without the cavity reflection and transmission coefficients of the emitter are given by Eqs. (3.12), that we also recast below for convenience

$$r(\omega) = \frac{i\gamma_{1D}}{\omega_0 - \omega - i(\gamma_{1D} + \gamma)}, t(\omega) = 1 + r(\omega) = \frac{\omega_0 - \omega - i\gamma}{\omega_0 - \omega - i(\gamma_{1D} + \gamma)} \quad (9.34)$$

Now we can obtain the reflection coefficient from the combined system mirror+emitter+mirror

by first calculating the reflection coefficient from emitter and the right mirror

$$r' = r + \frac{r_{\text{mirror}} t^2}{1 - r r_{\text{mirror}} e^{i\varphi}} e^{i\varphi} \quad (9.35)$$

and then from the whole cavity:

$$\tilde{r} = r_{\text{mirror}} + \frac{r' t_{\text{mirror}}^2}{1 - r' r_{\text{mirror}} e^{i\varphi}} e^{i\varphi} \quad (9.36)$$

where $\varphi = \omega d/c$ (compare with approach in Sec. 5 and in particular Fig. 5.1).

We can now find the resonance frequency is found from the condition that the denominator of Eq. (9.36) is equal to zero, which leads to

$$\frac{\omega - \omega_0 + i\gamma}{\gamma_{1D}} = -i \frac{1 + r e^{i\varphi}}{1 - r e^{i\varphi}}. \quad (9.37)$$

The same answer could have been obtained even faster, if we use the cavity Green function Eq. (9.10) we just derived. Then we can just use the general answer

$$\omega - \omega_0 + i\gamma = \frac{1}{2\pi q} \gamma_{1D} G(0, 0) \quad (9.38)$$

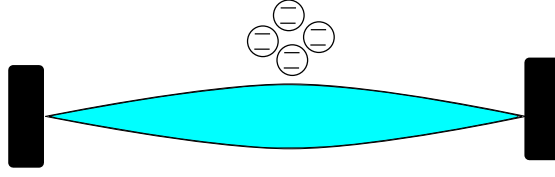
where G is given by Eq. (9.10) (compare with Eq. (3.23)), which immediately yields Eq. (??).

2do: unify factors in definition of G

Note that, in general, Eq. (9.37) is a transcendental equation to be solved for ω because the right-hand side can depend on ω . In the now-familiar Markovian approximation, we assume that the environment response is faster than the system dynamics, that is, it slowly changes in frequency. In this we can neglect the frequency dependence of the right-hand-side and evaluate it at $\omega = \omega_0$. Then the imaginary part of the right-hand-side provides the radiative decay rate of an emitter in a cavity and the real part yields the correction to the emitter frequency. In the next section we are going to analyze the regime, when the strong coupling with the cavity mode is realized, and the Markovian approximation breaks down.

9.3 Collective Rabi splitting

Let us now consider N identical emitters with resonant frequencies ω_0 , radiative decay rates γ_{1D} , and zero nonradiative decay rates placed in the center of a symmetric cavity and located


 Figure 9.5: Schematics of N emitters coupled to a cavity mode

at the close points z_n . We assume that the emitter-emitter distance is much smaller than the photon wavelength, the cavity size d satisfies the condition $\omega_{\text{cav}}d/c = \pi$. Our goal is to obtain the frequencies of the coupled system emitter+cavity photons.

In order to find the resonance frequencies of the coupled system, we can write the coupled dipoles equations in the absence of the external field

$$(\omega_0 - \omega)p_n = \frac{1}{2\pi q} \gamma_{1D} \sum_{n'=1}^N G(z_n, z_{n'}) p_{n'} . \quad (9.39)$$

We will use Eq. (9.11) for the Green function. Since the emitters are close to each other, we find $G(z_n, z_{n'}) = \text{const}(n, n') \equiv G$. Then we can sum all the equations Eq. (9.39) over $n = 1 \dots N$ and find

$$(\omega_0 - i\gamma - \omega)P = \frac{2N\gamma_{1D}\omega_{\text{cav}}}{\omega_{\text{cav}} - \omega - i\frac{\omega_{\text{cav}}}{2Q}} P, \quad P \equiv \sum_{n=1}^N p_n . \quad (9.40)$$

Assuming that $P \neq 0$ we can divide Eq. (9.40) by P and recover Eq. (9.41). On the other hand, if $P = 0$, the right-hand-side of Eq. (9.39) is zero and so $\omega = \omega_0$. It is now clear that the weak coupling approximation corresponds to ignoring the resonant frequency dependence in the right-hand side of Eq. (9.40) and setting $\omega = \omega_0$. This can be done only if this dependence is weak, that is, if Q is low so that the cavity resonance is spectrally broad enough.

In total, the system of equations Eqs. (9.40) should have $N + 1$ eigenmodes, corresponding to N modes of emitters hybridized with one mode of the cavity. The two eigenmode frequencies are given by

$$\omega_{\pm} = \frac{\omega_0 + \omega_{\text{cav}} - i\gamma - i\gamma_{\text{cav}}}{2} \pm \sqrt{2N\gamma_{1D}\omega_{\text{cav}} - \left(\frac{\omega_0 - \omega_{\text{cav}} - i\gamma + i\gamma_{\text{cav}}}{2} \right)^2} , \quad (9.41)$$

They describe the mode of the emitter array hybridized with the cavity mode. For $\gamma = 0$ and

zero detuning $\omega_0 = \omega_{\text{cav}}$ and $Q \gg 1$ the modes exhibit the collective vacuum Rabi splitting of

$$2g\sqrt{N} \equiv 2\sqrt{2N\gamma_{1D}\omega_{\text{cav}}} \quad (9.42)$$

. Importantly, the splitting between the modes ω_{\pm} is collectively enhanced by the factor of \sqrt{N} . Here we introduced the coupling strength between a single atom and a single photon $g \equiv \sqrt{2\gamma_{1D}\omega_{\text{cav}}}$. The answer Eq. (9.41) corresponds to the single-excited states of a so-called Tavis-Cummings model [3].

The remaining $N - 1$ modes are the degenerate dark modes $\omega_{\nu} = \omega_0$, corresponding to $P = 0$. They are called dark since they do not couple to light and have zero radiative decay rate, $\text{Im } \omega = 0$ for $\gamma = 0$.

It is also instructive to see how Eq. (9.41) transforms in the weak coupling regime. For simplicity, we assume zero detuning, $\omega_0 = \omega_{\text{cav}}$. Then the answer can be obtained by just setting ω in the right-hand side of Eq. (9.40) to ω_0 :

$$\omega_0 - i\gamma - i\frac{2N\gamma_{1D}\omega_{\text{cav}}}{\gamma_{\text{cav}}} \equiv \omega_0 - i\gamma - i\frac{g^2}{\gamma_{\text{cav}}} \equiv \omega_0 - i\gamma(1 + NC_1), \quad (9.43)$$

Here we have again written explicitly $\gamma_{\text{cav}} = \omega_{\text{cav}}/(2Q)$ and introduced the single-atom cooperativity C

$$C = \frac{g^2}{\gamma_{\text{cav}}\gamma} \quad (9.44)$$

that describes the ratio between the single atom emission in the photonic modes and into the other channels. Equation tells us that the decay rate of the atom in the cavity is enhanced due to the Purcell effect. The enhancement increases proportionally to the number of atoms N , which is a typical feature of a collective superradiant mode.

9.4 Additional reading

Light-matter interaction in microcavities: A. Kavokin et al., *Microcavities* (Clarendon Press, Oxford, 2006)

Chapter 10

Array of quantum emitters

Starting from this chapter, we will proceed to the quantum optical regime. No longer can the emitters be considered as classical oscillators, but their quantum nature becomes important. This can be already seen from a simple model of a quantum emitter is a two-level atom with two states, the ground state $|g\rangle$ and the excited state $|e\rangle$. When an atom absorbs a photon an electron is excited and the atom's optical response changes completely: a second photon can no longer be absorbed. Thus, such an atom presents an inherently nonlinear optical system. This demands a separate quantum description. However, many of the collective effects described in the previous chapter survive, and also new effects, such as Dicke superradiance, appear in the quantum regime. In this chapter we will present a theoretical description for an array of atoms collectively interacting with light and we will describe several basic effects.

10.1 Jaynes–Cummings model

We start the discussion with writing down the basic Hamiltonian describing an array of atoms interacting with a single photonic mode:

$$H = H_{\text{at}} + H_{\text{phot}} + H_{\text{int}} . \quad (10.1)$$

Here H_{at} , H_{phot} and H_{int} are the Hamiltonians of atoms, photons, and their coupling, respectively:

$$H_{\text{at}} = \omega_0 \sum_{j=1}^N \sigma_j^\dagger \sigma_j, \quad H_{\text{phot}} = \omega_{\text{cav}} a^\dagger a, \quad H_{\text{int}} = g \sum_j (a \sigma_j^\dagger + a^\dagger \sigma_j) . \quad (10.2)$$

$\sigma_j^\dagger|g_j\rangle = |e_j\rangle$ and $\sigma_j|e_j\rangle = |g_j\rangle$ are the atomic raising and lowering operators acting in the space of each atoms ground $|g_j\rangle$ and excited states $|e_j\rangle$, ω_0 and ω_{cav} are the atom and cavity photon resonance frequencies and the constant g describes atom-photon coupling. We use the rotating wave approximation and disregard the terms $\propto a\sigma_j, a^\dagger\sigma_j^\dagger$.

It is instructive to study the eigenstates of the coupled atom-photon system already in the simplest case of one atom $N = 1$. This corresponds to the exactly solvable Jaynes-Cummings model, introduced in Ref. [1]. To solve the model we notice that the Hamiltonian commutes with the operator of the total number of excitatons in the system $a^\dagger a + \sigma^\dagger \sigma$. Thus, the number of excitations $m = 0, 1, 2$ is a good quantum number. We look for the general eigenstate with m excitations

$$\psi_m = A|m-1, e\rangle + B|m, g\rangle \quad (10.3)$$

as a superposition of a states with $m-1$ cavity photons and excited atom or m photons and atom in the ground state. The Schrödinger equation in the subspace with m excitations reads

$$H\psi_m = \omega\psi_m, \quad H_m = \omega_{\text{cav}}(m-1) + \begin{pmatrix} \omega_0 & g\sqrt{m} \\ g\sqrt{m} & \omega_{\text{cav}} \end{pmatrix}, \quad (10.4)$$

and the eigenfrequencies are given by

$$\omega_{m,\pm} = \omega_{\text{cav}}(m-1) + \frac{\omega_0 + \omega_{\text{cav}}}{2} \pm \sqrt{g^2 m + \left(\frac{\omega_0 - \omega_{\text{cav}}}{2}\right)^2}. \quad (10.5)$$

The spectrum is schematically illustrated in Fig. 10.1. It is formed by avoided crossings of the many-photon resonances with the atomic resonance. The Rabi splitting between the resonances increases with the number of excitations $\propto \sqrt{m}$. This means that the more photons are in the cavity the stronger their electric field and the stronger the light-matter coupling.

10.2 Collective Dicke states and Tavis-Cummings model

We are now ready to proceed to the case of $N > 1$ emitters. This is in general a very complicated problem since the Hilbert space grows as 2^N . However, it can be simplified in the considered case when all the emitters are the same.

In order to make use of the symmetry between the emitters we introduce the collective

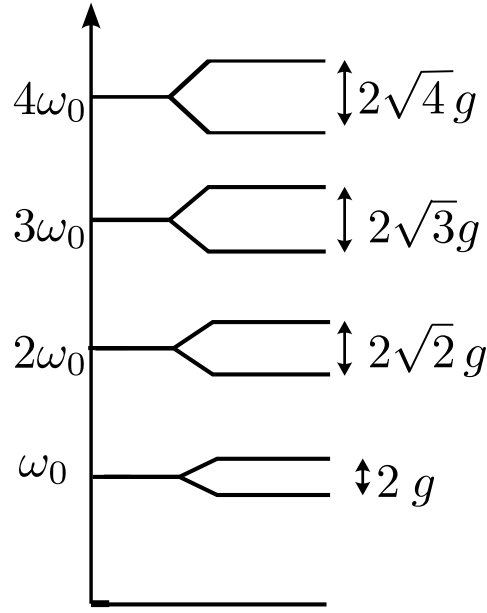


Figure 10.1: Schematic illustration of energy spectrum in the Jaynes-Cummings model [1], describing a two-level atom in a cavity

(pseudo)spin raising and lowering operators J_{\pm} :

$$\sum_{j=1}^N \sigma_j = J_-, \quad \sum_{j=1}^N \sigma_j^\dagger = J_+. \quad (10.6)$$

This operators satisfy the usual algebra of the momentum operators, in particular $[J_+, J_-] = 2iJ_z$. Using the collective spin operators the Hamiltonian Eq. (10.2) assumes the following form:

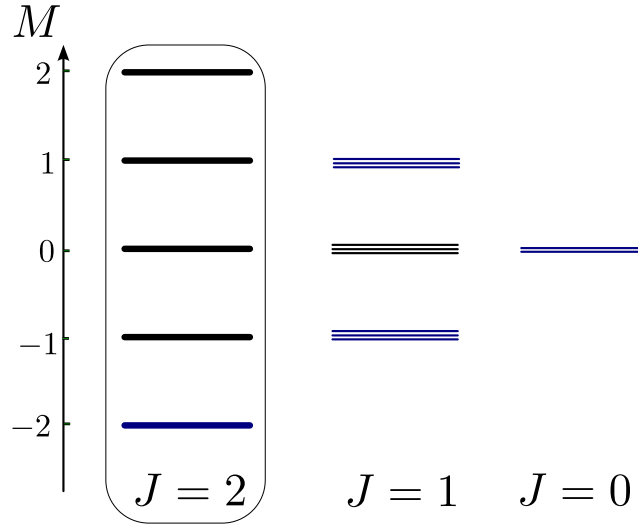
$$H_{\text{at}} = \omega_0 J_z + \frac{N\omega_0}{2}, \quad H_{\text{int}} = g(aJ_+ + a^\dagger J_-). \quad (10.7)$$

In order to understand its spectrum we remember that the total momentum in the system of N spins-1/2 can take the following values:

$$J = N/2, N/2 - 1, \dots \quad (10.8)$$

Figure 10.2 illustrates the possible states of the atomic array and their degeneracies, characterized by their total momentum and its projection on the z axis for the particular case of $N = 4$. The value of collective spin projection onto z axis M encodes the number of excitations in the system: $M = -N/2$ ($+N/2$) corresponds to all atoms being in the ground (excited) states.

Of all the states in Fig. 10.2, the most important are the $N + 1$ states with $J_{\text{tot}} = N/2$.


 Figure 10.2: Illustration of a Dicke ladder of states for $N = 4$ emitters

The reason is that if we start with all atoms in the ground state $|J_{\text{tot}} = N/2, M = -N/2\rangle$, only this subset will be excited due to the symmetry of the problem, because the interaction H_{int} with light preserves J_{tot} . It is worth writing them down explicitly;

$$\begin{aligned}
 |M = -\frac{N}{2}, J = \frac{N}{2}\rangle &\equiv |0\rangle \equiv |g_1 g_2 \dots g_N\rangle, \\
 |M = -\frac{N}{2} + 1, J = \frac{N}{2}\rangle &\equiv \frac{1}{\sqrt{N}} (|e_1 g_2 \dots g_N\rangle + |g_1 e_2 \dots g_N\rangle + \dots + |g_1 g_2 \dots e_N\rangle), \\
 |M = -\frac{N}{2} + 2, J = \frac{N}{2}\rangle &\equiv \frac{1}{\sqrt{N(N-1)}} (|e_1 e_2 \dots g_N\rangle + |g_1 e_2 \dots e_N\rangle + \dots + |e_1 g_2 \dots e_N\rangle), \\
 |M = \frac{N}{2}, J = \frac{N}{2}\rangle &\equiv |e_1 e_2 \dots e_N\rangle.
 \end{aligned} \tag{10.9}$$

We can see that this *Dicke states* correspond to symmetric combinations with one atom excited, two atoms excited, and so on.

The spectrum of the Hamiltonian (10.7) can be found exactly [2]. It assumes the most simple form in the case of zero detuning, when $\omega_0 = \omega_{\text{cav}}$. We can then write

$$E_{J,M,\pm} = \omega_0 J_z + \frac{N\omega_0}{2} \pm \sqrt{2g|[J_+]_{M-1,M}|}, \quad [J_+]_{M,M+1} = \sqrt{(J-M+1)(J+M)}. \tag{10.10}$$

Let us consider the particular case of just one excitation. In this case we have $M = -N/2 + 1$ and either $J_{\text{tot}} = N/2$ or $J_{\text{tot}} = N/2 - 1$ (see Fig. 10.2). The first case corresponds to $E_{N/2, -N/2+1, \pm} = \omega_0 \pm \sqrt{Ng}$ and the latter to $N-1$ degenerate states $E_{N/2-1, -N/2+1} = \omega_0$. This agrees with the results we have obtained before in Sec. ?? in the strong coupling regime. For

$J_{\text{tot}} = N/2$ we see the collectively enhanced Rabi splitting, and the states with $J_{\text{tot}} = N/2 - 1$ are the degenerate dark states that do not interact with light. The states with $J_{\text{tot}} < N/2$ are in general degenerate. We will discuss them in more detail in Chapter 12 when we will consider subradiant states.

The agreement between the results of the semiclassical description in Sec. ?? above and the quantum description is not a coincidence. When we have just one photon in the system, the results are generally the same as in a semiclassical model. The reason is that the anharmonicity of the two-level atom potential is not manifested for one excitation: one photon does not encounter another photon to interact with. There is however one important difference: in Sec. ?? we were able to obtain a quasistationary states that have a finite lifetime. The quantum description in this section considers a closed system with a purely Hermitian Hamiltonian and infinite lifetimes, all energies are real. However, there is a way to consider quantum systems with dissipation. We will do that in the next section.

10.3 Weak coupling: collective spontaneous emission

In the previous section we considered an array of emitters resonantly coupled to the mode of a perfect cavity with infinite lifetime. Here, we will consider an entirely opposite setup of waveguide QED. Instead of being trapped in a cavity the photons will freely propagate and have a continuum spectrum $\omega_k = ck$ where k is the photon wave vector. As such, they can carry the energy away from the atoms. This obviously leads to the energy dissipation. What is important, however, that the dissipation will be collective, since the same propagating photon can be coupled to several atoms. Moreover, the photons will also mediate the coupling between the atoms.

We start by writing the photon Hamiltonian

$$H_{\text{phot}} = \sum_k \omega_k a_k^\dagger a_k \quad (10.11)$$

and the interaction Hamiltonian

$$H_{\text{int}} = - \sum_{k,j} \sqrt{\frac{2\pi\omega_k}{L}} [d e^{-ikz_j} \sigma_j a_k^\dagger + d^* e^{ikz_j} a_k \sigma_j^\dagger]. \quad (10.12)$$

Here, d is the dipole matrix element describing atom-photon coupling and L is the normalization

length; $\sum_k \equiv L \int_{-\infty}^{\infty} dk / (2\pi)$. The polarization degrees of freedom are disregarded for simplicity.

Since the photons can carry energy away, the atoms are generally in a mixed state and should be characterized by a density matrix ρ . We show in Appendix F, that such a matrix satisfies the Lindblad master equation [3, 4]

$$\frac{\partial \rho}{\partial t} = -\gamma_{1D} \sum_{j,j'} \text{Im} \mathcal{G}(z_j, z_{j'}) \left[\sigma_j^\dagger \sigma_{j'} \rho(t) + \rho(t) \sigma_j^\dagger \sigma_{j'} - 2\sigma_j \rho(t) \sigma_{j'}^\dagger \right] - i[H, \rho]. \quad (10.13)$$

Importantly, this master equation features collective dissipation: the decay terms are nonlocal. The Hamiltonian

$$H = -\gamma_{1D} \sum_{j,j'} \text{Re} \mathcal{G}(z_j, z_{j'}) \sigma_j^\dagger \sigma_{j'} \quad (10.14)$$

describes the dispersive photon-mediated coupling between the atoms due to the photon exchange. Here,

$$\mathcal{G}(z, z', \omega) = \lim_{\Delta \rightarrow +0} \int_{-\infty}^{\infty} \frac{dk}{2\pi} \frac{e^{ik(z-z')}}{\omega_k - \omega - i\Delta} = \frac{i}{c} e^{i\omega|z-z'|/c} \quad (10.15)$$

is the photon Green function. The master equation can also be rewritten as

$$\frac{\partial \rho}{\partial t} = 2\gamma_{1D} \sum_{j,j'} \text{Im} \mathcal{G}(z_j, z_{j'}, \omega_0) \sigma_j \rho(t) \sigma_{j'}^\dagger - i(H_{\text{eff}} \rho - \rho H_{\text{eff}}^\dagger), \quad (10.16)$$

where we have isolated the quantum jump term and the effective non-Hermitian Hamiltonian

$$H_{\text{eff}} = -\frac{g_0^2}{L} \sum_{j,j'} \mathcal{G}(z_j, z_{j'}, \omega_0) \sigma_j^\dagger \sigma_{j'} \quad (10.17)$$

that describes the dynamics in the absence of quantum jumps. Identifying the single atom spontaneous emission rate in the cavity as $\gamma_{1D} = g_0^2/c$, (wher $g_0 = \sqrt{2\pi\omega_0}d$) we see, that the non-Hermitian Hamiltonian generalizes the non-Hermitian Hamiltonian we obtained before (Eq. (3.25)) for the multiple excited case.

This Lindblad master equation assumes that without the atom-photon interaction the photons in a waveguide are at vacuum. Otherwise, if photons are described by some effective nonzero temperature, the decay to the reservoir is enhanced due to the stimulated emission. One has also to include the processes where the photons are absorbed from the waveguide. It is also possible to generalize the master equation for the case when the photons in the waveguide

are in a squeezed state [5].

We note that while we have presented the derivation for the waveguide with linear dispersion, the general form of the master equation remains the same also for more complicated setups if the photon Green function is properly calculated. Such a more general derivation is contained in Appendix F.

It is also instructive to consider the case when all the atoms are either close to each other $z_j = 0$ or separated by a wavelength $z_j = 2\pi c/\omega_0$, so that $G(z_j, z_{j'}) = -i\gamma_{1D}$. In this case there is no photon-mediated dispersive coupling and only collective dissipation remains

$$H = 0, H_{\text{eff}} = -i\gamma_{1D}, \quad (10.18)$$

$$\frac{\partial \rho}{\partial t} = \gamma_{1D}[2J_- \rho(t) J_+ - J_+ J_- \rho(t) - \rho(t) J_+ J_-], \quad (10.19)$$

where the collective spin raising operators J_{\pm} have been introduced in the previous section, Eq. (10.6). Equation (10.19) would be also the same if the atoms are placed in the bad cavity with low cooperativity, so that the cavity dynamics can be eliminated. It describes the collective spontaneous emission of the atoms in the environment, when all the emitted photons interfere constructively. This constructive interference leads to the Dicke superradiance that will be described in the next chapter.

10.4 Additional reading

References

- ¹E. T. Jaynes and F. W. Cummings, “Comparison of quantum and semiclassical radiation theories with application to the beam maser”, *Proc. IEEE* **51**, 89 (1963).
- ²M. Tavis and F. W. Cummings, “Exact Solution for an N -Molecule—Radiation-Field Hamiltonian”, *Phys. Rev.* **170**, 379–384 (1968).
- ³K. Lalumière, B. C. Sanders, A. F. van Loo, A. Fedorov, A. Wallraff, and A. Blais, “Input-output theory for waveguide qed with an ensemble of inhomogeneous atoms”, *Phys. Rev. A* **88**, 043806 (2013).
- ⁴R. H. Lehmberg, “Radiation from an N -atom system. I. General Formalism”, *Phys. Rev. A* **2**, 883–888 (1970).
- ⁵J. You, Z. Liao, S.-W. Li, and M. S. Zubairy, “Waveguide quantum electrodynamics in squeezed vacuum”, *Physical Review A* **97**, 023810 (2018).

Chapter 11

Dicke superradiance

In the previous chapter we have developed theoretical approaches to describe collective light-matter interaction in the quantum regime. We are now ready to apply these approaches and consider the basic collective quantum effect, Dicke superradiance [1]. We start in Sec. 11.1 with the original Dicke formulation of a problem of collective spontaneous decay for an initially fully excited atom array. Next, in Sec. 11.2 we will proceed to the Dicke phase transition, that happens in driven systems.

11.1 Superradiant burst

Let us assume, that at $t = 0$ the array of emitters is fully excited, that is, it is in the state with the total momentum $J = N/2$ and momentum projection $M = N/2$ (see Fig. 10.2). After that, the atoms will start to spontaneously emit photons. The main finding will be that the emission rate in the array is faster than the rate γ_{1D} for a single atom by a factor $\propto N$ and the peak emission intensity is larger by a factor of N^2 .

The emission dynamics is described by the Lindblad master equation (10.19). The master equation is readily solved numerically. The rate of photon emission is given just by

$$I(t) = 2\gamma_{1D}\text{Tr}(J_-\rho J_+), \quad (11.1)$$

since each quantum jump corresponds to a photon being emitted. The results of numerical calculation of emission dynamics are presented in Fig. 11.1. We see, that instead of a slow

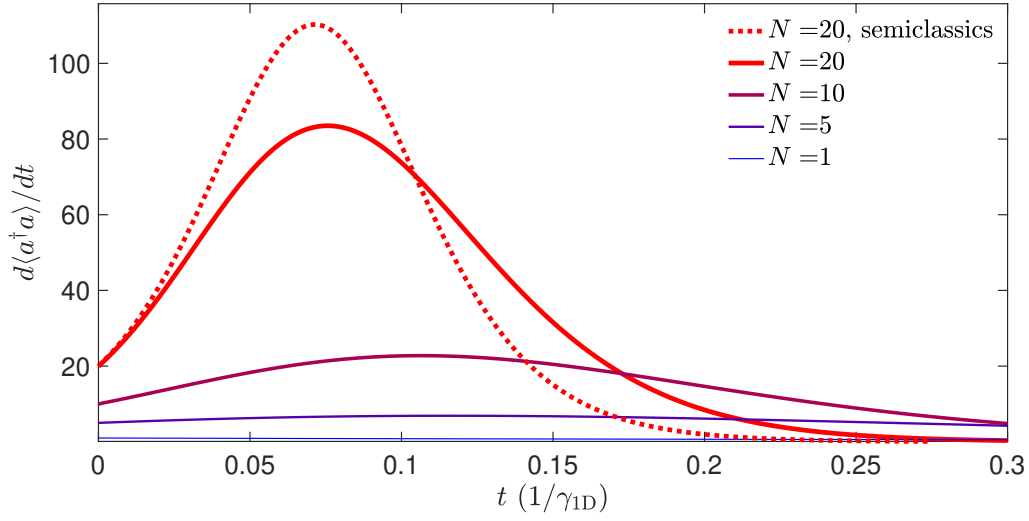


Figure 11.1: Superradiant burst in the Dicke model. The curves show time-dependent emission intensity for different numbers of emitters. Dotted curve presents the semiclassical result Eq. (11.8).

monotonous decay for a single atom, $I(t) = 2\gamma_{1D} \exp(-2\gamma_{1D}t)$, the intensity develops a short and high *superradiant burst*. At $t = 0$ the intensity is given by just $I(t = 0) = 2N\gamma_{1D}$, which corresponds to an uncorrelated spontaneous emission, with the intensity just proportional to the number of atoms. However, later on, the emission becomes coherent and fast.

The dynamics of the superradiant burst can be described analytically in a semiclassical approximation [2]. We start by looking for the solution in the form

$$\rho = \sum_{M=1}^N \rho_M |M\rangle \langle M|, \quad (11.2)$$

where ρ_M are the populations of the Dicke states Eq. (10.9) and rewrite the master equation in this basis as

$$\frac{\partial \rho_M}{\partial t} = 2\gamma_{1D}(J - M)(J + M + 1)(\rho_{M+1} - \rho_M) \quad (11.3)$$

Next, we introduce the average spin projection $\langle M \rangle$. Each act of spontaneous emission corresponds to a transition one step down the ladder of Dicke states, decreasing M by one. If we assume that the projection is a good quantum number, we can just apply Eq. (11.11) directly to describe its dynamics

$$\frac{\partial \langle M \rangle}{\partial t} = -2\gamma_{1D}(J - \langle M \rangle)(J + \langle M \rangle + 1), \quad (11.4)$$

where $J = N/2$ and the initial condition reads $\langle M(t = 0) \rangle = N/2$. The solution of this

differential equation yields

$$\langle M \rangle = \frac{N}{2} \frac{(N - e^{2\gamma_{1D}t(1+N)} + 2)}{N + e^{2\gamma_{1D}t(1+N)}}. \quad (11.5)$$

The rate of emission then becomes

$$\frac{\partial \langle M \rangle}{\partial t} = 2\gamma_{1D} \frac{(N+1)^2}{N} \frac{N^2 e^{2\gamma_{1D}t(1+N)}}{(N + e^{2\gamma_{1D}t(1+N)})^2}. \quad (11.6)$$

By solving the condition $\frac{\partial \langle M \rangle}{\partial t} = 0$ we can find the expression for the emission maximum

$$t_D = \frac{\gamma_{1D} \ln N}{2(N+1)} \quad (11.7)$$

and rewrite the intensity as

$$I(t) = \gamma_{1D} \frac{(N+1)^2}{2} \frac{1}{\cosh^2[2\gamma_{1D}(N+1)(t - t_D)]}. \quad (11.8)$$

Equations (11.7), (11.8) clearly show the speedup of the emission dynamics and the enhancement of the peak emission intensity. The result of the calculation following Eq. (11.8) is shown in Fig. ?? by the dotted curve that qualitatively agrees with the full master equation simulation. The error results from the fact that Eq. (11.4) where M has been replaced it by the averaging value, does not fully capture the actual distribution of M . More detailed modern discussion of the analytical approaches to the superradiant burst in various setups can be found in Ref. [3].

11.2 Dicke phase transition

The Dicke superradiant burst phenomenon is a speed-up of emission from an excited system that then evolves freely, without an external driving. In this section, we describe another collective phenomenon, Dicke phase transition, that happens for a driven system [4, 5].

We consider an array of atoms, that are coupled to the same photon mode and subjected to a resonant periodic driving, described by the interaction term

$$V = \Omega_R \sum_{j=1}^N (\sigma_j e^{-i\omega_0 t} + \sigma_j^\dagger e^{i\omega_0 t}), \quad (11.9)$$

where the Rabi frequency Ω_R characterizes the driving strength. In the frame, rotating with

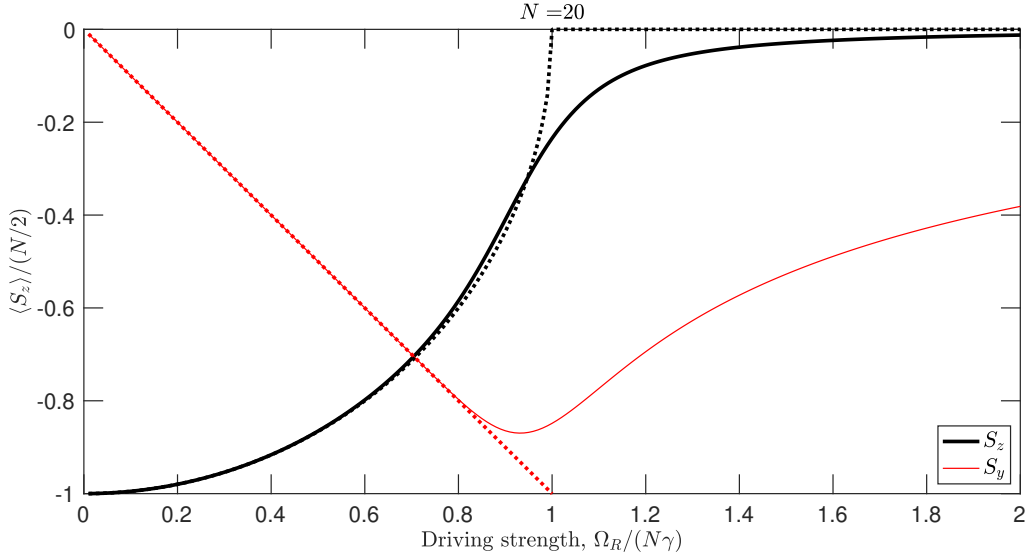


Figure 11.2: Dicke phase transition in the driven array of N atoms. Solid curve show the dependence of the collective spin components S_z and S_y on the drive strength calculated numerically from the master equation Eq. (11.11), dotted lines present the analytical results Eqs. (11.17). Calculation has been performed for $N = 20$.

the frequency ω_0 the driving term becomes time-independent, and assumes the following simple form

$$V = 2\Omega_R J_x . \quad (11.10)$$

Here, $J_x \equiv \sum_{j=1}^N (\sigma_j + \sigma_j^\dagger)/2$ is the collective spin operator, introduced in the previous chapter. The master equation for the density matrix then assumes the following form

$$\frac{\partial \rho}{\partial t} = \gamma_{1D} (2J_- \rho J_+ - J_+ J_- \rho - \rho J_+ J_-) - 2i\Omega_R [S_x, \rho] , \quad (11.11)$$

it differs from Eq. (10.19) that we considered before by the presence of the driving term.

Before proceeding to the rigorous numerical solution it is instructive to analyze Eq. (11.11) in the semiclassical approximation. This approximation applies to large number of atoms, and large expectation values of the momentum projection operators J_α ($\alpha = x, y, z$), when they can be approximated by the complex numbers:

$$S_\alpha = \langle J_\alpha \rangle, S_\alpha S_\beta = \langle J_\alpha J_\beta \rangle . \quad (11.12)$$

In order to derive the semiclassical equations we start from the following exact operator for

the operators J_α that follows from Eq. (11.11):

$$\dot{J}_\alpha = \text{Tr} \left[J_\alpha \frac{\partial \rho}{\partial t} \right] = i \text{Tr} ([V, J_\alpha] \rho) + \gamma_{1D} (2J_+ J_\alpha J_- - J_+ J_- J_\alpha - J_\alpha J_+ J_-). \quad (11.13)$$

In particular, we find

$$\dot{J}_z = 2\Omega_R J_y - 2\gamma_{1D} J_+ J_- \quad (11.14)$$

In the limit of $J \gg 1$ we can neglect the commutator between J_+ and J_- and write $2J_+ J_- = J_+ J_- + J_- J_+ + 2J_z \approx J_+ J_- + J_- J_+$, which results in

$$\dot{J}_z = 2\Omega_R J_y - 2\gamma_{1D} (J_+ J_- + J_- J_+) = 2\Omega_R J_y - 2\gamma_{1D} (J_x^2 + J_y^2). \quad (11.15)$$

Next, we replace the operators and their products by the corresponding expectation values following Eq. (11.12). This procedure results in the following system of coupled equations for the collective spin [5]:

$$\begin{aligned} \dot{S}_x &= 2\gamma_{1D} S_z S_x, \\ \dot{S}_y &= -2\Omega_R S_z + 2\gamma_{1D} S_z S_y, \\ \dot{S}_z &= 2\Omega_R S_y - 2\gamma_{1D} (S_x^2 + S_y^2). \end{aligned} \quad (11.16)$$

The equations have a following transparent interpretation. The driving term Ω_R acts as an effective magnetic field along x axis, leading to the spin rotation about this axis. The spontaneous emission leads to the decay of the spin towards the point $S_x = S_y = 0$, while preserving the length of the spin vector $S_x^2 + S_y^2 + S_z^2 = (N/2)^2 = \text{const.}$ The competition of the driving and the spontaneous emission can lead to the interesting spin dynamics. The stationary point of Eqs. (11.16) reads

$$S_x = 0, S_y = \frac{\Omega}{\Omega_c}, \quad S_z = -\sqrt{1 - \frac{\Omega_R^2}{\Omega_c^2}}, \quad (11.17)$$

It shows that when $\Omega < \Omega_c$, ($\Omega_c = N\gamma_{1D}$), there exists a stationary nontrivial solution for the spin. The point $\Omega = \Omega_c$ corresponds to the dissipative first-order phase transition, where S_z has a square-root singularity. We remind, that the value of S_z describes the population inversion for the array; $S_z = -N/2$ ($+N/2$) corresponds to all atoms being in the ground (excited) state.

The dependence of the spin projections on the driving strength is shown in Fig. 11.2. Solid curves present the numerical solution of the master equation Eq. (11.11), while dotted curves show the analytical semiclassical result Eq. (11.17). The calculations are in good agreement despite the fact that the array is relatively small and has only $N = 20$ atoms.

The same system of equations also describes an array of atoms in a cavity, with γ_{1D} being replaced by the single-atom decay rate of the cavity mode γ . When the driving strength Ω_R is above the critical frequency Ω_c , the system of nonlinear equations Eq. (11.16) has a long-living oscillating solution [6]. This solution oscillates with the frequency $2\sqrt{\Omega_R^2 - \Omega_c^2}$ and decays with the rate on the order of γ .

In Ref. [5] it has been noted, that in order to properly define the macroscopic limit for the array of atoms, when $J = N/2 \gg 1$, the decay rate has to be additionally renormalized, that is, divided by a factor on the order of N [5], $\gamma \rightarrow \gamma/N$. After such a renormalization, the oscillating solution becomes long-living, its decay rate scales as γ/N . This solution has been termed a so-called time-crystalline phase [5].

Such a phase transition has been experimentally observed in Ref. [7] for a Bose-Einstein condensate of atoms in an optical cavity. The so-called oscillating time-crystalline phase, predicted in Ref. [5], has been experimentally observed in Ref. [8].

11.3 Additional reading

Reviews on superradiance: A. V. Andreev et al., “Collective spontaneous emission (Dicke superradiance)”, [Soviet Physics Uspekhi](#) **23**, 493 (1980) M. S. Feld and J. C. MacGillivray, “Superradiance”, in *Coherent nonlinear optics: recent advances*, edited by M. S. Feld and V. S. Letokhov (Springer Berlin Heidelberg, Berlin, Heidelberg, 1980), pp. 7–57, M. Gross and S. Haroche, “Superradiance: An essay on the theory of collective spontaneous emission”, [Physics Reports](#) **93**, 301–396 (1982)

References

- ¹R. H. Dicke, “Coherence in Spontaneous Radiation Processes”, [Phys. Rev.](#) **93**, 99 (1954).
- ²M. Gross and S. Haroche, “Superradiance: An essay on the theory of collective spontaneous emission”, [Physics Reports](#) **93**, 301–396 (1982).
- ³R. Holzinger and S. F. Yelin, *Collective superradiance: estimating the peak emission rate and time*, 2025, [arXiv:2504.09985 \[quant-ph\]](#).
- ⁴H. J. Carmichael, “Analytical and numerical results for the steady state in cooperative resonance fluorescence”, [Journal of Physics B: Atomic and Molecular Physics](#) **13**, 3551 (1980).
- ⁵F. Iemini, A. Russomanno, J. Keeling, M. Schiró, M. Dalmonte, and R. Fazio, “Boundary time crystals”, [Phys. Rev. Lett.](#) **121**, 035301 (2018).
- ⁶N. Leppenén and E. Shahmoon, *Quantum bistability at the interplay between collective and individual decay*, 2024, [arXiv:2404.02134 \[quant-ph\]](#).
- ⁷K. Baumann, C. Guerlin, F. Brennecke, and T. Esslinger, “Dicke quantum phase transition with a superfluid gas in an optical cavity”, [Nature](#) **464**, 1301–1306 (2010).
- ⁸H. Keßler, P. Kongkhambut, C. Georges, L. Mathey, J. G. Cosme, and A. Hemmerich, “Observation of a dissipative time crystal”, [Phys. Rev. Lett.](#) **127**, 043602 (2021).
- ⁹A. V. Andreev, V. I. Emel’yanov, and Y. A. Il’inskii, “Collective spontaneous emission (Dicke superradiance)”, [Soviet Physics Uspekhi](#) **23**, 493 (1980).
- ¹⁰M. S. Feld and J. C. MacGillivray, “Superradiance”, in *Coherent nonlinear optics: recent advances*, edited by M. S. Feld and V. S. Letokhov (Springer Berlin Heidelberg, Berlin, Heidelberg, 1980), pp. 7–57.
- ¹¹G. Ferioli, A. Glicenstein, I. Ferrier-Barbut, and A. Browaeys, “A non-equilibrium superradiant phase transition in free space”, [Nature Physics](#) **19**, 1345–1349 (2023).

REFERENCES

Modern discussion of superradiant burst: R. Holzinger and S. F. Yelin, *Collective superradiance: estimating the peak emission rate and time*, 2025, [arXiv:2504.09985 \[quant-ph\]](#)

Comparison of Monte-Carlo and master equation techniques for the Dicke phase transition: N. Leppenen and E. Shahmoon, *Quantum bistability at the interplay between collective and individual decay*, 2024, [arXiv:2404.02134 \[quant-ph\]](#).

Analogue of the Dicke phase transition in a free-space cavity-free setup G. Ferioli et al., “A non-equilibrium superradiant phase transition in free space”, *Nature Physics* **19**, 1345–1349 (2023).

Chapter 12

Multiple-excited subradiant states

In the previous sections, we considered the collective quantum dynamics in the array of two-level atoms, focussing on the symmetric superradiant Dicke states. However, the full Hilbert space size for an array of N two-level atoms scales as 2^N , while the Dicke-type models have probed only a reduced $N + 1$ -dimensional space of symmetric states. The abundance of unexplored physics becomes especially evident for subradiant states: to paraphrase the beginning of Tolstoy’s “Anna Karenina,” *all superradiant states are similar to each other, but all subradiant states are different*. The question “what is the darkest state?”, that we focused on, is apparently harder than the question “what is the brightest state?”.

To be more precise, the photons emitted from a subradiant state interfere destructively so that the rate of spontaneous emission from an array becomes smaller than that for an individual atom. There are many different inequivalent ways to realize such destructive interference — the Hilbert subspace of dark states in atomic arrays with multiple excitations is highly degenerate, and there are many linearly independent wavefunctions with destructive interference. Understanding dark states is useful because arrays of quantum emitters coupled to photons are a promising platform for deterministic quantum information processing, and knowledge of how to control the spontaneous emission rate can help to enhance the excitation lifetime [1].

We will start this section by re-examining the subradiant states in the Dicke model, and then will proceed to the more complicated waveguide QED model.

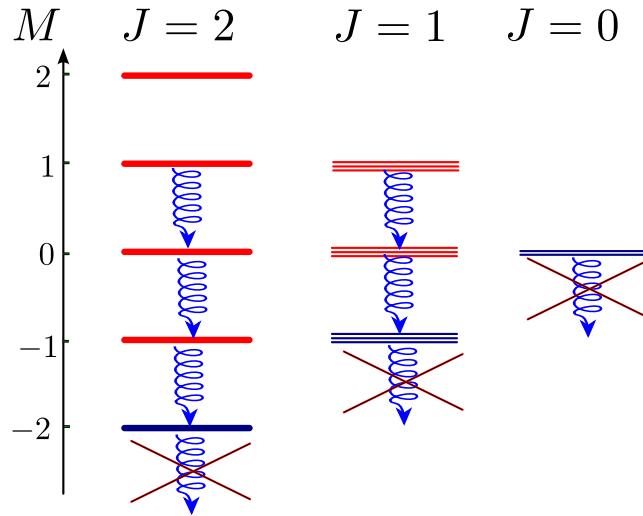


Figure 12.1: Illustration of a Dicke ladder of states for $N = 4$ emitters. Curvy arrows illustrate spontaneous emission processes, that conserve the total momentum J . The lowest-energy states with given J are dark states, because spontaneous emission from them is not possible.

12.1 Subradiant states in the Dicke ladder

Let us consider the spontaneous emission of photons from an array of identical two-level atoms. As discussed in Sec. 10.2, it is instructive to describe such an array in the basis of states with a given total momentum J and momentum projection M . All possible states for an array of $N = 4$ atoms are illustrated in Fig. 12.1. If all the atoms are the same, the spontaneous emission process preserves the spherical symmetry, that is, it conserves the total momentum J . As such, the spontaneous emission processes can be considered independently for sets of states with different J . For a given J , emission of a photon decreases M by unity. The lowest- M state for a given J , however, is dark: there are no more atomic states with the same symmetry to decay to, and spontaneous emission is impossible. There exist $C_N^{[N/2]}$ such dark states, including the ground state [2], that form the kernel of the jump operator J_- [3, 4]. The picture Fig. 12.1 immediately shows that there are no subradiant states with the fill-factor more than $1/2$ (with $M > 0$). This is a very general finding. It is not restricted to the Dicke model and, as will be discussed in the following section, is also applied to the waveguide QED setup [2, 5].

12.2 Subradiant states in waveguide QED

Let us answer a following question:

“what is the darkest (least radiant) state with a given amount of excitations?” for an array of emitters coupled to the waveguide.

In order to better explain the question and the answer, we start from the simplest case of $N = 2$ two-level atoms, interacting with photons in the waveguide, see Fig. 12.2. As discussed in Chapter 5, the subradiant state for the two atoms with the spacing smaller than half of the wavelength is the dimer state,

$$|\text{dimer}\rangle = \frac{1}{\sqrt{2}}(\sigma_1^\dagger - \sigma_2^\dagger)|0\rangle, \quad (12.1)$$

that is an antisymmetric superposition of the single-excited state of each of the atoms [Fig. 12.2(a)]. Here $|0\rangle$ is the ground state of the array and σ^\dagger are the atomic raising operators, so this dimer state has a superposition of just two single-excited states. Due to the “ $-$ ” sign, the photon emission processes from the two atoms interfere destructively. The spontaneous emission lifetime τ for the state Eq. (12.1) has been calculated in Sec. 5, Eq. (5.32). The answer is recalled below

$$\frac{1}{\tau} = \frac{1}{\tau_1} \min |1 - \cos \varphi|, \quad (12.2)$$

and contains an interference term where $\varphi = \omega_0 d/c$ is the phase gained by light between the two atoms. Here, $\tau_1 \equiv 1/(2\gamma_{1D})$ is the lifetime for a single atom. Clearly, when φ is close to an integer number of 2π (the spacing d is an integer number of wavelengths λ), the two interfering terms in Eq. (12.2) cancel each other and the lifetime τ becomes longer than τ_1 by a factor on the order of $1/\varphi^2$, $1/(\varphi - 2\pi)^2$, etc.

While this subradiant dimer state is almost trivial and well known [6], answering the question “what is the darkest state?” becomes harder in an array with more than $N = 2$ atoms, even for just a single excitation. For example, for $N = 3$ atoms there are two candidates for the darkest single-excited state, $\propto (\sigma_1^\dagger - \sigma_3^\dagger)|0\rangle$ and $\propto (\sigma_1^\dagger + \sigma_3^\dagger - 2\sigma_2^\dagger)|0\rangle$, and it is not immediately obvious which linear combination has the longest lifetime. In 2019, Molmer and Zhang [7] presented a general answer for the 1D problem for the subradiant single-excited state [see Fig. 12.2(b)]:

$$|\text{standing wave}\rangle = \sqrt{\frac{2}{N}} \sum_{m=1}^N (-1)^m \sin \left[\frac{\pi\nu}{N} \left(m - \frac{1}{2} \right) \right] \sigma_m^\dagger |0\rangle, \quad (12.3)$$

where $\nu = 1$ for the darkest state and the lifetime decreases with $\nu = 1, 2, \dots$ as $1/\nu^2$. We have discussed this in more detail in Sec. 7.1. The answer Eq. (12.3) is relatively intuitive: first, the factor $(-1)^m$ ensures destructive interference of emission from different atoms, second,

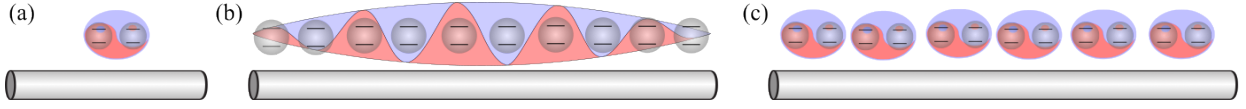


Figure 12.2: (a) Subradiant dimer: two atomic excitations destructively interfering in photon emission, see Eq. (12.1). (b) Subradiant standing wave [7], Eq. (12.3). (c) Subradiant dimer product Eq. (12.5), [2, 5].

the excitation amplitude decays towards the edge of the array, which further suppresses the probability of photon escape from the array.

Another important prediction of Refs. [7, 8] was that the ansatz Eq. (12.3) remains valid for more than one excitation, if the fill-factor of excitations is small, $f \ll 1$. To be more precise, the darkest state with several excitations can be obtained as a fermionized antisymmetric combination of the standing waves Eq. (12.3) with different values of ν . Indeed, the problem of photons propagating in a one-dimensional array and coupled to atoms under certain conditions can be mapped to the problem of interacting hard-core bosons. The interaction is provided by the strong anharmonicity of the two-level atom potential. However, the fate of fermionization and the structure of the darkest states in the strongly excited regime remained unclear. In the Ref. [9], it has been predicted that for two excitations and four atoms, the dark states differ strongly from Eq. (12.3). It has also been found that these double-excited subradiant states manifest as sharp resonances in the two-photon inelastic scattering spectra, in the same way as single-excited states can be seen as resonances in single-photon reflection and transmission spectra.

In light of our results [9], the validity region for the fermionized ansatz by Zhang and Mølmer [7, 8] thus was a puzzle. There were several types of discrepancies. First, the dispersion of polaritons in the waveguide QED is strongly nonparabolic. Fermionization is applicable only to hard-core bosons with parabolic dispersion. For polaritons, this is an approximation, valid only near the edge of the Brillouin zone, $k \sim \pi/d$, as can be seen from Fig. ?? . As such, while the darkest states could be described by the ansatz, it has been shown that the general subradiant state wavefunction becomes chaotic due to the nonparabolic dispersion [10].

The second discrepancy with fermionization was related to bound states. When the period of the array was close to $1/12$ of the light wavelength at the atom resonance, $d = \lambda/12$, the numerical calculations indicated that the darkest state was not the fermionized standing wave state but the bound state of two photons [11]. This puzzle can be resolved by analyzing the dispersion of bound pairs $E(K)$ in the infinite array. The bound state wavefunction can be

approximated by

$$|\text{bound}\rangle = \sum_{m_1, m_2} e^{iK(m_1+m_2)} \Phi_{|m_1-m_2|} \sigma_{m_1}^\dagger \sigma_{m_2}^\dagger |0\rangle, \quad (12.4)$$

where $K = k_1 + k_2$ is the center-of-mass wave vector. The amplitude $\Phi_{|m_1-m_2|}$ describes the relative motion of the two particles, it decays as $|m_1 - m_2|$ increases. One can analytically prove that for $d = \lambda/12$ the effective mass of the bound pairs diverges, $\partial^2 E / \partial K^2 = 0$ at $K = \pi/d$ [12]. As such, the bound pairs become heavy, it becomes hard for them to escape the array, and the spontaneous emission time increases. More detailed calculations of the dispersion of the bound photon pairs can be found in Refs. [13, 14].

Another discrepancy with the prediction of the fermionization ansatz occurs at large excitation fill factors, when the fermionization breaks down. It was found that with the increase in the number of excitations, the darkest subradiant states transform from antisymmetrized products of plane waves to the product of localized dimer excitations [2], see also Fig. 12.2(c):

$$|\text{dimer}, N\rangle = \frac{1}{2^{N/4}} (\sigma_1^\dagger - \sigma_2^\dagger)(\sigma_3^\dagger - \sigma_4^\dagger) \dots (\sigma_{N-1}^\dagger - \sigma_N^\dagger) |0\rangle. \quad (12.5)$$

Another finding was that when the number of excitations is above half the number of emitters (fill factor f above one-half), dark states do not exist. This result is obvious for $N = 2$ atoms, where the state Eq. (12.5) with $f = 1/2$ is a totally occupied symmetric state $\sigma_1^\dagger \sigma_2^\dagger |0\rangle$, but was less obvious for a general N . For $N = 4$ atoms, the double-excited state corresponds to $f = 1/2$ fill factor, and this is exactly the state we first found in Ref. [9]. Another interesting feature of the answer Eq. (12.5) is that the dimers are formed by nearest atoms, e.g., that the state $\propto (\sigma_1^\dagger - \sigma_2^\dagger)(\sigma_3^\dagger - \sigma_4^\dagger) |0\rangle$ is darker than the one $\propto (\sigma_1^\dagger - \sigma_3^\dagger)(\sigma_2^\dagger - \sigma_4^\dagger) |0\rangle$. This can be explained intuitively by the fact that the closer the two excitations in a dimer are, the longer the spontaneous emission lifetime, see Eq. (12.2). Thus, the product state of the smallest possible dimers, formed by adjacent atoms, maximizes the lifetime.

For a single excitation, the eigenstates can be readily probed as resonances of the light reflection and transmission coefficients. This has been systematically done for subradiant states in an array of superconducting qubits coupled to the waveguide in Refs. [15, 16]. More details on these experiments can also be found in the review [17]. Predicted dimer states with two excitations were recently observed experimentally in an array of four superconducting qubits in experiments done by Gerhard Kirchmair's group [18]. Two excitations for four qubits

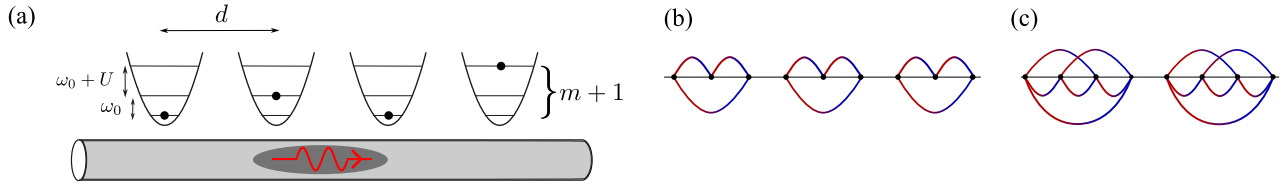


Figure 12.3: Adapted from Ref. [5]: (a) Illustration of an equidistant array of multi-level atoms coupled via photons in a waveguide. (b,c) Schematics of trimer and tetramer states in the array. Each red-blue line from site j to site j' in the diagrams corresponds to a subradiant dimer excitation $\sigma_j^\dagger - \sigma_{j'}^\dagger$.

correspond exactly to the $f = 1/2$ fill factor.

Very recent theoretical results by a group from the University of Padova, Italy, indicate that such dimer states are also relevant for two-dimensional atom arrays [19]. According to their findings, the most subradiant state in this setup is well described by a coherent superposition of all possible quantum dimer coverings: a resonating valence bond (RVB) liquid state.

In 2024 the answer Eq. (12.1) has been generalized to an array of waveguide-coupled multilevel atoms with an anharmonic potential [5], illustrated in Fig. 12.3. The result was that for strong anharmonicity, the darkest possible states are, in general, multimode excitations that depend on the number of levels per atom, the number of atoms in the array, and the excitation fill factor. While a general eigenstate is an entangled one, there exist eigenstates that are products of dimers, trimers, or tetramers, depending on the size of the system and the fill factor. At half-filling, these product states acquire a periodic structure with all-to-all connections inside each multimode and become the most subradiant ones. For example, for $N = 6$ three-level atoms, the darkest state is the trimer state

$$|\text{trimer}\rangle = (\sigma_1^\dagger - \sigma_2^\dagger)(\sigma_2^\dagger - \sigma_3^\dagger)(\sigma_3^\dagger - \sigma_1^\dagger) \times (\sigma_4^\dagger - \sigma_5^\dagger)(\sigma_5^\dagger - \sigma_6^\dagger)(\sigma_6^\dagger - \sigma_4^\dagger)|0\rangle, \quad (12.6)$$

as illustrated in Fig. 12.3(b). Figure 12.3(c) illustrates the quadrumer subradiant state, which is the darkest for $N = 8$ four-level atoms.

In two-level atom arrays with chiral one-way atom-photon coupling, somewhat similar steady-state patterns have been theoretically predicted already in Ref. [20]. However, contrary to the product states studied here for the non-chiral setup, the states in Ref. [20] are entangled.

12.3 Additional reading

Observation of a double-excited subradiant state for 4 qubits coupled to a waveguide: [18]

Multiple-excited subradiant states: Y.-X. Zhang and K. Mølmer, “Theory of subradiant states of a one-dimensional two-level atom chain”, *Phys. Rev. Lett.* **122**, 203605 (2019), A. V. Poshakinskiy and A. N. Poddubny, “Dimerization of many-body subradiant states in waveguide quantum electrodynamics”, *Phys. Rev. Lett.* **127**, 173601 (2021), J. Shi and A. N. Poddubny, “Multimer states in multilevel waveguide QED”, *Phys. Rev. A* **110**, 053707 (2024)

Localized subradiant states: R. Holzinger et al., “Control of localized single- and many-body dark states in waveguide QED”, *Phys. Rev. Lett.* **129**, 253601 (2022).

References

- ¹A. Asenjo-Garcia, M. Moreno-Cardoner, A. Albrecht, H. J. Kimble, and D. E. Chang, “Exponential improvement in photon storage fidelities using subradiance and “selective radiance” in atomic arrays”, *Phys. Rev. X* **7**, 031024 (2017).
- ²A. V. Poshakinskiy and A. N. Poddubny, “Dimerization of many-body subradiant states in waveguide quantum electrodynamics”, *Phys. Rev. Lett.* **127**, 173601 (2021).
- ³F. Damanet, D. Braun, and J. Martin, “Cooperative spontaneous emission from indistinguishable atoms in arbitrary motional quantum states”, *Phys. Rev. A* **94**, 033838 (2016).
- ⁴N. Shammah, N. Lambert, F. Nori, and S. De Liberato, “Superradiance with local phase-breaking effects”, *Phys. Rev. A* **96**, 023863 (2017).
- ⁵J. Shi and A. N. Poddubny, “Multimer states in multilevel waveguide QED”, *Phys. Rev. A* **110**, 053707 (2024).
- ⁶R. G. DeVoe and R. G. Brewer, “Observation of superradiant and subradiant spontaneous emission of two trapped ions”, *Phys. Rev. Lett.* **76**, 2049–2052 (1996).
- ⁷Y.-X. Zhang and K. Mølmer, “Theory of subradiant states of a one-dimensional two-level atom chain”, *Phys. Rev. Lett.* **122**, 203605 (2019).
- ⁸Y.-X. Zhang and K. Mølmer, “Subradiant emission from regular atomic arrays: universal scaling of decay rates from the generalized bloch theorem”, *Phys. Rev. Lett.* **125**, 253601 (2020).
- ⁹Y. Ke, A. V. Poshakinskiy, C. Lee, Y. S. Kivshar, and A. N. Poddubny, “Inelastic scattering of photon pairs in qubit arrays with subradiant states”, *Phys. Rev. Lett.* **123**, 253601 (2019).

- ¹⁰A. V. Poshakinskiy, J. Zhong, and A. N. Poddubny, “Quantum chaos driven by long-range waveguide-mediated interactions”, [Phys. Rev. Lett. **126**, 203602 \(2021\)](#).
- ¹¹Y.-X. Zhang, C. Yu, and K. Mølmer, “Subradiant bound dimer excited states of emitter chains coupled to a one dimensional waveguide”, [Phys. Rev. Research **2**, 013173 \(2020\)](#).
- ¹²A. N. Poddubny, “Quasiflat band enabling subradiant two-photon bound states”, [Phys. Rev. A **101**, 043845 \(2020\)](#).
- ¹³G. Calajó and D. E. Chang, “Emergence of solitons from many-body photon bound states in quantum nonlinear media”, [Phys. Rev. Research **4**, 023026 \(2022\)](#).
- ¹⁴B. Bakkensen, Y.-X. Zhang, J. Bjerrin, and A. S. Sørensen, *Photonic bound states and scattering resonances in waveguide QED*, 2021, [arXiv:2110.06093 \[quant-ph\]](#).
- ¹⁵J. D. Brehm, A. N. Poddubny, A. Stehli, T. Wolz, H. Rotzinger, and A. V. Ustinov, “Waveguide bandgap engineering with an array of superconducting qubits”, [npj Quantum Materials **6**, 10 \(2021\)](#).
- ¹⁶J. D. Brehm, R. Gebauer, A. Stehli, A. N. Poddubny, O. Sander, H. Rotzinger, and A. V. Ustinov, “Slowing down light in a qubit metamaterial”, [Appl. Phys. Lett. **121**, 204001 \(2022\)](#).
- ¹⁷A. S. Sheremet, M. I. Petrov, I. V. Iorsh, A. V. Poshakinskiy, and A. N. Poddubny, “Waveguide quantum electrodynamics: collective radiance and photon-photon correlations”, [Rev. Mod. Phys. **95**, 015002 \(2023\)](#).
- ¹⁸M. Zanner, T. Orell, C. M. F. Schneider, R. Albert, S. Oleschko, M. L. Juan, M. Silveri, and G. Kirchmair, “Coherent control of a multi-qubit dark state in waveguide quantum electrodynamics”, [Nat. Phys. **18**, 538–543 \(2022\)](#).
- ¹⁹G. Calajó, M. Tečer, S. Montangero, P. Silvi, and M. D. Liberto, *Many-body quantum dimerization in 2D atomic arrays*, 2025, [arXiv:2504.07207 \[quant-ph\]](#).
- ²⁰H. Pichler, T. Ramos, A. J. Daley, and P. Zoller, “Quantum optics of chiral spin networks”, [Phys. Rev. A **91**, 042116 \(2015\)](#).
- ²¹R. Holzinger, R. Gutiérrez-Jáuregui, T. Hönigl-Decrinis, G. Kirchmair, A. Asenjo-Garcia, and H. Ritsch, “Control of localized single- and many-body dark states in waveguide QED”, [Phys. Rev. Lett. **129**, 253601 \(2022\)](#).

Appendix A

Resonant susceptibility

Here, we provide more intuition into Eq. (3.6) for the resonant emitter susceptibility. Let us consider a toy model for an atom interacting with the electric field. The model represents a charge q with mass m moving in a harmonic potential $m\omega_0^2 z^2/2$ with the resonance frequency ω_0 around a charge $-q$. The moving charge then satisfies the Newton equation of motion

$$m\ddot{z} - 2m\gamma\dot{z} + m\omega_0^2 z = q[E(z)e^{-i\omega t} + E^*(z)e^{i\omega t}], \quad (\text{A.1})$$

where the right-hand side is the force acting upon the atom because of the time-dependent electromagnetic field $E(z, t) = E(z)e^{-i\omega t} + E^*(z)e^{i\omega t}$. We have also introduced a phenomenological friction force described by the coefficient γ . The dipole moment of the atom is given by $p_{\text{tot}} = qz(t)$ and can be sought in the form $p_{\text{tot}}(t) = p \exp[-i\omega t] + c.c.$ Solving Eq. (A.1) for $p(t) \propto e^{-i\omega t}$ we find

$$p = \alpha E, \quad \alpha = \frac{q^2}{m[\omega_0^2 - \omega^2 - 2i\omega\gamma]}. \quad (\text{A.2})$$

It is easy to show that for $\gamma \ll \omega_0$ Eq. (A.2) becomes equivalent to Eq. (3.6) with $a = q^2/(m\omega_0)$.

Appendix B

Green function for the Helmholtz equation

Here we will find the Green function $G(z)$ of the one-dimensional Helmholtz equation, satisfying the equation

$$\frac{d^2 G(z)}{dz^2} + q^2 G(z) = -4\pi q^2 \delta(z). \quad (\text{B.1})$$

where $q = \omega/c$ is the light wavevector. At $z \rightarrow \pm\infty$, the Green function should describe the outgoing wave, that is, it should satisfy the radiating boundary conditions.

We first note that for $z > 0$ or $(z < 0)$ the right-hand side of Eq. (B.1) is zero. Hence, we can choose the Green function in the form of plane waves, that satisfy the homogeneous wave equation:

$$G(z) = \begin{cases} A_+ e^{iqz} + A_- e^{-iqz}, & (z > 0) \\ B_+ e^{iqz} + B_- e^{-iqz}, & (z < 0). \end{cases} \quad (\text{B.2})$$

We also use the radiation boundary conditions $A_- = 0$ and $B_+ = 0$, that is we assume that the answer can not contain any terms corresponding to the waves incident on the source, only the terms propagating from the source. Due to mirror symmetry of the original equation $A_+ = B_- \equiv A$ and the Green function can be sought as

$$G(z) = \begin{cases} A e^{iqz}, & (z > 0) \\ A e^{-iqz}, & (z < 0). \end{cases} \equiv A e^{iq|z|}. \quad (\text{B.3})$$

Now we need to satisfy the equation also at $z = 0$, that is, to find A . To this end, we can

formally substitute the expression $Ae^{iq|z|}$ in the left-hand side. Using the identities

$$\frac{d}{dz}|z| = \text{sign } z, \quad \frac{d}{dz} \text{sign } z = 2\delta(z) \quad (\text{B.4})$$

we find that

$$\frac{d^2 G(z)}{dz^2} + q^2 G(z) = 2iqA\delta(z) \quad (\text{B.5})$$

which results in the answer

$$G(z) = 2\pi iq e^{iq|z|}. \quad (\text{B.6})$$

The same answer for the Green function can also be obtained by calculating it in the reciprocal space. To this end, we write

$$G(z) = \int \frac{dk}{2\pi} e^{ikz} G_k \quad (\text{B.7})$$

and substitute it into Eq. (B.1) which yields

$$G_k(q^2 - k^2) = -4\pi q^2. \quad (\text{B.8})$$

Thus, the result reads

$$G(z) = -4\pi q^2 \int \frac{dk}{2\pi} \frac{e^{ikz}}{k^2 - q^2}. \quad (\text{B.9})$$

The expression in Eq. (B.9) has a singularity at $k = \pm q$ and is generally not well defined. In order to define it in a more proper way we need to assume the presence of some losses in the system, that is, to set

$$q \rightarrow q + i\Delta \quad (\text{B.10})$$

with $\Delta > 0$ and then take the limit $\Delta \rightarrow 0$. Physically, this means setting the radiation condition that ensures the radiation being emitted away from the source. In order to calculate the integral we extend the contour to include either the half-circle $z = |R| \exp(i\varphi)$ that is either in the upper half plane, with $\varphi = 0 \dots \pi$ or in the lower half plane, with $\varphi = 0 \dots -\pi$. The half-circle is chosen in such a way that $\exp(ikz)$ is exponentially decaying, which means pper half-plane for $z > 0$ or in lower half-plane for $z < 0$. Then the integral can be evaluated using the Cauchy theorem. Depending on the contour, the integral is determined either by the pole

at $k = q + i\Delta$ or by the pole at $k = -q - i\Delta$:

$$G(z) = -2q^2 \times \lim_{\Delta \rightarrow 0} \begin{cases} -2\pi i \operatorname{Res} \frac{e^{ikz}}{k^2 - q^2} \Big|_{k=q+i\Delta} & z > 0, \\ 2\pi i \operatorname{Res} \frac{e^{ikz}}{k^2 - q^2} \Big|_{k=-q-i\Delta} & z < 0. \end{cases} \quad (\text{B.11})$$

The sign “ $-$ ” for $z > 0$ appears because the integral is taken counterclockwise, $\arg z = 0 \dots \pi$. Evaluating the residues we recover Eq. (B.6).

In what follows, it will be also prove one more Green function, using the rotating wave approximation (RWA):

$$\mathcal{G} = \lim_{\Delta \rightarrow +0} \int_{-\infty}^{\infty} \frac{dk}{2\pi} \frac{e^{ikz}}{\omega_k - \omega - i\Delta} \equiv \int_{-\infty}^{\infty} \frac{dk}{2\pi} \frac{e^{ikz}}{\omega_k - \omega - i0} = \frac{i}{c} e^{i\omega|z|/c}, \quad (\text{B.12})$$

where $\omega_k = c|k|$. In order to prove this identity we write

$$\begin{aligned} \int_{-\infty}^{\infty} \frac{dk}{2\pi} \frac{e^{ikz}}{\omega_k - \omega - i0} &= \int_0^{\infty} \frac{dk}{2\pi} \frac{e^{ikz}}{ck - \omega - i0} + \int_{-\infty}^0 \frac{dk}{2\pi} \frac{e^{ikz}}{-ck - \omega - i0} \\ &\approx \int_{-\infty}^{\infty} \frac{dk}{2\pi} \frac{e^{ikz}}{ck - \omega - i0} + \int_{-\infty}^{\infty} \frac{dk}{2\pi} \frac{e^{ikz}}{-ck - \omega - i0} \\ &= -\frac{2\omega}{c} \int_{-\infty}^{\infty} \frac{dk}{2\pi} \frac{e^{ikz}}{k^2 - (\omega/c)^2 - i0}. \end{aligned} \quad (\text{B.13})$$

Here, the key approximation was made in the second line, where we assume that the integration can be extended from the half-infinite ranges to the whole frequency range. This means assuming that the integral is determined only by the interaction with the photons with frequencies close to ω , which is the essence of the RWA.

Appendix C

Electromagnetic Green function in free space

In this appendix we will revisit the problem of dipole radiation in free space and derive its electric field. We start from the Maxwell equations for the electric and magnetic fields \mathbf{E} and \mathbf{H} at the frequency ω [1, 2]:

$$\text{rot } \mathbf{E} = \frac{i\omega}{c} \mathbf{H} , \quad (\text{C.1})$$

$$\text{rot } \mathbf{H} = -\frac{i\omega}{c} [\mathbf{E} + 4\pi \mathbf{p} \delta(\mathbf{r})] , \quad (\text{C.2})$$

$$(\text{C.3})$$

where the term $\mathbf{p} \delta(\mathbf{r})$ is the polarizability of a point dipole \mathbf{p} located at the coordinate origin. Calculating the curl of the first equation we arrive at

$$\text{rot rot } \mathbf{E}(\mathbf{r}) - q^2 \mathbf{E}(\mathbf{r}) = 4\pi q^2 \mathbf{p} \delta(\mathbf{r}) \quad (\text{C.4})$$

where $q = \omega/c$. The divergence of Eq. (C.2) is zero, which means that

$$\text{div}[\mathbf{E} + 4\pi \mathbf{p} \delta(\mathbf{r})] = 0 . \quad (\text{C.5})$$

As a result, we can use the identity $\text{rot rot } \mathbf{E} = \text{grad div } \mathbf{E} - \Delta \mathbf{E}$ in Eq. (C.4) and express $\text{div } \mathbf{E}$ as $-4\pi \text{div } \mathbf{p} \delta(\mathbf{r})$. The result reads

$$(\Delta + q^2) \mathbf{E}(\mathbf{r}) = -4\pi(q^2 + \text{grad div}) \mathbf{p} g . \quad (\text{C.6})$$

The solution of this equation

$$\mathbf{E}(\mathbf{r}) = \frac{1}{q^2} (q^2 + \text{grad div}) \mathbf{p} g \quad (\text{C.7})$$

where $g(\mathbf{r})$ is a Green function of a scalar wave equation .

$$(\Delta + q^2) g = -4\pi q^2 \delta(\mathbf{r}) \quad (\text{C.8})$$

It can be found by transforming the equation to the reciprocal space, similar to Eq. (B.9):

$$g = -4\pi q^2 \int \frac{d^3 k}{(2\pi)^3} \frac{e^{i\mathbf{k} \cdot \mathbf{r}}}{k^2 - q^2} = -4\pi q^2 \int_0^{2\pi} d\varphi \int_0^\pi \sin \theta d\theta \int_0^\infty \frac{k^2 dk}{(2\pi)^3} \frac{e^{ikr \cos \theta}}{k^2 - q^2} \quad (\text{C.9})$$

Here we introduced the spherical coordinates with the polar and azimuthal angles θ and φ . Integrating over the angles, we obtain

$$g = 4\pi i q^2 \frac{1}{r} \int_0^\infty \frac{k dk}{(2\pi)^2} \frac{e^{ikr} - e^{-ikr}}{k^2 - q^2} . \quad (\text{C.10})$$

The expression under the integral is an even function of k , so the integral can be extended over the whole real axis:

$$g = 2\pi i q^2 \frac{1}{r} \int_{-\infty}^\infty \frac{k dk}{(2\pi)^2} \frac{e^{ikr} - e^{-ikr}}{k^2 - q^2} . \quad (\text{C.11})$$

We deal with the singularity at $k = q$ similar to the one-dimensional case, Eq.(B.11), by setting $q \rightarrow q + i\Delta$ and taking the limit $\Delta \rightarrow +0$:

$$g = \frac{iq^2}{2\pi r} \left[-2\pi i \text{Res} \frac{ke^{ikr}}{k^2 - q^2} \Big|_{k=q} + 2\pi i \text{Res} \frac{ke^{-ikr}}{k^2 - q^2} \Big|_{k=-q} \right] , \quad (\text{C.12})$$

which results in

$$g = \frac{q^2 e^{iqr}}{r} \quad (\text{C.13})$$

The electric field can be written as

$$\mathbf{E}(\mathbf{r}) = (q^2 + \text{grad div}) \mathbf{p} \frac{e^{iqr}}{r}, \quad (\text{C.14})$$

or, after the tensor Green function $G_{\alpha\beta}$, as

$$E_\mu = G_{\mu\nu} p_\nu, \text{ or } G_{\mu\nu} = \left(q^2 \delta_{\alpha\beta} + \frac{\partial^2}{\partial x_\mu \partial x_\nu} \right) \frac{e^{iqr}}{r}. \quad (\text{C.15})$$

In what follows, it will be instructive to use one more representation of Eq. (C.13):

$$\frac{q^2 e^{iqr}}{r} = \iint \frac{d^2 k}{(2\pi)^2} \frac{2\pi i q^2}{\sqrt{q^2 - k^2}} e^{i\mathbf{k} \cdot \boldsymbol{\rho} + i\sqrt{q^2 - k^2}|z|} \quad (\text{C.16})$$

where $\boldsymbol{\rho} \equiv (x, y)$. To prove this equation we can just check directly that Eq. (C.13) satisfies Eq. (C.8):

$$\begin{aligned} (\Delta + q^2) \iint \frac{d^2 k}{(2\pi)^2} \frac{2\pi i q^2}{\sqrt{q^2 - k^2}} e^{i\mathbf{k} \cdot \boldsymbol{\rho} + i\sqrt{q^2 - k^2}|z|} \\ = \frac{2\pi i q^2}{\sqrt{q^2 - k^2}} \iint \frac{d^2 k}{(2\pi)^2} e^{i\mathbf{k} \cdot \boldsymbol{\rho}} \left(\frac{d^2}{dz^2} + q^2 - k^2 \right) e^{i\sqrt{q^2 - k^2}|z|} \\ = -4\pi q^2 \delta(z) \iint \frac{d^2 k}{(2\pi)^2} e^{i\mathbf{k} \cdot \boldsymbol{\rho}} = -4\pi q^2 \delta(\mathbf{r}) \end{aligned} \quad (\text{C.17})$$

where in the second line we used the Green function of the 1D Helmholtz equation, obtained in Appendix B.

Appendix D

Emitter polarizability with radiative corrections

In this section we consider the radiative corrections to the resonant polarizability of the emitter interactign with photons in free space. We assume, that without the interaction the polarizability is a resonant function of frequency

$$\alpha_0 = \frac{A}{\omega_0 - \omega - i\gamma} . \quad (\text{D.1})$$

Our goal will be to show, that Eq. (D.1) is changed when the interaction of the emitter with the photons is taken into account. The derivation is inspired by the review [3].

We start by writing the definition of the polarizability, that is, the relation between the dipole moment \mathbf{p} and the incident electric field at the dipole origin \mathbf{E}_0 :

$$\mathbf{p} = \alpha_0 \mathbf{E}_0 . \quad (\text{D.2})$$

The subtle point in Eq. (D.10) is the definition of \mathbf{E}_0 . Strictly speaking, this should be the total electric field at the dipole origin, and not the field of the incident wave. That is, in Eq. (D.10) we forgot to include the field, emitted by the dipole. So it is better to make the replacement

$$\mathbf{E}_0 \rightarrow \mathbf{E}_0 + \hat{G}(0)\mathbf{p}_0 , \quad (\text{D.3})$$

where $\hat{G}(0)$ is the tensor electromagnetic Green function, defined by Eq. (C.15). The problem

with this expression is however that the Green function diverges at the coordinate origin. If our point dipole is actually a model for a small particle, with the size much smaller than the light wavelength, it is physically reasonable to regularize the Green function by taking its average over the particle volume V .

We will now obtain an approximate expression for Eq. (C.15) for $qr \ll 1$. This requires a certain care, because

$$\frac{\partial^2}{\partial x_\alpha \partial x_\beta} \frac{1}{r} = -\frac{4\pi}{3} \delta_{\alpha\beta} \delta(\mathbf{r}) \quad (\text{D.4})$$

In order to prove this relation we notice that

$$\int_{r < R} d^3r \frac{\partial^2}{\partial x^2} \frac{1}{r} = \frac{1}{3} \int_{r < R} d^3r \left(\frac{\partial^2}{\partial x^2} + \frac{\partial^2}{\partial y^2} + \frac{\partial^2}{\partial z^2} \right) \frac{1}{r} = \frac{1}{3} \int_{r < R} d^3r [-4\pi \delta(\mathbf{r})] = -\frac{4\pi}{3}. \quad (\text{D.5})$$

This allows us to write

$$G_{xx}(r) = \left(q^2 + \frac{d^2}{dx^2} \right) \frac{e^{iqr}}{r} = \left(q^2 + \frac{d^2}{dx^2} \right) \frac{1 + iqr - \frac{(qr)^2}{2} - i\frac{(qr)^3}{6}}{r}, \quad (\text{D.6})$$

and

$$\text{Im } G_{xx}(0) = q^3 - \frac{q^3}{6} \frac{d^2}{dx^2} (x^2 + y^2 + z^2) = \frac{2q^3}{3}. \quad (\text{D.7})$$

Therefore, near the origin, the Green's function can be represented as

$$\hat{G}(\mathbf{r}) \approx G_1(\mathbf{r}) + G_2(\mathbf{r}) + G_3(\mathbf{r}) \equiv -\frac{4\pi}{3} \delta(\mathbf{r}) + \frac{2iq^3}{3} + \frac{3\mathbf{r} \otimes \mathbf{r} - r^2 \hat{\mathbf{1}}}{r^5}, \quad qr \ll 1. \quad (\text{D.8})$$

The averaging results in

$$\overline{G_1} = -\frac{4\pi}{3V}, \quad \overline{G_2} = \frac{2iq^3}{3}, \quad \overline{G_3} = 0. \quad (\text{D.9})$$

Substituting $G(0) = \overline{G_1} + \overline{G_2}$ into

$$\mathbf{p} = \alpha_0 [\mathbf{E}_0 + G(0)\mathbf{p}]. \quad (\text{D.10})$$

and solving the resulting equation we find

$$\mathbf{p} = \frac{\alpha_0}{1 - (\overline{G_1} + \overline{G_2})\alpha_0} \mathbf{E}_0 = \alpha \mathbf{E}_0, \quad (\text{D.11})$$

$$\alpha = \frac{\alpha_0}{1 - \frac{2i}{3} \left(\frac{\omega}{c}\right)^3 \alpha_0 + \frac{4\pi}{3V} \alpha_0}, \quad (\text{D.12})$$

If the radiative corrections are small, we can neglect their frequency dependence in the vicinity of the resoance

$$\alpha = \frac{A}{\omega_0 - \omega - i\gamma - \frac{2i}{3} \left(\frac{\omega}{c}\right)^3 A} \approx \frac{A}{\omega_0 - \omega - \frac{2i}{3} \left(\frac{\omega_0}{c}\right)^3 A + \frac{4\pi}{3V} A}. \quad (\text{D.13})$$

This allows us to introduce the radiative decay rate of the emitter

$$\gamma_0 = \frac{2i}{3} \left(\frac{\omega_0}{c}\right)^3 A \quad (\text{D.14})$$

and to rewrite the renormalized polarizability in the form

$$\alpha = \frac{3ic^3}{2\omega_0^3} \frac{\gamma_0}{\tilde{\omega}_0 - \omega - i(\gamma_0 + \gamma)}, \quad (\text{D.15})$$

with

$$\tilde{\omega}_0 = \omega_0 + \frac{4\pi}{3V} A. \quad (\text{D.16})$$

being the resonance frequency, shifted due to the interaction with the photons. The term $4\pi/(3V)$ is a analogue to the Lamb shift in quantum electrodynamics, that naturally arises in our simplified emitter model. From now on, in particular in Eq. (4.2) in the main text, we will assume that this shift is already included in the definition of ω_0 and will not write it explicitly.

Appendix E

Lattice summation details

The sum in Eq. (4.5) can be readily evaluated directly for arrays with hundreds or tens of atoms, occurring in practice [4]. However, the convergence is relatively slow due to the far-field terms. The commonly used approach to evaluate the lattice sum is the Ewald summation, which is based on splitting the sum into two parts. The first part, corresponding to smaller values of r in the near field zone, is evaluated in the real space, and the second part, corresponding to the far field zone $r \gtrsim c/\omega$, is Fourier transformed into the reciprocal space using the identity

$$\sum_{\mathbf{r}_j} \frac{e^{i\omega|\mathbf{r}-\mathbf{r}_j|/c}}{|\mathbf{r}-\mathbf{r}_j|} = \sum_{\mathbf{b}} \frac{2\pi i}{k_b a^2} e^{ik_b|z|+i\mathbf{b}\cdot\boldsymbol{\rho}}, \quad (\text{E.1})$$

where $\mathbf{r} = (\mathbf{r}, z)$, \mathbf{r}_j form a square lattice with the period a , the reciprocal lattice vectors \mathbf{b} form a square lattice with the spacing $2\pi/a$, $k_b \equiv \sqrt{(\omega/c)^2 - b^2}$. To prove this identity we replace each term in the sum in the left hand side using Eq. (C.16):

$$\begin{aligned} \sum_{\mathbf{r}_j} \frac{e^{i\omega|\mathbf{r}-\mathbf{r}_j|/c}}{|\mathbf{r}-\mathbf{r}_j|} &= \sum_{\mathbf{r}_j} \iint \frac{d^2k}{(2\pi)^2} \frac{2\pi i q^2}{\sqrt{q^2 - k^2}} e^{i\mathbf{k}\cdot\boldsymbol{\rho} + i\sqrt{q^2 - k^2}|z|} \\ &= \iint d^2k \frac{2\pi i q^2}{\sqrt{q^2 - k^2}} e^{i\sqrt{q^2 - k^2}|z|} e^{i\mathbf{k}\cdot\boldsymbol{\rho}} \left(\frac{1}{(2\pi)^2} \sum_{\mathbf{r}_j} e^{-i\mathbf{k}\cdot\mathbf{r}_j} \right) \\ &= \iint d^2k \frac{2\pi i q^2}{\sqrt{q^2 - k^2}} e^{i\mathbf{k}\cdot\boldsymbol{\rho} + i\sqrt{q^2 - k^2}|z|} \frac{1}{a^2} \sum_{\mathbf{b}} \delta(\mathbf{b} - \mathbf{k}) = \sum_{\mathbf{b}} \frac{2\pi i}{k_b a^2} e^{ik_b|z|+i\mathbf{b}\cdot\boldsymbol{\rho}} \quad (\text{E.2}) \end{aligned}$$

where we used the Poisson summation formula

$$a \sum_n e^{ikan} = 2\pi \sum_n \delta\left(k - \frac{2\pi}{a}n\right). \quad (\text{E.3})$$

The easiest way to remember this formula is to take the limit $ka \rightarrow 0$ when the summation in the left-hand-side can be replaced by integration and it reduces to the usual identity $\int dx \exp(ikx) = 2\pi\delta(k)$.

More details on the Ewald summation can be found e.g. in Ref. [5]. In our experience a more efficient approach is the Floquet summation technique developed in [6]. Specifically, the sum is given by Eq. (A37) of Ref. [6] that has to be complex conjugated and also multiplied by 4π to take into account the time dependence convention $e^{j\omega t}$ and a different definition of the Green's function used in Ref. [6]. We now discuss how to obtain the approximate expression Eq. (4.9) in the main text. The first term $2\pi i\omega/(ca^2)$ is given by the term with $b = 0$ in Eq. (E.1) multiplied by q^2 . It describes the radiative decay due to the emission of the waves propagating normally to the array, where $b = 0$, or, in another words, results from far-field radiative coupling between the atoms. The last term $S/2$ is given by the near field and can be obtained by setting ω in Eq. (4.5) to zero:

$$\frac{S}{2} = \sum_{\mathbf{r} \neq 0} \frac{\partial^2}{\partial x^2} \frac{1}{r} \equiv \sum_{\mathbf{r} \neq 0} \frac{3x^2 - r^2}{r^5} = \frac{1}{2} \sum_{\mathbf{r} \neq 0} \frac{1}{r^3} \approx \frac{9.03}{2a^3}. \quad (\text{E.4})$$

For the square lattice this sum converges rapidly enough and can be calculated directly. The term $S'(\omega/c)^2/2$ results from the field in Eq. (4.5) in the intermediate zone between the far field and the near field reads

$$\frac{S'(\omega/c)^2}{2} = \sum_{\mathbf{r} \neq 0} \frac{1 - (x/r)^2}{r} \frac{e^{i\mathbf{b} \cdot \mathbf{r} + i\omega r/c}}{r}. \quad (\text{E.5})$$

The term $1 - (x/r)^2$ for the square lattice can be replaced by its angle-averaged value $1/2$, and we can write it as

$$S' = \lim_{z \rightarrow 0} \lim_{\omega \rightarrow 0} \left(\text{Re} \sum_{\mathbf{r}} \frac{e^{i\omega\sqrt{r^2+z^2}/c}}{\sqrt{r^2+z^2}} - \frac{e^{i\omega|z|/c}}{|z|} \right). \quad (\text{E.6})$$

Taking the Fourier transformation of the first term with the help of Eq. (E.1), we find

$$S' = \lim_{z \rightarrow 0} \lim_{\omega \rightarrow 0} \left(\frac{2\pi i}{a} \sum_{\mathbf{b}} \frac{e^{i\sqrt{q^2-b^2}|z|}}{\sqrt{(\omega/c)^2 - b^2}} - \frac{e^{i\omega|z|/c}}{|z|} \right) = \lim_{z \rightarrow 0} \left(\frac{2\pi}{a} \sum_{\mathbf{b}} \frac{e^{-b|z|}}{b} - \frac{1}{|z|} \right). \quad (\text{E.7})$$

Let us first check the cancellation of the singular diverging terms $\propto 1/z$ in (E.7). To do this,

we can replace the summation by integration:

$$\frac{2\pi}{a} \sum_b \frac{e^{-bz}}{b} \approx \int_0^\infty b db \frac{e^{-b|z|}}{b} = \frac{1}{|z|}. \quad (\text{E.8})$$

Thus, the terms $1/z$ cancel each other and Eq. (E.7) has a finite limit of the order $1/a$. Numerical calculation for a square lattice yields to

$$S' = \lim_{z \rightarrow 0} \left(\frac{2\pi}{a} \sum_b \frac{e^{-b|z|}}{b} - \frac{1}{|z|} \right) = -\frac{3.90}{a}. \quad (\text{E.9})$$

Appendix F

Lindblad master equation for an emitter array

In this Appendix we will derive a master equation describing collective photon-mediated coupling and dissipation for a one-dimensional array of two-level atoms coupled to a reservoir of photonic modes. The system Hamiltonian reads

$$H = H_0 + H_{\text{phot}} + H_{\text{int}} \quad (\text{F.1})$$

where

$$H_0 = \sum_n \omega_0 \sigma_n^\dagger \sigma_n \quad (\text{F.2})$$

is the atom Hamiltonian (σ_n being the atomic raising operators and ω_0 the atom resonance frequency),

$$H_{\text{phot}} = \sum_k \omega_k a_k^\dagger a_k \quad (\text{F.3})$$

is the Hamiltonian of propagating photons with the frequencies ω_k and

$$H_{\text{int}} = - \sum_{k,j} \sqrt{2\pi\omega_k} [df_k^*(z_j) \sigma_j a_k^\dagger + d^* f_k(z_j) a_k \sigma_j^\dagger] \quad (\text{F.4})$$

is the interaction Hamiltonian. Here d is the dipole moment and $f_k(z)$ are the electric field eigenmodes and a_k are the corresponding photon annihilation operators. In the particular case

of photons propagating in a waveguide, we have

$$f_k(z) = \frac{1}{\sqrt{L}} \exp(ikz), \quad \omega_k = c|k|, \quad \sum_k \equiv \int_{-\infty}^{\infty} \frac{Ldk}{2\pi}, \quad (\text{F.5})$$

where L is the normalization length.

It is convenient to rewrite the atom-photon coupling Hamiltonian in the interaction representation

$$\tilde{H}_{\text{int}} = - \sum_{k,j} g_k [f_k^*(z_j) \sigma_j a_k^\dagger e^{i(\omega_k - \omega_0)t} + f_k(z_j) a_k \sigma_j^\dagger e^{-i(\omega_k - \omega_0)t}] \quad (\text{F.6})$$

where $g_k = \sqrt{2\pi\omega_k}d$ is the coupling constant.

The equation for the density matrix of a total system of atoms and photons reads

$$\frac{\partial \rho}{\partial t} = -i[\tilde{H}_{\text{int}}(t), \rho(t)]. \quad (\text{F.7})$$

We are interested in tracing out the photons and obtain an effective master equation describing the atom density matrix. To this end, we eliminate the reservoir dynamics by first integrating Eq. (F.7) over t and then substituting the result back into Eq. (F.7):

$$\frac{\partial \rho}{\partial t} = -[\tilde{H}_{\text{int}}(t), \int_0^{t'} dt' [\tilde{H}_{\text{int}}(t'), \rho(t')]] \quad (\text{F.8})$$

Next, we assume that the reservoir dynamics is fast, so we can replace $\rho(t')$ in the right-hand-side by $\rho(t)$:

$$\frac{\partial \rho}{\partial t} = -[H_{\text{int}}(t), \int_0^{t'} dt' [H_{\text{int}}(t'), \rho(t)]] \quad (\text{F.9})$$

and average over the reservoir degrees of freedom. We assume, that the reservoir is in vacuum, so the only nonzero average is

$$\langle a_k a_{k'}^\dagger \rangle = \delta_{kk'}. \quad (\text{F.10})$$

The result reads

$$\begin{aligned}
 - \left\langle \left[H_{\text{int}}(t), \int_0^{t'} dt' [H_{\text{int}}(t'), \rho(t)] \right] \right\rangle &= \sum_{k,j,j'} \frac{g_k^2}{L} \int_0^{t'} dt' \left[\right. \\
 &\quad - \sigma_j^\dagger \sigma_{j'} f_k(z_j) f_k^*(z_{j'}) e^{-i(\omega_k - \omega_0)(t-t')} \rho(t) - \rho(t) \sigma_j^\dagger \sigma_{j'} f_k(z_j) f_k^*(z_{j'}) e^{i(\omega_k - \omega_0)(t-t')} \\
 &\quad \left. + \sigma_j \rho(t) \sigma_{j'}^\dagger f_k^*(z_j) f_k(z_{j'}) [e^{-i(\omega_k - \omega_0)(t-t')} + e^{i(\omega_k - \omega_0)(t-t')}] \right] \quad (\text{F.11})
 \end{aligned}$$

We now again make the use of Markovian approximation, and replace $g_k^2 \rightarrow g_0^2$, which means that the coupling takes place only with the close-to-resonant photons where $\omega_k \approx \omega_0$. Now we can perform the integration over k

$$\begin{aligned}
 \sum_k f_k(z_j) f_k^*(z_{j'}) \int_0^{t'} dt' e^{-i(\omega_k - \omega_0)(t-t')} &= \sum_k f_k(z_j) f_k^*(z_{j'}) \int_{-\infty}^{t'} dt' e^{-i(\omega_k - i0 - \omega_0)(t-t')} \\
 &= -i \sum_k \frac{f_k(z_j) f_k^*(z_{j'})}{\omega_k - \omega_0 - i0} = -i \mathcal{G}(z_j, z_{j'}) \quad (\text{F.12})
 \end{aligned}$$

where we explicitly introduced the photon Green function

$$\mathcal{G}(z_j, z_{j'}, \omega_0) = \sum_k \frac{f_k(z_j) f_k^*(z_{j'})}{\omega_k - \omega_0 - i0}. \quad (\text{F.13})$$

In a similar fashion, we can write

$$\sum_k f_k(z_j) f_k^*(z_{j'}) \int_0^{t'} dt' e^{i(\omega_k - \omega_0)(t-t')} = i \mathcal{G}^*(z_{j'}, z_j) = i \mathcal{G}^*(z_j, z_{j'}). \quad (\text{F.14})$$

Here we restricted ourselves to the time-inversion symmetric case, when $\mathcal{G}(z_j, z_{j'}) = \mathcal{G}(z_{j'}, z_j)$.

Using the equations above we can express the integrals in Eq. (F.11) via the Green function:

$$\begin{aligned}
 - \left\langle \left[H_{\text{int}}(t), \int_0^{t'} dt' [H_{\text{int}}(t'), \rho(t)] \right] \right\rangle &= \frac{g_0^2}{L} \sum_{j,j'} \left[\right. \\
 &\quad i \sigma_j^\dagger \sigma_{j'} \rho(t) \mathcal{G}(z_j, z_{j'}) - i \rho(t) \sigma_j^\dagger \sigma_{j'} \mathcal{G}^*(z_j, z_{j'}) + \sigma_j \rho(t) \sigma_{j'}^\dagger [i \mathcal{G}(z_j, z_{j'}) - i \mathcal{G}^*(z_j, z_{j'})] \left. \right]. \quad (\text{F.15})
 \end{aligned}$$

Here, as usual, $-i0$ means a complex number with a vanishingly small negative imaginary part, that is introduced in order for the system to have non-vanishing losses. The Lindblad master

equation assumes the form [1, 2]

$$\frac{\partial \rho}{\partial t} = -\frac{g_0^2}{L} \sum_{j,j'} \text{Im} \mathcal{G}(z_j, z_{j'}) \left[\sigma_j^\dagger \sigma_{j'} \rho(t) + \rho(t) \sigma_j^\dagger \sigma_{j'} - 2\sigma_j \rho(t) \sigma_{j'}^\dagger \right] - i[H, \rho], \quad (\text{F.16})$$

where the Hamiltonian

$$H = -\frac{g_0^2}{L} \sum_{j,j'} \text{Re} \mathcal{G}(z_j, z_{j'}) \sigma_j^\dagger \sigma_{j'} \quad (\text{F.17})$$

describes photon-mediated coupling between the atoms. It is sometimes instructive to rewrite the master equation as

$$\frac{\partial \rho}{\partial t} = \frac{2g_0^2}{L} \sum_{j,j'} \text{Im} \mathcal{G}(z_j, z_{j'}) \sigma_j \rho(t) \sigma_{j'}^\dagger - i(H_{\text{eff}} \rho - \rho H_{\text{eff}}^\dagger), \quad (\text{F.18})$$

where

$$H_{\text{eff}} = -\frac{g_0^2}{L} \sum_{j,j'} \mathcal{G}(z_j, z_{j'}) \sigma_j^\dagger \sigma_{j'} \quad (\text{F.19})$$

is the effective non-Hermitian Hamiltonian. In particular case when the reservoir is presented by the photons with linear dispersion we can use Eq. (B.12) for the Green function:

$$-\frac{g_0^2}{L} \mathcal{G}(z_j, z_{j'}) = -i \frac{g_0^2}{c} e^{i\omega_0 |z_j - z_{j'}|/c}. \quad (\text{F.20})$$

Identifying spontaneous decay rate in the waveguide as $\gamma_{1D} = g_0^2/c$ we recover the usual effective non-Hermitian Hamiltonian in the form

$$H_{\text{eff}} = -i\gamma_{1D} e^{i\omega_0 |z_j - z_{j'}|/c}. \quad (\text{F.21})$$

Bibliography

- ¹K. Lalumière, B. C. Sanders, A. F. van Loo, A. Fedorov, A. Wallraff, and A. Blais, “Input-output theory for waveguide qed with an ensemble of inhomogeneous atoms”, [Phys. Rev. A **88**, 043806 \(2013\)](#).
- ²R. H. Lehmberg, “Radiation from an N -atom system. I. General Formalism”, [Phys. Rev. A **2**, 883–888 \(1970\)](#).